INCORPORATING MICROCLIMATE INTO HABITAT SUITABILITY ANALYSIS FOR PLETHODONITD SALAMANDERS

BY

SAMUEL FITZSIMONS STICKLEY

DISSERTATION

Submitted in partial fulfillment of the requirements
for the degree of Doctor of Philosophy in Natural Resources and Environmental Sciences
in the Graduate College of the
University of Illinois Urbana-Champaign, 2021

Urbana, Illinois

Doctoral Committee:

Professor Robert Schooley, Chair
Associate Professor Jennifer Fraterrigo, Director of Research
Assistant Professor Kaiyu Guan
Dr. John Crawford, National Great Rivers Research and Education Center

ABSTRACT

Climate has substantial influence on the distribution of species, and climate change puts many species at risk of extirpation or extinction due to diminishing range sizes. Understanding how organisms may respond to climate change is important for spatially predicting suitable habitat for conservation planning. However, current approaches to modeling suitable habitat typically rely on climate data that do not account for important buffering effects of vegetation on near-surface microclimates and are produced at spatiotemporal scales irrelevant to a variety of organisms that thrive in microenvironments. Furthermore, commonly used species distribution models may not account for mechanistic aspects, like physiology, that are relevant to the biology and performance of a species. This dissertation integrates aspects from three main components of a species' niche (the habitat, trait, and performance components) into robust correlative and mechanistic models for habitat suitability analysis at the microscale. This involved the development and evaluation of an approach that incorporates vegetation structure across the entire vertical profile of forests into predictions of microclimatic temperature at a highly spatially resolved scale. The resulting maps of microclimatic temperature (habitat component) were incorporated into a physiological model (trait component) that included a novel method that accounts for body-mass elevation effects for predicting the metabolic rate of three plethodontid salamander species of varying sizes, sexes, and stage classes. Predictions of suitable climatic habitat, vapor pressure deficit, and salamander physiology were combined (performance component) at varying spatial scales and temporal periods to assess spatiotemporal agreement between model approaches and to target suitable habitat at relevant biological scales to plethodontid salamanders in Great Smoky Mountains National Park.

Understory vegetation structure was found to be an important addition to canopy cover in buffering near-surface temperatures and improved accuracy of microclimatic temperature estimates. The combined effects of microclimatic temperature variation with increasing plethodontid body mass along elevational gradients resulted in spatiotemporal differences in salamander energetics across species, sexes, and stage classes. Integrating physiological models with predicted suitable habitat demonstrated important spatiotemporal mismatches between model approaches, highlighting a problem with relying on static species distribution models, which neglect important temporal changes in energetic demand of plethodontid salamanders. Furthermore, this dissertation validates the importance of incorporating microclimate into species distribution models and demonstrates approaches to integrating multiple model types for spatiotemporal targeting of suitable habitat that account for temporal variations in energetic demand as well as variations among species and across stage classes. The results from this dissertation reveal the importance of predicting microclimate more accurately by accounting for the proper vegetation and biophysical buffers to near-surface temperature, and highlight the use of multiple model approaches, correlative and mechanistic, developed at proper spatial and temporal scales for spatially analyzing and targeting suitable habitat, especially for species vulnerable to climate change.

ACKNOWLEDGEMENTS

The research conducted for this dissertation was partially funded by National Science Foundation award #1339944. Chapter two of this dissertation was reproduced with permission from Springer Nature, and was first published in [*Landscape Ecology*, 36, 1197–1213, 2021] by Springer Nature.

For their help with the data used in this project, I thank Jason Fridley for providing the iButton logger dataset in Great Smoky Mountains National Park, and John Crawford, William Peterman, and Daniel Hocking for providing the salamander body mass dataset. Thomas Jordan was also very helpful in assisting with the Tennessee LiDAR dataset, and Doug Newcomb gave great advice on developing vegetation structure with LiDAR data.

At the University of Illinois, I first want to acknowledge and thank my advisor, Jennifer Fraterrigo, for all of her help and guidance over the many years that we worked together on this research, other projects, and teaching courses. It has been a real pleasure and a great experience. I also thank the rest of my doctoral committee members, Robert Lee Schooley, Kaiyu Guan, and John Crawford, for all of their time and effort in helping me with the development and completion of this work. Each member of my doctoral committee has truly contributed a unique perspective to this project based on their areas of expertise. A special thanks to Eric Larson for his review and comments on aspects of this research, to all of the Fraterrigo lab members and graduate student cohorts that I have had the pleasure of working with, and to all of the students that I have enjoyed teaching and working with so much over the years.

Finally, I would not be finishing this project without the support of my family and friends, so I thank all of you for being such an important part of my life.

This dissertation is dedicated to my parents, Bob and Sharon, for their unwavering support throughout my life, and to my wife, Emily, for all of her encouragement as I worked towards completion of my doctoral degree.

TABLE OF CONTENTS

CHAPTER 1: LITERATURE REVIEW AND RESEARCH APPROACH …….……1

CHAPTER 2: UNDERSTORY VEGETATION CONTRIBUTES TO MICORLCIMATIC BUFFERING OF NEAR-SURFACE TEMPERATURES IN TEMPERATE DECIDUOUS FORESTS ……..…….8

CHAPTER 3: SPATIOTEMPORAL PATTERNS OF ENERGETIC MAINTENANCE COSTS ARE INCONSISTENT WITH SUITABLE CLIMATIC HABITAT FOR PLETHODONTID SALAMANDERS …….…..…….36

CHAPTER 4: TARGETING AREAS OF HIGH CONSERVATION VALUE FOR PLETHODONTID SALAMANDERS THREATHEANED FROM CLIMATE-INDUCED RANGE LOSS …….…….63

CHAPTER 5: SUMMARY AND CONCLUSIONS ……....94

APPENDIX A: CHAPTER 2 SUPPLEMENTARY MATERIAL ……..…….97

APPENDIX B: CHAPTER 3 SUPPLEMENTARY MATERIAL …….……....111

APPENDIX C: CHAPTER 4 SUPPLEMENTARY MATERIAL …….……....126

REFERENCES …….....140

CHAPTER 1: LITERATURE REVIEW AND RESEARCH APPROACH

Literature Review

Many species are shifting their distributions towards higher latitudes or higher elevations as they track suitable climatic conditions, and ecologists now confronted with one of the most important challenges of our time, developing a better understanding of organismal responses to climate change (Hoegh-Guldberg et al. 2008; Chen et al. 2011; Tingley et al. 2012; Lenoir and Svenning 2015). Climate change is a main driver to extinction risk (Urban 2015), because species' ranges and areas of suitable climatic habitat are diminishing (Thomas et al. 2004; Maclean and Wilson 2011; Urban 2015). Because global biodiversity is declining at unparalleled rates (Hoffmann et al. 2010; WWF 2020), there is a need to develop conservation approaches that provide spatially explicit outcomes and reduce uncertainty under future climate conditions (Groves et al. 2012; Schmitz et al. 2015; Jones et al. 2016). Protecting areas of microclimatic refugia or areas that promote functional connectivity is critically important for species vulnerable to climate change (Groves et al. 2012; Jones et al. 2016; Evans et al. 2015).

Amphibians are the most vulnerable vertebrates in the world with over 40% of the species estimated to be at risk of extinction globally, mostly due to habitat loss, fragmentation, and climate change (Cushman 2006; Blaustein et al. 2010; IUCN 2020). Because amphibians are rarely capable of functioning at temperatures near their upper critical limits and loss of suitable climatic habitat reduces dispersal ability, many species are at risk of extinction (Carey and Alexander 2003; Milanovich et al., 2010). This is the case for many salamander species in the family Plethodontidae which are vulnerable to regional extirpation or extinction for multiple reasons (Bernardo and Spotila, 2006; Milanovich et al., 2010). Plethodontid salamanders are terrestrial, lungless ectotherms that require cool, moist conditions to avoid water loss (Feder

1983; Lutterschmidt and Hutchison 1997; Bernardo and Spotila 2006). Increases in temperature may increase desiccation risk, vulnerability to pathogens (Blaustein and Kiesecker 2002; Carey and Alexander 2003; Blaustein et al. 2010), diminish growth rates and body size (Caruso et al. 2014), alter reproductive cycles, and increase physiological stress (Feder and Pouoh 1975; Blaustein et al. 2010; Homyack et al. 2010, 2011). Plethodontid energy budgets may be affected by increasing temperatures, decreasing availability of water, and overall climatic variability, resulting in increased physiological stress which can create ecological tradeoffs that affect overall fitness (Pough 1980; Sears 2005; DuRant et al. 2007; Homyack et al. 2010). Therefore, these species may be unable to physiologically adapt to increasing temperatures or migrate to new areas through unsuitable microclimatic conditions across the landscape matrix due to limited dispersal ability within species-specific elevational ranges (Bernardo and Spotila 2006; Lutterschmidt and Hutchinson 1997; Milanovich et al. 2010).

Furthermore, certain plethodontid species are high elevation specialists that have been shown to increase in body size with cooler, moister climates that accompany elevational gain (Peterman et al. 2016). Because energetic demand of plethodontids increases with body size (Feder 1976) and increased temperatures (Pough 1980; Sears 2005; Homyack et al. 2010), there is potential for physiological variation along climatic and elevational gradients. Characterizing physiological responses to changing microclimatic regimes is important for understanding plethodontid surface activity and distribution, but current approaches to assessing suitable habitat are typically not resolved at proper spatiotemporal scales and neglect physiology or other mechanistic considerations (Kearney and Porter 2009; Lembrechts et al. 2018).

Small organisms, like plethodontid salamanders, rely on microclimatic conditions, but species distribution models (SDMs), the most commonly used approaches to assessing suitable

habitat and range size (Elith et al. 2008; Lentini and Wintle 2015; Araújo et al. 2019), are commonly produced with bioclimatic variables based on free-air temperature predictions and at average spatial resolutions 10,000-fold larger than the organisms being studied (Potter et al. 2013; Lenoir et al. 2017; Lembrechts et al. 2018). Although temporal resolutions vary in studies using SDMs, they are often inadequate as well (Lembrecths et al. 2018). The "spatial resolution paradox" suggests that SDMs developed with coarse resolution climate data may overestimate suitable habitat regionally, but underestimate suitable habitat at the local scale, an issue for accurately predicting organismal responses to climate change (Trivedi et al. 2008; Gillingham et al. 2012a, b; Franklin et al. 2013; Lenoir et al. 2017). Furthermore, SDMs typically do not account for physiological responses at relevant spatial and temporal scales, neglecting potentially important biological information on performance and fitness of organisms (Kearney and Porter 2009; Barton and Terblanche 2014; Evans et al. 2015). To bridge this spatiotemporal gap in habitat suitability predictions, there is a need to develop robust microclimate datasets for use in modeling species distributions and amphibian bioenergetics (Kearney and Porter 2009; Bramer et al. 2018; Lembrecths et al. 2018). Although advances in developing physiological models at relevant biological scales have been made (Kearney and Porter 2016), there remains a need to better understand the patterns and drivers of microclimatic variability to enhance accuracy of microclimate predictions at fine spatial resolutions (Bolstad et al. 1998; Lenoir et al. 2017; Lembrechts et al. 2018).

Microclimate is controlled by many environmental factors that contribute to the buffering of solar radiation and large scale climate patterns; factors that free-air temperature predictions are unable to capture (Davis et al. 2018; De Frenne et al. 2019; Zellweger et al. 2019a; Stickley and Fraterrigo 2021). In heterogenous landscapes, near surface temperature may vary among

locations only a few meters apart or deviate from free-air temperatures at greater magnitudes compared to temperature measurements only a few meters above the ground (Fridley 2009; Davis et al. 2018). Fine-scale variations in microclimatic temperature are due to the buffering effects from topography (e.g., elevation, slope), shading from forest cover and vegetation characteristics (e.g. vegetation density, vegetation height), vicinity to water (Fridley 2009; Geiger et al. 2009), and ground substrate (e.g., leaf litter, downed woody debris, rocks), which also act as microrefugia for terrestrial salamanders (Ashcroft et al. 2008; Caruso et al. 2015; O'Donnell et al. 2014). Topoclimatic variables, such as solar heat transfer varying with topographic complexities have long been the focus of variability in climatic regimes (Geiger et al. 2009; Lembrechts et al. 2018). However, vegetation is also an important, yet commonly disregarded, factor to altering climate near the surface of the earth (Geiger et al. 2009; Davis et al. 2018; Stickley and Fraterrigo 2021).

The forest canopy has been shown to act as a thermal insulator that cools maximum temperatures (Chen and Franklin 1997; Davis et al. 2018), warms minimum temperatures (De Frenne et al. 2019), and reduces temperature variability at the forest floor (Chen et al. 1999; Vanwalleghem and Meentemeyer 2009). Important biophysical effects and the structure of sub-canopy vegetation layers may also buffer direct and diffuse (i.e., scattered and transmitted from atmosphere) solar radiation, alter localized wind patterns, and modify evapotranspiration rates (Geiger et al. 2009; Bramer et al. 2018). Despite increasing availability of fine resolution elevation datasets and remote sensing technologies for characterizing vegetation structure (Lefsky et al. 2002; Zellweger et al. 2019b), there is limited development of microclimatic datasets at broad extents (Lembrechts et al. 2018).

The use of coarse resolution, free-air climate data, which neglect important buffering effects of vegetation on near-surface temperatures and disregard mechanistic responses from organisms, is problematic for assessing suitable habitat for small, ground-dwelling organisms (Kearney and Porter 2009; Helmuth et al. 2010). There is now a critical need to incorporate microclimate into species distribution models and mechanistic modeling approaches to estimate suitable habitat at scales relevant to a multitude of organisms reliant on climatic regimes near the surface of the earth (Lembrechts et al. 2018), but there remains a gap in our understanding of the biophysical processes that drive spatiotemporal variability of microclimatic regimes and techniques for estimating organismal responses to climate change at microscales are poorly developed (Bolstad et al. 1998; Lenoir et al. 2017; Lembrechts et al. 2018). Integrating multiple model types at proper spatiotemporal resolutions can provide independent results that strengthen predictions in areas of agreement or provide insights on model disagreement (Kearney and Porter 2009; Morin and Thuiller 2009), information especially relevant for the prioritization of conservation assets for species vulnerable to climate change (Cushman 2006; Hoegh-Guldberg et al. 2008; Kearney and Porter 2009; Clusella-Trullas et al. 2011). Furthermore, an integration of these models may allow for robust targeting of important conservation assets, such as microclimatic refugia and areas of connectivity between important habitat locations (Groves et al. 2012; Jones et al. 2016).

Research Approach

The primary goal of this dissertation was to integrate components of a species' niche (Kearney and Porter 2009) to analyze and spatially locate climatically and physiologically suitable habitat at microscales relevant to plethodontid salamanders (Fig. 1.1). In Chapter 2, I

aimed to capture a habitat component (Fig. 1.1) by developing and evaluating an approach that incorporates complex vegetation structure into statistical models for the robust prediction of microclimatic temperatures across the Great Smoky Mountains National Park (GSMNP; North Carolina and Tennessee, US). I also identified the factors influencing spatiotemporal patterns in microclimatic temperature, predicting a priori that understory vegetation layers would be important buffers of microclimatic temperatures along with canopy vegetation. Additionally, I characterized spatiotemporal mismatches between free-air, coarse resolution temperature models and sub-canopy, microclimatic temperature predictions. In Chapter 3, I aimed to capture a trait component (Fig. 1.1), by incorporating the microclimatic temperature maps developed in Chapter 2 with a physiological model that accounts for body mass-elevation relationships to estimate fine resolution predictions of standard metabolic rate (SMR) for three plethodontid species of varying sizes, sexes, and stage classes. Additionally, I evaluated the agreement of fine resolution salamander bioenergetics with predictions from coarse resolution SDMs to assess spatiotemporal mismatches between model approaches. In Chapter 4, I aimed to capture a performance component (Fig. 1.1) by integrating current and future predictions of fine resolution suitable climatic habitat (i.e., correlative model) and salamander physiology (i.e., mechanistic model) during increased periods of surface activity (March-November) for the three plethodontid species. I quantified future changes in salamander physiology and suitable climatic habitat, and integrated models to spatially target areas with low energetic cost of maintenance within suitable climatic habitat locations and areas of functional connectivity between suitable climatic habitat locations. In Chapter 5, I summarize the main results and conclusions from this dissertation, and discuss potentially important future needs in this field of research.

Figure

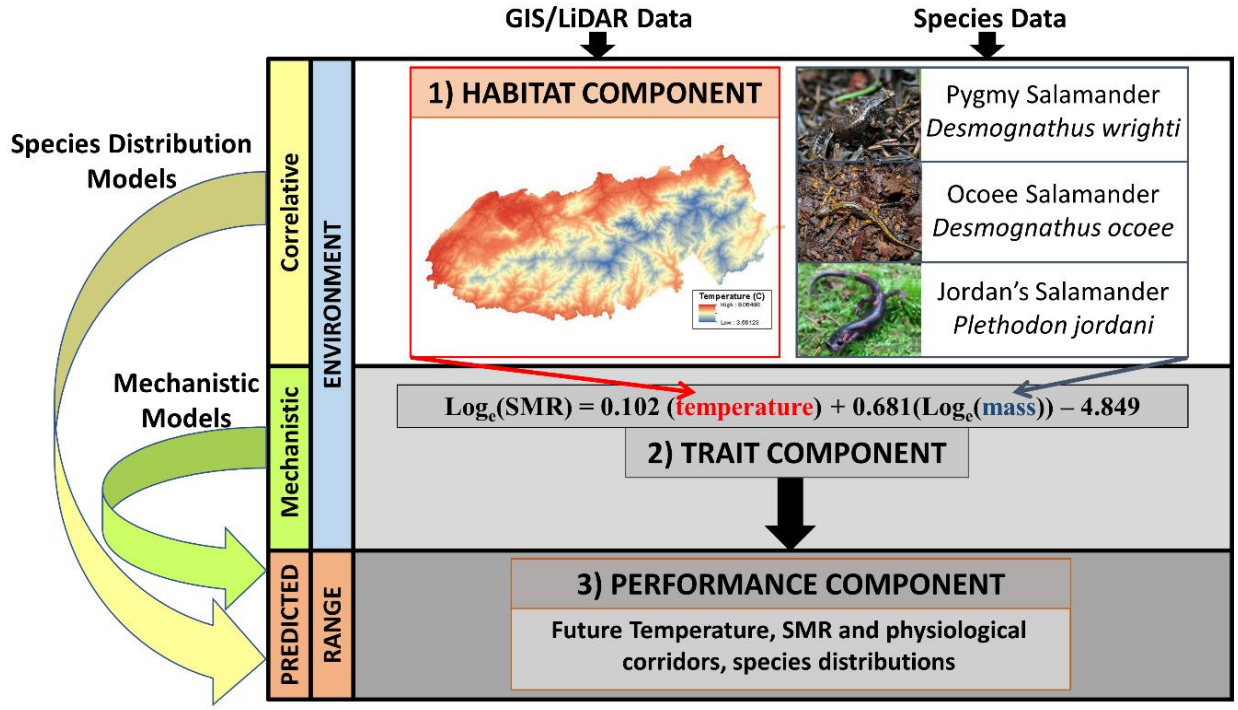

Figure 1.1 Conceptual diagram that depicts the use of a habitat and trait component to integrate physiology and suitable climatic habitat into a performance component for plethodontid salamanders at a microscale

CHAPTER 2: UNDERSTORY VEGETATION CONTRIBUTES TO MICROCLIMATIC BUFFERING OF NEAR-SURFACE TEMPERATURES IN TEMPERATE DEDICUOUS FORESTS

Introduction

One of the greatest ecological challenges of our time is understanding how organisms may respond to climate change. Because climate is the underlying factor in determining species' distributions, there has been renewed interests in studying microclimate (De Frenne and Verheyen 2016; Jucker et al. 2018) or the climatic conditions at localized areas near the surface of the earth (Geiger et al. 2009). Developing accurate microclimate datasets at biologically relevant scales has become a high priority for predicting potential species' range shifts in response to climate change (Kearney and Porter 2009; Bramer et al. 2018) and identifying climatic microrefugia, i.e., areas essential to the various species reliant on locally persistent climatic regimes under regionally changing climatic conditions (Ashcroft 2010; Hannah et al. 2014; Lenoir et al. 2017). However, techniques for predicting microclimate are poorly developed and there is limited understanding of the patterns and drivers of spatiotemporal variability of microclimatic regimes, especially in montane forests (Bolstad et al. 1998; Lenoir et al. 2017; Lembrechts et al. 2018). To enhance the availability and use of microclimate datasets for environmental and conservation planning, it is important to advance methods for characterizing microclimate and quantify uncertainties (Potter et al. 2013; Lembrechts et al. 2018).

Free-air, macroclimate can differ substantially from the microclimatic conditions that organisms experience in their natural habitat, resulting in spatiotemporal mismatches (Fridley 2009; Geiger et al. 2009; Potter et al. 2013). In microhabitat, organisms generally experience 5 °C deviations in seasonal mean temperatures compared to free-air macroclimate, but these deviations can increase up to 20 °C within heterogeneous landscapes (Scherrer and Körner 2010;

Suggitt et al. 2011; Zellweger et al. 2019a). In montane forests, near-surface temperatures can vary at locations only a few meters apart (Fridley 2009; Geiger et al. 2009; Bramer et al. 2018) and deviate from free-air temperatures at greater magnitudes compared to temperature measurements only a few meters above the ground (Davis et al. 2018). Fine-scale temperature variability has typically been attributed to the interactions between topoclimatic variables, such as solar heat transfer varying with topographic complexities (Geiger et al. 2009; Lembrechts et al. 2018). However, vegetation also alters forest microclimates (Geiger et al. 2009; Davis et al. 2018; Lembrechts et al. 2018).

Forest canopy characteristics such as canopy cover, canopy height, and leaf area index, strongly affect sub-canopy temperature, acting as a thermal insulator that cools maximum temperatures (MaxT; Chen and Franklin 1997; Davis et al. 2018), warms minimum temperatures (MinT; De Frenne et al. 2019), and reduces temperature variability at the forest floor (Chen et al. 1999; Vanwalleghem and Meentemeyer 2009). For instance, sub-canopy MaxT of forest interiors have been shown to be more than 5 °C lower than adjacent clear-cut areas (Chen et al. 1999), and there tends to be increased variability in MaxT and MinT in forests with limited canopy cover (Chen et al. 1999; Vanwalleghem and Meentemeyer 2009). Forest layers below the canopy may also be important buffers of direct and diffuse (i.e., scattered and transmitted from atmosphere) solar radiation (Geiger et al. 2009), but relatively few studies have evaluated their role in determining microclimate. By contributing to structural complexity, sub-canopy vegetation layers may produce variations in solar radiation levels, localized wind patterns and evapotranspiration (Geiger et al. 2009; Bramer et al. 2018), which could result in further alterations of near-surface microclimate. Additionally, vegetation layers below the canopy may interact with other landscape physiographic variables such as cold-air-drainage and distance-to-

stream, creating spatiotemporal variations in microclimate (Kiefer and Zhong 2013; Day and Monk 1974). Despite increasing availability of datasets for characterizing vegetation structure (Lefsky et al. 2002; Zellweger et al. 2019b), there is limited understanding of its mediating effects on microclimatic regimes.

Accounting for sub-canopy forest layers and biophysical interactions may improve our understanding of microclimatic processes and increase the accuracy of microclimatic temperature predictions within forests, an important step in developing biologically relevant datasets at broad extents. Therefore, we developed and evaluated an approach that incorporates complex vegetation structure into statistical models for the robust prediction of microclimatic temperatures across the Great Smoky Mountains National Park (GSMNP). Using these models, we identified the factors influencing spatiotemporal patterns in microclimatic temperature. Previous studies have shown that canopy cover buffers microclimatic temperatures (Chen and Franklin 1997; Geiger et al. 2009; Davis et al. 2018); we predicted a priori that understory vegetation layers would also be important buffers of microclimatic temperatures. Additionally, we identified vegetation and physiographic factors contributing to spatiotemporal mismatches between free-air, macroclimatic temperature models and sub-canopy, microclimatic temperature predictions.

Materials and methods

Study area

This study was conducted in Great Smoky Mountains National Park and included a 150-meter buffer of the park boundary for a total area of 2430 km2 (Fig. 2.1). Situated along the North Carolina (NC) and Tennessee (TN) border, GSMNP ranges in elevation from

approximately 267 to 2025 m above sea level (Fig. 2.1) and is one of the most ecologically diverse areas in the U.S. Deciduous forests cover approximately 80% of the park extent, with the distributions of the five major forest types (Cove Hardwood, Northern Hardwood, Pine-and-Oak, Hemlock, and Spruce-fir) greatly influenced by elevation, topography, and moisture gradients (Whittaker 1956). The structural characteristics of these differing plant communities, along with topographic heterogeneity, contribute to fine-scale variations in microclimatic temperatures.

Temperature data collection

Our goal was to model daily MaxT and MinT during the months of March through November to capture microclimatic variation during the growing season. We obtained daily MinT and MaxT measurements from 159 climate dataloggers deployed from 2006 to 2010 by Fridley (2009). Climate dataloggers (iButton and HOBO H8 loggers) were placed 1 m above the forest floor and recorded temperature in 2-h intervals. Approximately 120 dataloggers were initially set up in two focal watersheds in central GSMNP. Both watersheds, roughly 50 km2 in area, were chosen for their extensive coverage of overall aspect and elevational gradient. Dataloggers were typically deployed in transects of 10 with each logger spaced 50–500 m apart, starting at stream channels and moving upslope to the top of the ridge. Another 50 dataloggers were distributed parkwide in clusters of three, stratified by elevation and region of the park (Fridley 2009). To obtain regional, free-air temperatures, we downloaded daily MaxT and MinT measurements recorded at 11 local weather stations from 2006 to 2010 from the National Oceanic and Atmospheric Administration's National Climate Data Center (Fig. 2.1).

Characterizing vegetation structure and landscape physiography

To determine which biophysical features impact near-surface temperature, we characterized vegetation structure and landscape physiography with light detection-and-ranging (LiDAR) and Geographic Information Systems (GIS) data. For the TN side of GSMNP, we obtained airborne LiDAR data collected in 2011 and processed by The Center for Remote Sensing and Mapping Science at the University of Georgia and Photo Science, Inc. (Fig. 2.1; Jordan 2011). For the NC side of GSMNP, we downloaded NC phase 3, airborne LiDAR data collected and processed by the North Carolina Floodplain and Mapping Program (OCM Partners 2019).

Filtered LiDAR data points were categorized into ground, unassigned, and noise points (i.e., points unlikely to be vegetation). Unassigned points were used to estimate vegetation height (VH) at the top of the canopy, and vegetation structure (VS) per raster pixel. To estimate VS across multiple strata, we grouped the unassigned points into five height classes: low-understory = VS < 5 m; high-understory = VS ≥ 5 m to 10 m; low-canopy = VS ≥ 10 m to 15 m; mid-canopy = VS ≥ 15 m to 20 m; and high-canopy = VS ≥ 20 m. We divided the number of unassigned points per VS layer by the total number of unassigned points producing the percentage of vegetation within each stratum across every pixel of the study area raster (GRASS Development Team 2017).

To characterize landscape physiographic variables, we calculated slope, aspect, solar insolation, topographic convergence index (TCI), and distance-to-stream for each pixel of the 3 m2 digital elevation model (DEM). Topographic convergence index was used as a proxy for cold-air-drainage and soil moisture based on site water potential (Beven and Kirkby 1979). Spatial datasets were modeled using LAStools—efficient LiDAR processing software (version

160721, unlicensed), ArcGIS® software versions 10.4.1–10.6.1 by Esri Inc. (2020), and GRASS GIS version 7.2.0. Further details about modeling vegetation structure and landscape physiography are provided in Appendix A.

Statistical downscaling

To account for the influence of elevation on temperature, we modeled daily lapse rates (i.e., the rate at which temperature changes with elevation) of MinT and MaxT with simple linear models as a function of elevation using temperature measurements from the 11 weather stations, which range in elevation from 338 to 1979 m (Fig. 2.1). The elevational lapse rates produced from regional weather station measurements were used to downscale temperature to a 3 m2 DEM to produce a level one (L1) model. To estimate sub-canopy, near-surface temperatures based on biophysical variables, we fit linear mixed-effects (LME) models to daily MaxT and MinT data from the climate dataloggers as a function of the L1 model temperature predictions, vegetation structure, and landscape physiographic variables. Daily temperature predictions from the L1 model were treated as fixed effects in all candidate models because of the strong effect elevation has on temperature variation. The VS and landscape physiographic variables were included as additive fixed effects in candidate models (Appendix A Fig. A.1). We examined the correlation and covariance among vegetation layers. Vegetation height was strongly correlated with high-canopy VS ($r = 0.70$), so we excluded high-canopy VS to avoid collinearity. To investigate potential interactive effects, we included terms representing the interaction of vegetation characteristics with solar insolation, distance-to-stream, and TCI. Distance-to-stream values were log transformed to address the decreasing effect of stream proximity on temperature with distance (Lookingbill 2002). To account for potential non-independence of the residuals, we

treated datalogger locations as a random effect. Temporal autocorrelation of residuals was addressed by including a term that models temporal correlation as an exponential decay and allows for unequally spaced observations ("corCAR1" function in the "nlme" package of R; Singer and Willett 2003).

Models were fit using maximum likelihood estimation and candidate models were ranked using Akaike's Information Criterion (AIC) within an information theoretic approach (Burnham and Anderson 2002). We initially tested a global model including all terms and a null model including only the L1 model predictions. We then used a top-down method for model selection, retaining each candidate model within a 95% confidence set (i.e., cumulative Akaike's weight ≤ 0.95; Zuur et al. 2009). To validate the top ranked models, we randomly split the data into 70% training data for model fitting and used the remaining 30% as testing data for evaluation. We measured goodness-of-fit for each model using the coefficient of determination (R2). We report marginal R2, which reflects only the fixed effects, and conditional R2 which includes both the fixed and random effects of the LME models. Our aim was to maximize predictive accuracy, so we calculated mean absolute error (MAE) for each candidate model, selecting the model with the lowest MAE. Final selected models for MaxT and MinT were re-fit using restricted maximum likelihood to obtain parameter estimates (Zuur et al. 2009), which were used to predict MaxT and MinT for each 3 m2 pixel of the study area raster. We also estimated the parameters of the final models after independent variables were scaled and centered (mean = 0, standard deviation = 1) to enable direct comparisons of effect sizes. Statistical modeling was performed using R v. 3.5.0 software and the "nlme" library (R Core Team 2020; Pinheiro et al. 202006). Further details on statistical modeling and candidate models are in the Appendix A.

Free-air climate comparisons

To determine the spatiotemporal mismatch between free-air and microclimatic temperature, we obtained gridded, free-air temperature data from two widely-used climate models, Daymet (Thornton et al. 2018) at 1 km2 spatial resolution and Parameter–Elevation Regressions on Independent Slopes Model (PRISM; Daly et al. 1994) at 4 km2 spatial resolution. Daily MaxT and MinT were extracted from each of these datasets at each datalogger location to compare MAE to the LME model predictions. We also downloaded monthly temperature rasters (i.e., average monthly temperature per raster cell) to evaluate temperature mismatch at the monthly and seasonal time scale across the entire study extent of GSMNP. Temperature mismatch was quantified by calculating temperature differences (absolute and real values) for 5000 randomly selected points from across the study area, which equated to temperature predictions from the L1, Daymet or PRISM raster models less the temperature predictions from the final LME model. We also extracted landscape physiographic and VS variables at each point location and calculated Pearson correlation coefficients with temperature differences to quantify the covariance between biophysical factors and spatiotemporal mismatch. Further information on methods can be found in Appendix A. The datasets generated during and/or analyzed during the current study are available in the Illinois Data Bank, University of Illinois at Urbana-Champaign, https://doi.org/10.13012/B2IDB-0897344_V1.

Results

LME model results and accuracy

Across 159 climate dataloggers measuring near-surface temperatures, we obtained 123,945 daily temperature measurements from 2006 to 2010 for the months of March-

November. Daily datalogger measurements ranged from 0.4 to 35.1 °C ($\bar{x}$ = 17.4 °C) for MaxT and − 10.1 to 26.0 °C ($\bar{x}$ = 9.8 °C) for MinT. Variation in daily MaxT and MinT were analyzed as a function of the variables summarized in Table 2.1. Temperature predictions from the LME models were highly correlated to datalogger measurements for daily MaxT (r = 0.90) and MinT (Appendix A Fig. A.2; r = 0.95). The MaxT LME model (marginal R2 = 0.77, conditional R2 = 0.81) had an overall mean absolute error (MAE) of 2.1 °C. This was an increase in accuracy of 2.8 °C, 1.2 °C, and 2.1 °C compared to the L1 model, Daymet, and PRISM datasets, respectively (Fig. 2.2; L1 model R2 = 0.73, MAE = 4.9 °C; Daymet MAE = 3.3 °C; PRISM MAE = 4.2 °C). The three free-air datasets consistently overestimated MaxT throughout the study period (Fig. 2.2). Goodness of fit measures were better for MinT, but the MinT LME model (marginal R2 = 0.90, conditional R2 = 0.92) minimally outperformed the L1 MinT model (Table 2.1; Fig. 2.2; R2 = 0.88). The MinT LME model had an overall MAE of 1.6 °C, an increase in accuracy of only 0.08 °C compared to the L1 model (MAE = 1.6 °C) and increased accuracy of approximately 0.9 °C and 1.8 °C compared to the Daymet and PRISM datasets, respectively (Daymet MAE = 2.5 °C; PRISM MAE = 3.4 °C). Daymet and PRISM MinT predictions consistently underestimated MinT throughout the study period (Fig. 2.2).

For MaxT, the LME model was most accurate in the summer (MAE = 1.3 °C) with greater errors in spring (MAE = 2.9 °C) and fall (MAE = 2.0 °C). This temporal pattern of accuracy was synchronous with vegetation growth as indicated by the normalized difference vegetation index (Fig. 2.2b; Norman et al. 2017). The L1 model was asynchronous with vegetation growth, and overestimated MaxT by as much as 5.5 °C above datalogger temperatures in summer (Fig. 2.2). For MinT, patterns in temporal accuracy were similar for the LME and L1

models, both with lower MAEs in summer (LME = 1.4 °C; L1 = 1.3 °C) as compared to spring (LME = 1.5 °C; L1 = 1.6 °C) and fall (LME = 1.9 °C; L1 = 2.0 °C).

Effects of vegetation structure and landscape physiography on temperature

Temperature predictions from the L1 model explained the most variation in MaxT and MinT in the final LME models (Table 2.1; Fig. 2.3; ΔMaxT = 0.8 °C and ΔMinT = 0.7 °C with 1.0 °C from L1 model temperature prediction). This was expected due to strong influence of elevation on temperature in montane systems; patterns in the spatial distribution of error were visibly similar to elevational variation (Fig. 2.4). However, vegetation structure also had significant effects on microclimatic temperatures (Table 2.1; Figs. 2.3, 2.4). Across the study area, mean vegetation height (VH) was 20.2 m ± 9.2 (SD) and vegetation structure (VS) was characterized by higher density in the low-understory ($\bar{x}$ = 20.4% ± 17.4%), followed by the high-understory ($\bar{x}$ = 16.7% ± 14.2%), mid-canopy ($\bar{x}$ = 16.4% ± 12.3%), and low-canopy ($\bar{x}$ = 15.0% ± 12.1%). The vegetation layers were weakly correlated and we found no evidence of covariance (Appendix A Table A.1). Among these vegetation characteristics, variation in MaxT was best explained by the buffering effects of low-understory and low-canopy VS (Table 2.1; Figs. 2.3, 2.4). In both cases, MaxT decreased with VS in each stratum (ΔMaxT = − 0.3 °C and − 0.8 °C with 10% increase in VS, respectively). On average, areas with dense low-understory VS (≥ 75th percentile, 33.3%) were 2.2 °C cooler than areas with sparse low-understory VS for MaxT (Figs. 2.4, 2.5; ≤ 25th percentile, 9.5%). Areas with dense low-understory VS and low-canopy VS (≥ 75th percentile, 22.7%) were 3.4 °C cooler than areas with sparse low-understory VS and low-canopy VS for MaxT (Figs. 2.4, 2.5; ≤ 25th percentile, 8.5%). These buffering effects of MaxT were strongest during the summer (Fig. 2.5). Variation in MinT

was best explained by low-understory VS (ΔMinT = − 0.3 °C with 10% increase in VS); mid-canopy VS also had a slight positive or warming effect on MinT (Table 2.1; Fig. 2.3; ΔMinT = 0.1 °C with 10% increase in VS).

Compared to the other additive variables in the LME models, solar insolation best explained variation in MaxT and MinT (Table 2.1; Fig. 2.3). Although both MaxT and MinT increased with solar insolation (ΔMaxT = 0.4 °C and ΔMinT = 0.7 °C with 1000 Wh/m2/day−1), vegetation structure mediated these effects, with dense understories having the largest influence. At high solar insolation levels (≥ 75th percentile, 8143 Wh/m2/day−1), sites with dense low-understory VS (≥ 75th percentile, 33.3%) were 4.7 °C cooler than sites with sparse low-understory VS (≤ 25th percentile, 9.5%), indicating a large buffering effect during periods of increased solar insolation. At low solar insolation levels (≤ 25th percentile, 5516 Wh/m2/day−1) this buffering effect was present but minimized (ΔMaxT = − 2.0 °C). For MinT, sites with dense low-understory VS were 3.0 °C cooler than sites with sparse VS at high solar insolation levels, but only 1.4 °C cooler at low solar insolation levels. At high solar insolation levels, sites with dense mid-canopy VS (≥ 75th percentile, 25%) were, on average, 0.7 °C cooler than sites with sparse mid-canopy VS (≤ 25th percentile, 10.2%) for MinT; however, at low solar insolation levels, sites with dense mid-canopy VS were warmer (ΔMinT = 0.05 °C) than sites with sparse VS in this stratum.

Topographic convergence index and distance-to-stream had smaller effects on MaxT and MinT variation (Table 2.1; Fig. 2.3; TCI ΔMaxT = − 0.4 °C and ΔMinT = − 0.0 4 °C with TCI; distance-to-stream ΔMaxT = − 0.00094 °C and ΔMinT = 0.00162 °C with a 1% increase in distance). At high TCI levels (≥ 75th percentile, TCI = 5.7) MaxT averaged 0.8 °C cooler compared to areas with low TCI levels (Fig. 2.5; ≤ 25th percentile, TCI = 3). This cooling effect

from TCI was slightly increased in areas with dense low-canopy VS, especially during summer (Fig. 2.5; ΔMaxT = 0.9 °C on average, 1.2 °C in summer).

Spatiotemporal patterns of mismatch between microclimatic and free-air temperatures

The magnitude of mismatch between the MaxT predictions of the LME model and the predictions of the free-air temperature datasets covaried with landscape physiography; magnitudes were largest for elevation and solar insolation (Fig. 2.6; Appendix A Fig. A.7, A.8, A.9). For the L1 model, mismatch was consistently greater at lower elevations, ranging in monthly correlation from − 0.29 to − 0.69 (Figs. 2.4, 2.6ab, 2.7a). For the two coarse-grain datasets, elevation was more strongly correlated to mismatch with the 4 km2 PRISM dataset (monthly range in r = − 0.42 to 0.52) compared to the 1 km2 Daymet dataset (Fig. 2.6ab; monthly range in r = − 0.34 to 0.34). The PRISM dataset had greater mismatch at higher elevations during summer and lower elevations during spring and fall; however, the Daymet dataset showed the opposite temporal trend with elevation (Fig. 2.6ab). The PRISM dataset also exhibited seasonal and elevational trends in over- and underestimation of MaxT as compared to the LME model predictions, overestimating MaxT at the highest elevations during spring (≥ 90th percentile, 1458 m) but underestimating MaxT at the lowest elevations during summer (Fig. 2.7b; < 285 m). For all three free-air datasets, solar insolation covaried more strongly with mismatch during the spring and fall, with limited or no correlation during summer (Fig. 2.6b). For the L1 model, mismatch was negatively correlated to solar insolation during early spring months of March and April (monthly range in r = − 0.14 to − 0.36) and fall months of September–November (monthly range in r = − 0.49 to -0.61). The largest Daymet and PRISM mismatches were positively correlated to solar insolation during March (Daymet r = 0.49;

PRISM r = 0.38) and November (Daymet r = 0.42; PRISM r = 0.46), with smaller correlation magnitudes during the other months in spring and fall (Fig. 2.6b).

For MinT, mismatch was consistently greater at higher elevations for the L1 model (monthly range in r = 0.21 to 0.75) and Daymet dataset (monthly range in r = 0.30 to 0.68) across the entire study period, with higher magnitudes occurring in early spring and summer (Fig. 2.6a; L1 model monthly range in r = 0.68 to 0.75; Daymet monthly range in r = 0.54 to 0.68). In contrast, mismatches in MinT based on PRISM data were not well correlated with elevation (monthly range in r = − 0.23 to 0.01). Mismatches between MinT predictions from the LME model with the three free-air datasets showed similar temporal patterns of strong, positive correlations to solar insolation during spring (L1 model monthly range in r = 0.54 to 0.88; Daymet monthly range in r = 0.34 to 0.78; PRISM monthly range in r = 0.29 to 0.80) and fall (L1 monthly range in r = − 0.39 to 0.91; Daymet monthly range in r = 0.66 to 0.81; PRISM monthly range in r = 0.68 to 0.84), but low to moderate correlations during summer (Fig. 2.6b; L1 monthly range in r = − 0.02 to 0.45; Daymet monthly range in r = 0.26 to 0.45; PRISM monthly range in r = 0.22 to 0.46).

Discussion

It is well established that elevation is a primary factor affecting temperature in montane landscapes (Geiger et al. 2009; Vanwalleghem and Meentemeyer 2009), but other climate-forcing factors, such as solar insolation and cold-air-drainage, contribute to microclimatic variation in forests (Chen et al. 1999; Geiger et al. 2009; Ashcroft and Gollan 2012). However, the underlying biophysical processes that affect microclimatic regimes are not well understood, and climate models typically disregard complex vegetation structure (Lefsky et al. 2002), either

not accounting for vegetation or using simplified canopy characteristics (Jennings et al. 1999; Wilson 2011). We characterized vegetation structure across multiple levels and incorporated this information into statistical models to examine the influence of complex vegetation characteristics and landscape physiography on microclimatic temperature variation. Our results indicate that vegetation structure in multiple strata contribute to microclimatic buffering, and the inclusion of complex vegetation structure improves the accuracy of microclimatic temperature models (Table 2.1; Figs. 2.2, 2.3).

Numerous studies have demonstrated the importance of forest canopies in buffering microclimatic temperatures, reducing sub-canopy MaxT and increasing sub-canopy MinT (Chen and Franklin 1997; Bramer et al. 2018; De Frenne et al. 2019). Our results are consistent with these findings, but we also find that understory vegetation structure contributes to microclimatic buffering, substantially cooling near-surface temperatures and increasing the accuracy of microclimatic temperature predictions, especially for MaxT during the growing season (Table 2.1; Figs. 2.2b, 2.4, 2.5). Canopy cover reduces solar radiation levels in the understory of deciduous forests (Hicks and Chabot 1985; Chazdon 1988), but a substantial fraction of direct and diffuse (i.e., from atmospheric scattering) radiation penetrates the canopy (Detlef 1977; Jones 2014). Understory plants can use this remaining radiation for growth (Chazdon 1988), resulting in dense vegetation below forest canopies or understory plants can use direct radiation for growth within canopy gaps and in areas where canopy and understory do not co-occur (Washitani and Tang 1991; Koizumi and Oshima 1993). Consequently, understory vegetation may be the only buffer against solar radiation within canopy gaps or an important additional buffer against solar radiation below the canopy.

Although understory vegetation structure is seldom incorporated into microclimate models, previous empirical studies accounting for the presence of understory vegetation suggest its strong buffering effects. For instance, Clinton (2003) found that the presence of rhododendron (Rhododendron maximum), an important evergreen shrub typically growing within 8 m of the forest floor, moderated temperatures and lowered minimum, maximum, and mean soil temperatures in a North Carolina watershed near GSMNP (Clinton 2003). Similarly, understory vegetation characteristics influenced temperature variability during spring and summer in an old-growth forest located within the Cascade Mountains of central Oregon (Frey et al. 2016). Our results reinforce these findings at a substantially finer spatial resolution and with more complex vegetation analyses.

Our results also demonstrate that biophysical interactions can affect microclimate at a very fine scale. We found that vegetation structure moderates the magnitude and direction of solar insolation and topographic convergence index (TCI), altering microclimatic temperatures. Microclimatic buffering associated with vegetation structure was greatest at solar insolation extremes, cooling MaxT at high solar insolation levels and warming MinT at low solar insolation levels. These results are consistent with the finding that insulating effects from vegetation are greatest during temperature extremes (Davis et al. 2018). We also found that higher levels of moisture, based on TCI, reduce microclimatic temperatures, and this cooling effect is amplified in areas with dense canopy vegetation structure (Fig. 2.5). Soil moisture levels can reduce localized temperature by transforming energy into latent heat as opposed to sensible heat (Dai and Trenberth 1999), and it has been shown that microclimatic temperature buffering can vary with local water balance in forests of the western US (Davis et al. 2018). Our results also suggest

variation in microclimatic buffering due to plant-water interactions, even in the humid environment of the Great Smoky Mountains.

Collectively, our findings indicate that a failure to consider sub-canopy vegetation layers, and the moderating effects of vegetation on solar radiation and localized moisture, can limit the accuracy of microclimatic temperature models in montane, forested landscapes. Although our models improved the accuracy of microclimatic temperature predictions, there were limitations. For instance, we used TCI as a proxy for soil moisture because of the limited availability of soil moisture data, but in situ soil moisture measurements could bolster microclimate predictions (Lenoir et al. 2017). It has also been shown that atmospheric demand for water may be more important than soil moisture in limiting surface conductance and evapotranspiration (Novick et al. 2016), but we did not incorporate these data into our study because they are currently unavailable at high spatiotemporal resolution. Integrating high resolution soil moisture data and models for evaporative demand, such as vapor pressure deficit, with complex vegetation structure data is critically needed to better understand the mechanisms underpinning the biophysical effects on microclimatic variation.

Although complex vegetation data have typically been unavailable at broad spatial extents, the increasing availability of LiDAR (Lefsky et al. 2002; Zellweger et al. 2019b) means that there is potential for characterizing vegetation structure across multiple levels over large extents. In this study, we show the potential importance of understory vegetation structure for microclimate prediction, but we were limited to using leaf-off, airborne LiDAR data from two separate datasets. LiDAR with increased point density, or via waveform laser scanning, could create more accurate representations of vegetation at finer strata. Also, LiDAR data collected during leaf-on periods at finer temporal scales could enhance predictions of microclimatic

variation during vegetation growth and senescence, increasing accuracy of microclimate models during the growing season.

Accurately predicting microclimate is crucial for bridging the gap between coarse-grain, free-air climate layers and actual microclimatic conditions experienced by most organisms (Suggitt et al. 2011; Hannah et al. 2014; Lembrechts et al. 2018). Most currently available or obtainable climate data are missing relevant climate-forcing factors to accurately portray microclimatic regimes or are too coarse in scale to detect the fine variations in microclimate across complex landscapes (Randin et al. 2009; Elsen and Tingley 2015; Meineri and Hylander 2017). Our comparison of microclimatic temperature predictions with two coarse-grain climate datasets highlights these problems. Both datasets were found to have large error, but the PRISM dataset (4 km2 spatial resolution) was less accurate than the Daymet dataset (1 km2 spatial resolution), typically overestimating MaxT and underestimating MinT (Fig. 2.2). Here, we show error potentially associated with the spatial scale of these two widely-used datasets, but it is important to note that there are datasets available at higher spatial resolution which would likely have smaller error. Nevertheless, for MaxT, we found that the mismatch between microclimate and PRISM predictions was strongly correlated with elevation with a clear trend of temporally over- or underestimating MaxT in areas of increased topographic heterogeneity (Fig. 2.7b). The covariation of solar insolation with mismatches between free-air and microclimatic temperatures was, at least partially, due to the lack of solar insolation as a climate-forcing factor in the free-air temperature models. Temperature increases with solar radiation, but the free-air temperature datasets (L1, Daymet, and PRISM) did not indicate this known relationship (Fig. 2.7c). In contrast, MaxT predictions from the LME model were positively correlated with solar insolation during spring and fall, with a moderated effect during the summer months due to microclimatic

buffering of vegetation structure and TCI (Fig. 2.7c). These seasonal trends coincide with the covariation of solar insolation to temperature mismatches, suggesting that the inclusion of solar insolation in the LME models contributed to increased temperature mismatches for the free-air datasets in spring and fall (Fig. 2.6b). Taken together, we speculate that the direction and magnitude of mismatch between free-air and microclimatic temperature is dependent not only on spatial scale but also the relevant climate-forcing factors used in climate modeling, which can contribute to spatiotemporal inaccuracies (Fig. 2.6; Appendix A Fig. A.7, A.8, A.9).

There has been a call to integrate the appropriate climate-forcing factors and improved canopy cover estimates into climate models at relevant biological scales (Ashcroft et al. 2008; Kearney and Porter 2009; Ashcroft and Gollan 2012) to better understand how species may respond to climate change (Lenoir et al. 2017; Lembrechts et al. 2018). Species distribution models (SDMs) are potentially over- and underestimating suitable habitat at differing scales (Trivedi 2008; Gillingham 2012a, b; Franklin 2013; Lenoir et al. 2017), and temporally inaccurate climate data may cause the misdetection of suitable habitat as well. The use of accurate microclimate data for SDMs may be of particular importance for species that rely on microclimatic conditions, such as small, ectothermic, dispersal-limited, or ground-dwelling species (Kearney and Porter 2009; Helmuth et al. 2010). Our results suggest that the use of coarse-grain, free-air temperature models would result in overpredictions of MaxT and underpredictions of MinT with considerable spatiotemporal inaccuracy, problems that could greatly distort estimates of habitat suitability and connectivity for species that may be most vulnerable to climate change.

Here, we improved accuracy of microclimatic temperatures (3 m2 raster) over a broad extent (2430 km2 study area), helping to avoid the potential pitfalls that come with free-air,

coarse-grain predictions and demonstrating the plausibility of developing essential microclimate inputs for SDMs (Lembrechts et al. 2018). Accurately predicting microclimate across broad extents can help to identify potentially suitable habitat for a wide range of taxa, but is especially significant for evaluating rare or declining species. Such fine-scale maps of suitable habitat may provide the relevant detail for discovering new populations, targeting potential areas for species reintroductions, and locating potential climate change microrefugia.

In conclusion, we show that different vegetation structure layers and their interactions with landscape physiographic patterns buffer microclimatic temperatures of temperate deciduous forests in the Great Smoky Mountains, resulting in considerable spatiotemporal variation across the landscape. Future attempts at modeling microclimate may benefit from including spatially and temporally finer vegetation structure models and coupling these data with satellite-derived classifications, such as NDVI or leaf area index. This combination could bolster predictions of canopy and understory vegetation structure, further increasing our understanding of the underlying biophysical processes that control forest microclimates and increasing accuracy in microclimate predictions. With the effects of climate change intensifying, the improvement of climate data at biologically relevant scales is a crucial step that can lead to better predictions in the future, greatly benefiting environmental managers charged with prioritizing conservation efforts.

Figures

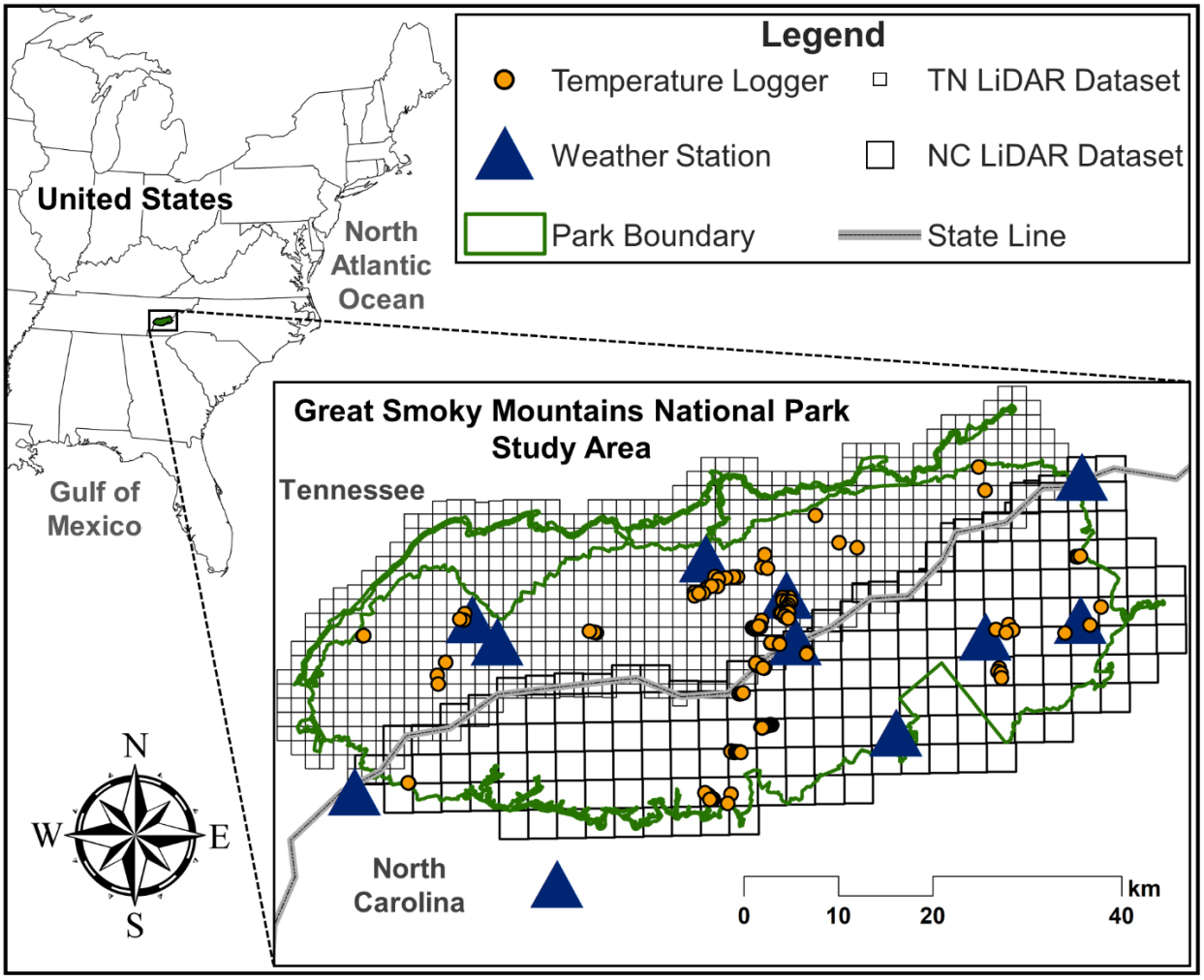

Figure 2.1 Location of Great Smoky Mountains National Park (GSMNP) study area on the border of North Carolina (NC) and Tennessee (TN), USA, in the southern Appalachian Mountains. The map shows the temperature dataloggers spread throughout the park (Fridley 2009), the locations of the 11 weather stations used for the level one model, the TN (1 km2 grids) and NC (2 km2 grid) LiDAR dataset boundaries, the GSMNP boundary, and the state line between NC and TN

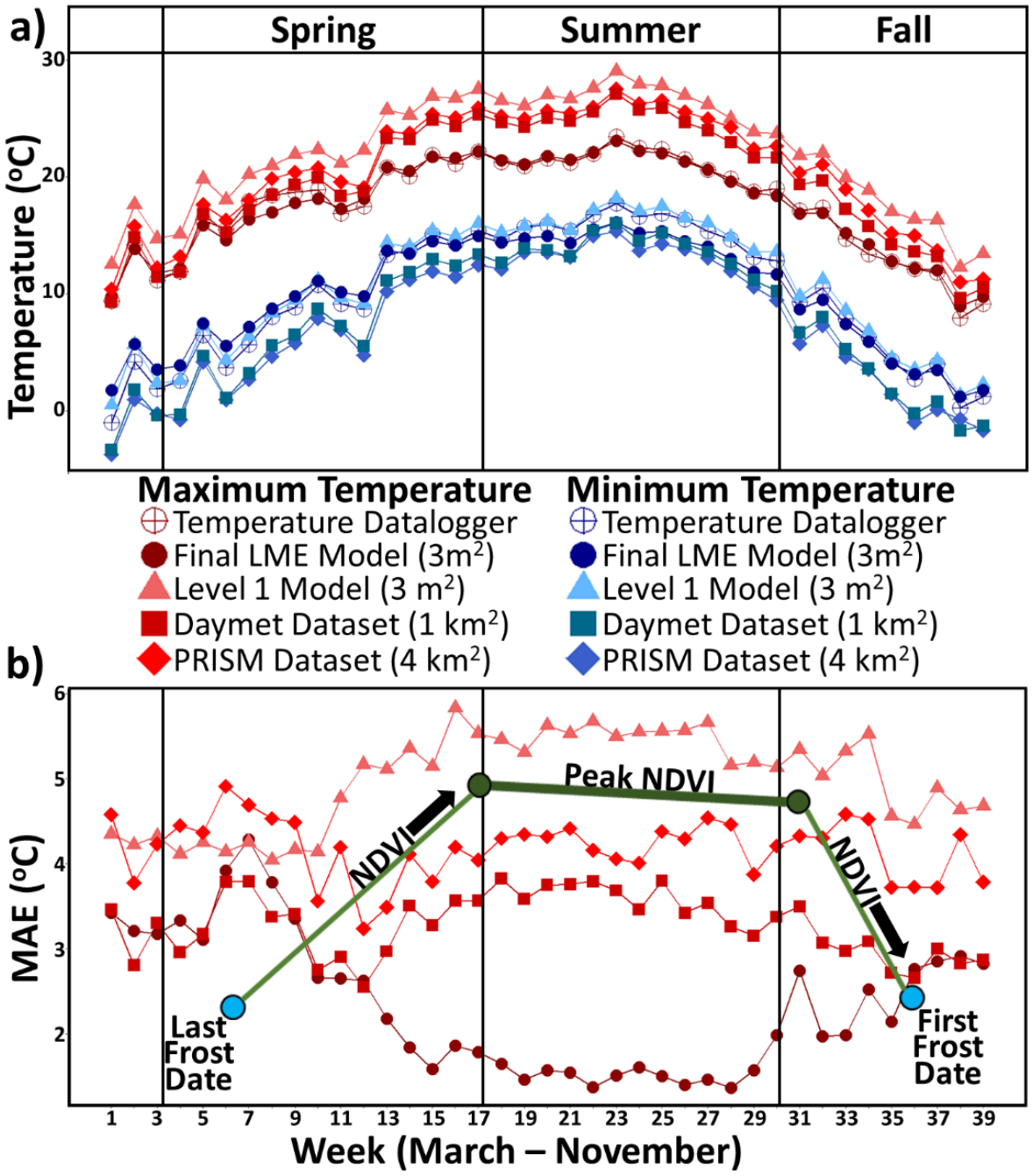

Figure 2.2 (a) Average weekly minimum and maximum temperatures (°C) from March–November of 2006–2010, including temperature averages from datalogger measurements, the final LME model predictions (3 m^2), the level one model predictions (3 m^2), the Daymet dataset (1 km2), and the PRISM dataset (4 km^2). (b) Weekly averaged mean absolute error (MAE in °C) for maximum temperature model predictions (Final LME Model, level one model, Daymet dataset, and PRISM dataset) from observed datalogger measurements. First and last frost date averaged from 2006 to 2010 and NDVI based on averages during time period (Norman et al. 2017). NDVI is overlaid on graph to show temporal synchrony with the final LME model predictions and asynchrony with the level one model predictions

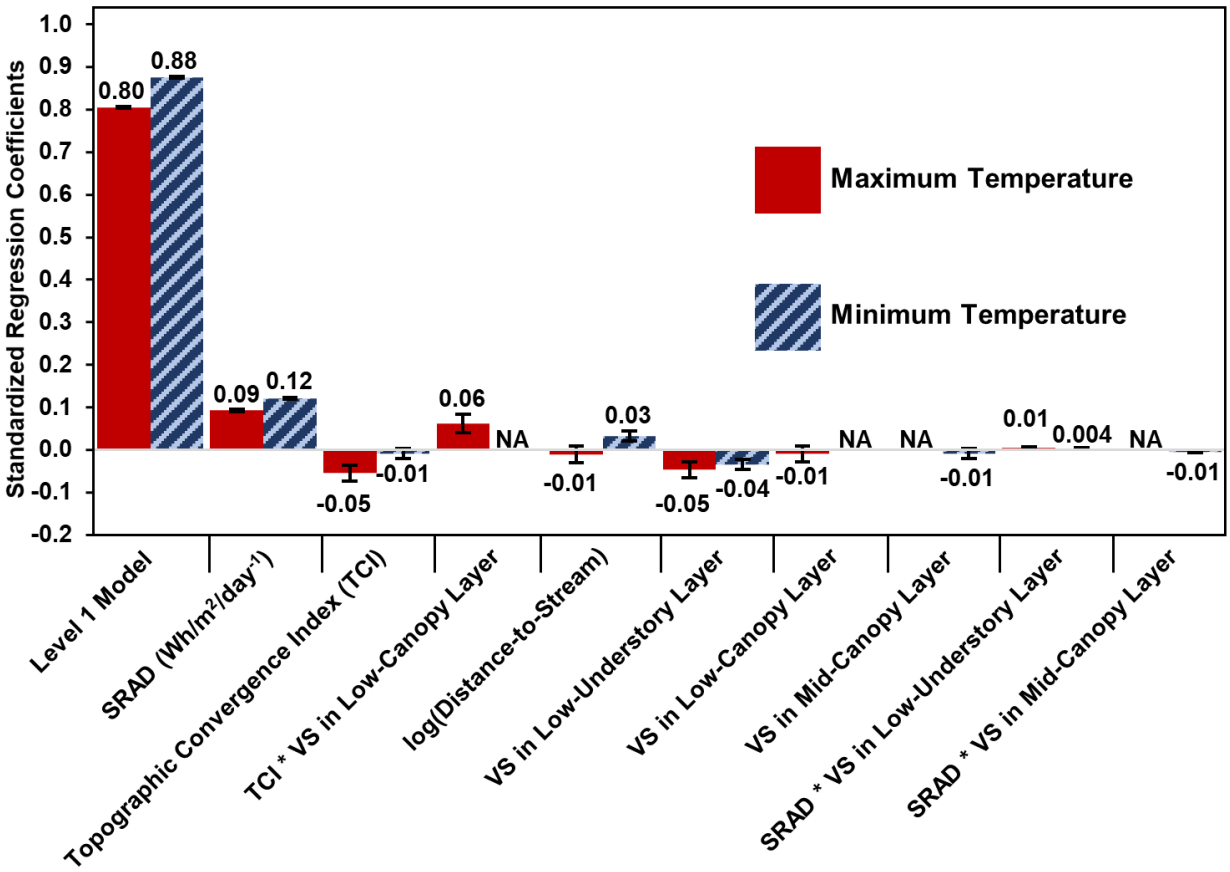

Figure 2.3 Variable importance based on standardized regression coefficients for the final AIC models for maximum (red) and minimum (blue stripes) temperature. Model summaries are in Table 2.1. TCI topographic convergence index, SRAD solar radiation (Wh/m2/day−1), VS vegetation structure

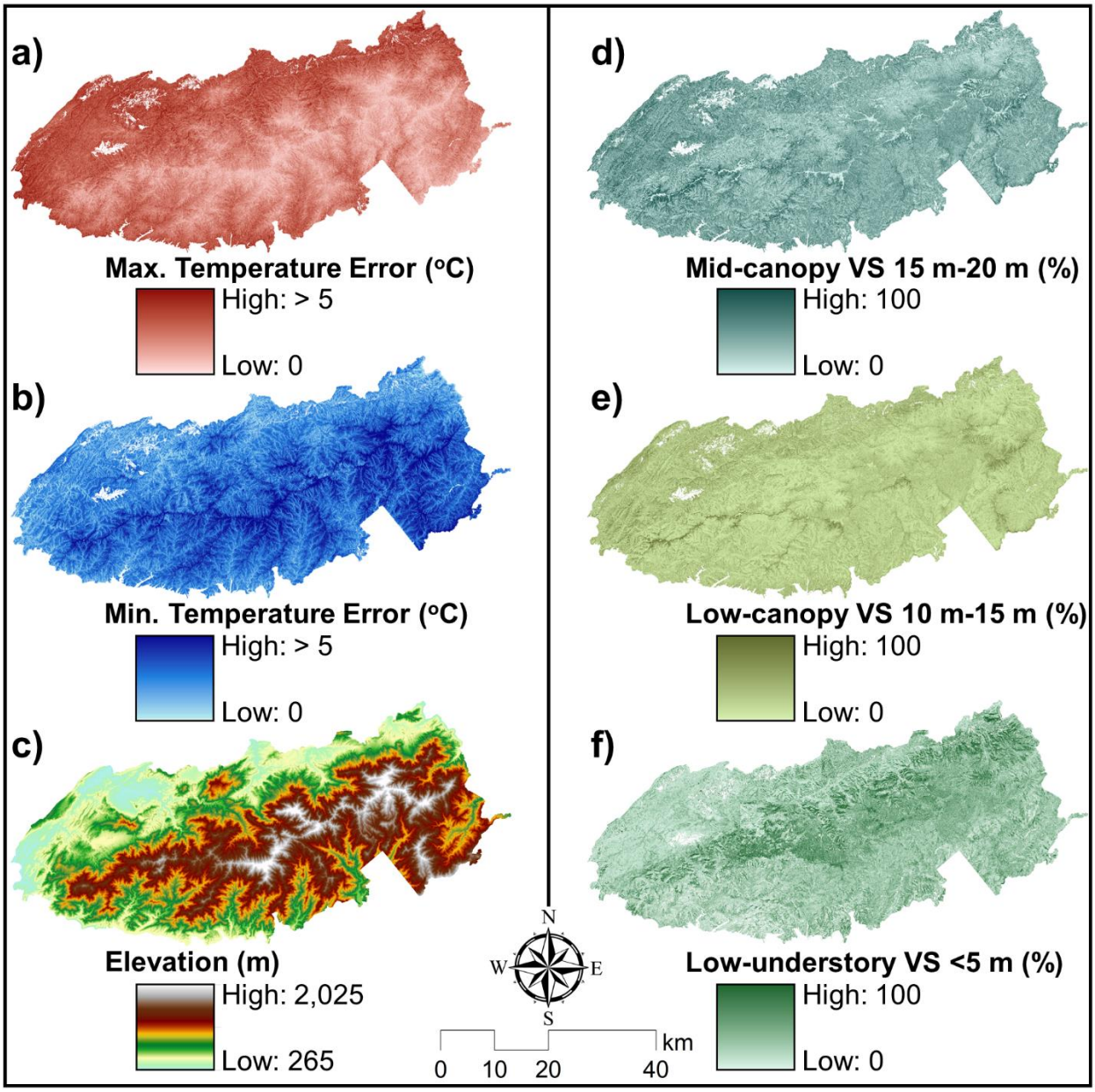

Figure 2.4 (a) Spatial distribution of model error for maximum temperature (°C) and (b) minimum temperature (°C). Model error is calculated as the difference between predictions from the final linear mixed-effects model and the level one model and averaged across study period. The darkest colors display error greater than 5 °C. (c) Elevation of Great Smoky Mountains National Park based on a 3 m digital elevation model. (d) Percentage of mid-canopy, (e)low-canopy, and (f) low-understory vegetation structure (VS)

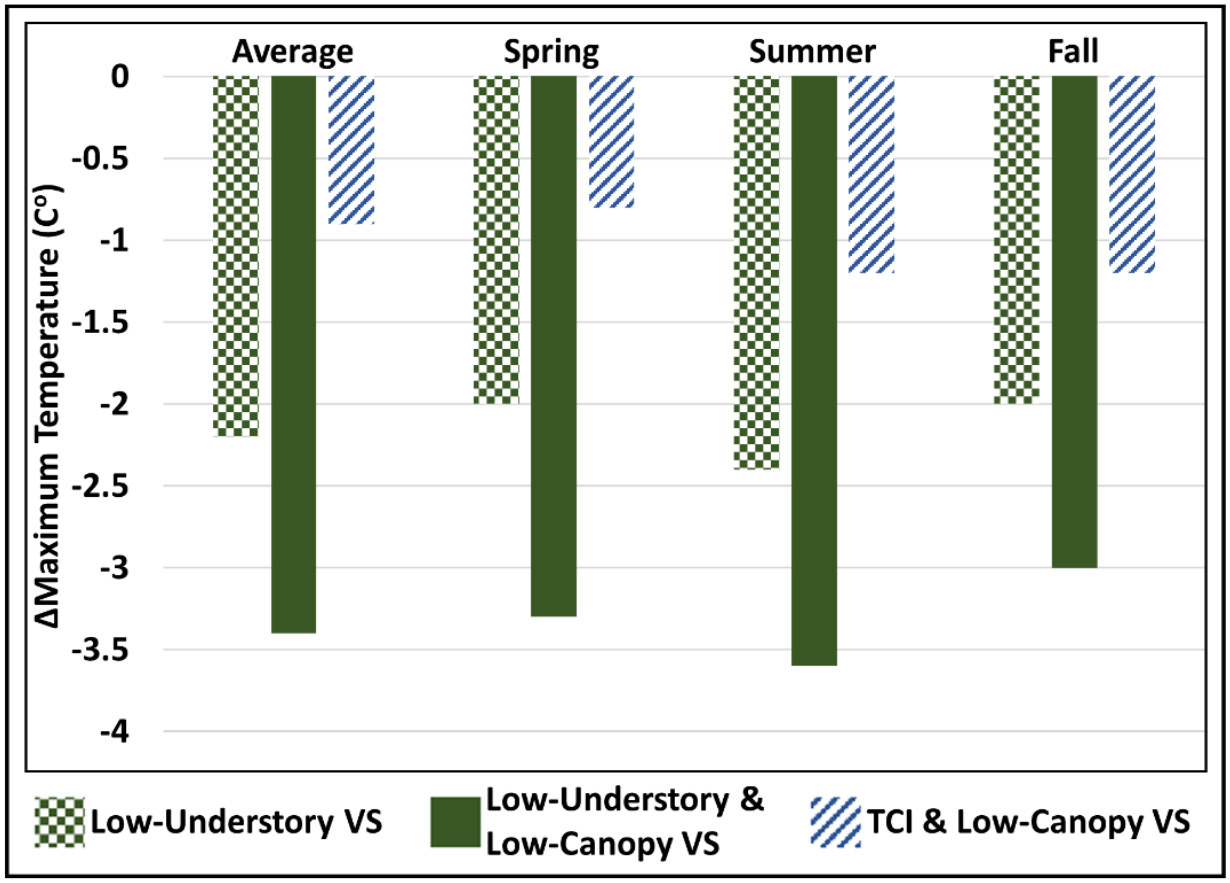

Figure 2.5 Magnitude of microclimatic buffering for maximum temperature (oC) by low-understory vegetation structure (VS), the combination of low-understory and low-canopy vegetation structure, and the combination of topographic convergence index (TCI) with low-canopy vegetation structure. Buffering magnitudes include the overall average for the entire study period and averages during spring, summer, and fall

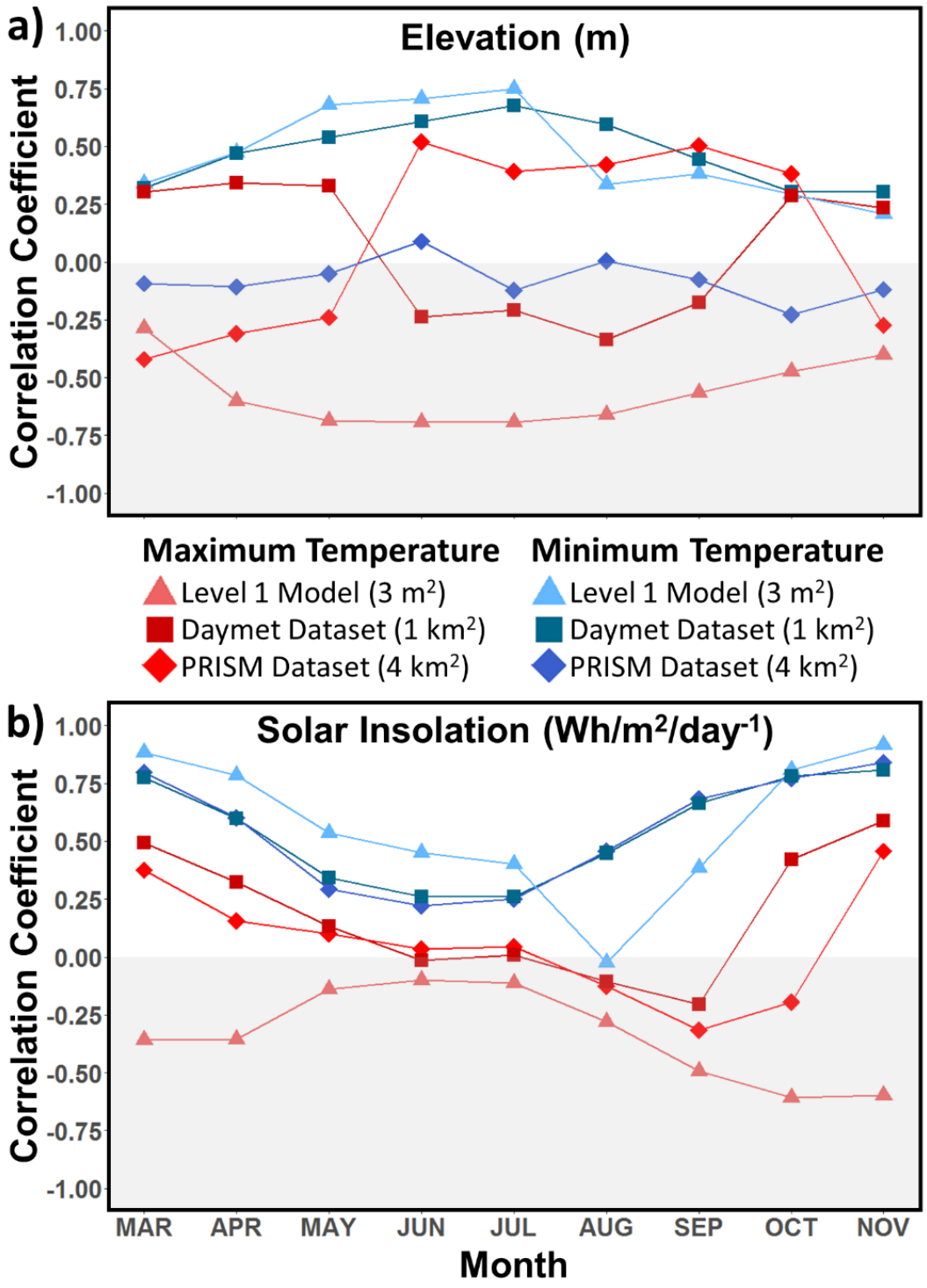

Figure 2.6 Monthly average correlation coefficients between temperature mismatch (absolute values from 2006 to 2010) and (a) elevation in meters and (b) solar insolation (Wh/m2/day−1). Temperature mismatch was calculated as the difference between free-air temperature estimates and microclimate predictions from the final LME models. Large positive or negative values for a given month indicate that the mismatch between microclimatic and free-air temperatures heavily covaried with the predictor variable

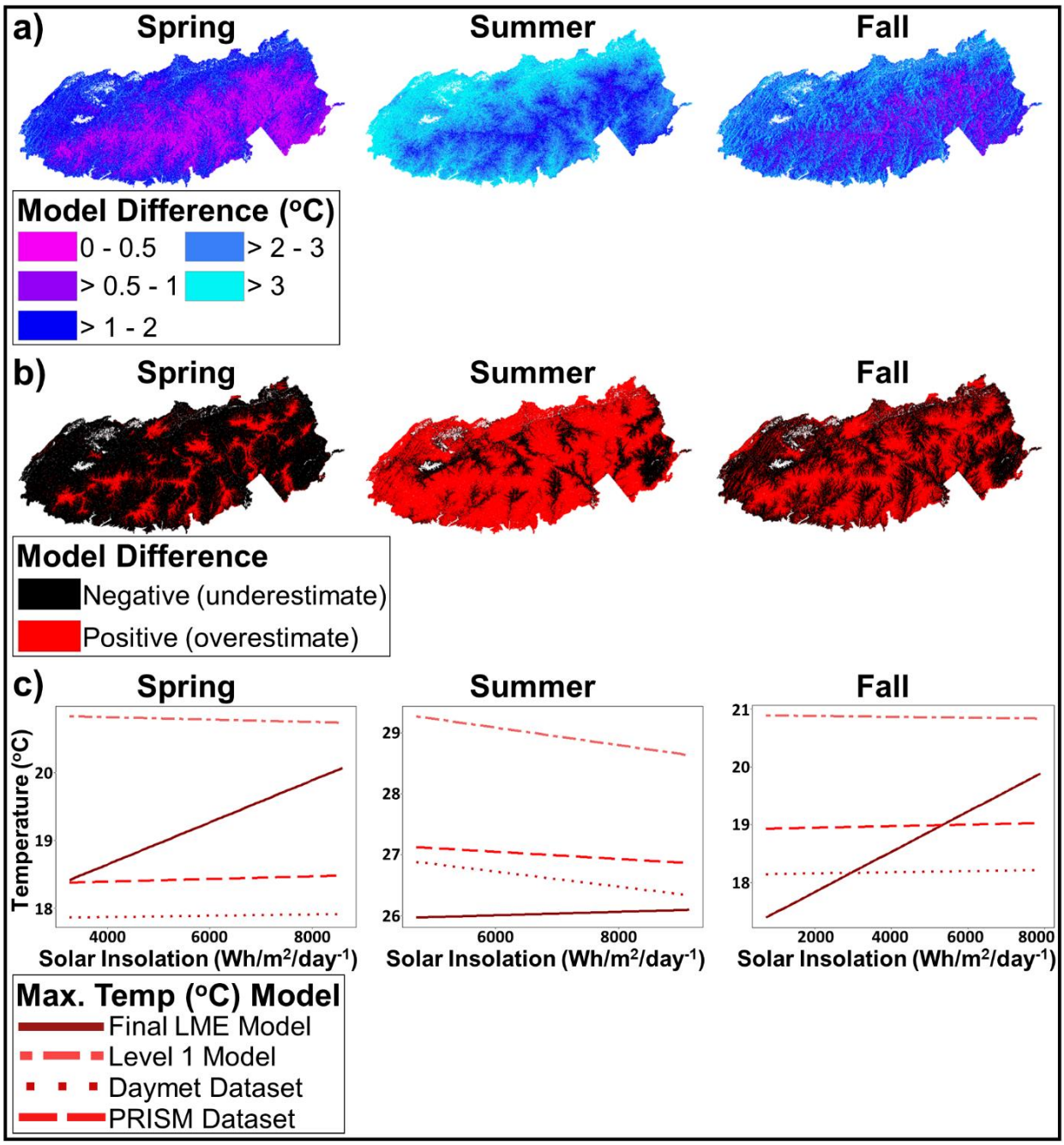

Figure 2.7 (a) Heat map showing the difference (absolute value) between predictions of average maximum temperature (°C) from the level one model and the final LME model for Spring, Summer, and Fall. (b) Heat map showing where the difference between PRISM estimates and predictions of the final LME model are either negative or positive, indicating that PRISM was underestimating or overestimating maximum temperature. c Final maximum temperature model predictions (°C) plotted against solar insolation (Wh/m2/day−1) using a smoothing function

Table

Table 2.1. Variable characteristics and model summaries for the final selected linear mixed-effects models. Daily minimum and maximum temperatures (°C) were modeled from March through November (2006–2010) using datalogger measurements as a function of the model variables shown here. The R^2 values shown are conditional and MAE is the mean absolute error between model predictions and datalogger observations. Also shown are variable names, units of measure, means and ranges of modeled data, final parameter estimates, the standard error of estimates (SE), degrees of freedom (df), *t*-values and *p*-values. The *p*-values shown (* *p*-value < 0.05, ** *p*-value < 0.01, and *** *p*-value < 0.001) were not used for model selection. Final model terms seen here were fit using restricted maximum likelihood. The level one model was a fixed effect and all other predictor variables were additive fixed effects. *TCI* topographic convergence index, *Solar* insolation, and *VS* vegetation structure.

Variable	Unit	Mean (Range)	Parameter estimate	SE	df	*t*-value	*p*-value
Minimum Temperature Model (MinT)							
Goodness of Fit: R^2 = 0.92 , MAE = 1.6							
(Intercept)	-		-2.2731135	0.5518857	124584	-4.12	***
Level 1 Model	°C	10.9 (-8.4 - 30.8)	0.7246783	0.0015900	124584	453.67	***
Solar Insolation	$Wh/m^2/day^{-1}$	6,709 (611 - 9,156)	0.0006632	0.0000211	124584	31.36	***
Distance-to-Stream	m	169 (0 - 483)	0.1627245	0.0848747	153	1.92	
Topographic Convergence Index	-	4.5 (0.8 - 20.2)	-0.0447740	0.0437462	153	-1.02	
Low-understory VS (below 5 m)	%	23.1 (0 - 100)	-0.0250879	0.0064067	153	-3.92	***
Mid-canopy VS (15 m-20 m)	%	18.1 (0 - 45)	0.0101210	0.0103495	153	0.98	
Low-understory VS*Solar	-	156,119 (0 - 902,712)	0.0000012	0.0000005	124584	2.40	*
Mid-canopy VS*Solar	-	118,714 (0 - 376,444)	-0.0000025	0.0000007	124584	-3.42	***
Maximum Temperature Model (MaxT)							
Goodness of Fit: R^2 = 0.81 , MAE = 2.4							
(Intercept)	-		1.3024726	0.7992080	124585	0.63	
Level 1 Model	°C	22.5 (4.6 - 41.0)	0.7541793	0.0023310	124585	323.55	***

Table 2.1. continued

Solar Insolation	$Wh/m^2/day^{-1}$	6,709 (611 - 9,156)	0.0003590	0.0000148	124585	24.33	***
Distance-to-Stream	m	169 (0 - 483)	-0.0941063	0.1144836	152	-0.82	
Topographic Convergence Index	-	4.2 (0 - 30.3)	-0.4351026	0.1130898	152	-3.85	***
Low-understory VS (below 5m)	%	23.1 (0 - 100)	-0.0273063	0.0080448	152	-3.39	***
Low-canopy VS (10 m-15 m)	%	16.1 (0 - 49.2)	-0.0826411	0.0271477	152	-3.04	**
Low-understory VS*Solar	-	156,119 (0 - 902,712)	0.0000012	0.0000005	124585	2.29	*
Low-canopy VS*TCI	-	23.1 (0 - 321.6)	0.0170228	0.0060343	152	2.82	**

CHAPTER 3: SPATIOTEMPORAL PATTERNS OF ENERGETIC MAINTENANCE COSTS ARE INCONSISTENT WITH SUITABLE CLIMATIC HABITAT FOR PLETHODONTID SALAMANDERS

Introduction

Species distribution models (SDMs) rely on a variety of correlative approaches for estimating species' distributional range limits and habitat suitability (Elith et al. 2006; Kearney and Porter 2009). Although widely used, SDMs have been criticized for rarely incorporating physiological responses at spatial and temporal scales that affect the performance and fitness of organisms (Kearney and Porter 2009; Barton and Terblanche 2014; Evans et al. 2015). Typically, SDMs are produced with coarse resolution climate data based on free-air temperature predictions and modeled at disproportionately broad scales compared to the microclimatic conditions that a myriad of organisms experience near the surface of the earth (Kearney and Porter 2009;Potter et al. 2013; Lenoir et al. 2017; Lembrechts et al. 2018). Furthermore, the bioclimatic inputs used in species distribution modeling may not account for climatic variability at proper temporal scales (Lembrechts et al. 2018). These spatiotemporal mismatches may simultaneously result in regional overestimations and local underestimations of suitable habitat (Trivedi et al. 2008; Gillingham et al. 2012a, b; Franklin et al. 2013). Leveraging microclimate datasets to address physiology at appropriate biological scales and to understand potential mismatches with SDMs is a priority, especially for small, ectothermic or dispersal limited species that are dependent upon climatic regimes at the microhabitat scale (Cushman 2006; Hoegh-Guldberg et al. 2008; Kearney and Porter 2009; Clusella-Trullas et al. 2011).

Salamanders in the family Plethodontidae are lungless ectotherms that require cool, moist microclimates to avoid water loss (Feder 1983; Lutterschmidt and Hutchison 1997; Bernardo and Spotila 2006). Temperature directly influences plethodontid salamanders by increasing

desiccation risk, increasing pathogens, decreasing available energy to catch prey, decreasing body size, altering reproductive cycles, and notably, increasing physiological stress (Feder and Pough 1975; Blaustein and Kiesecker 2002; Carey and Alexander 2003; Blaustein et al. 2010; Homyack et al. 2010, 2011). Higher temperatures and variability in climatic regimes alter the metabolic rate of plethodontids which in turn affects energy budgets (Pough 1980; Homyack et al. 2010). Changes in energy expenditure can intensify physiological stress, resulting in greater susceptibility to pathogenic infection and potentially creating ecological trade-offs that affect overall fitness (Sears 2005; DuRant et al. 2007). Because temperature affects the physiology, energy expenditure, performance and fitness of plethodontids, their distributional range limits and habitat suitability requirements are largely determined by climate, but climate is not the only factor that affects salamander energetics (Milanovich et al. 2010; Gifford and Kozak 2012).

Energetic demand increases with body size for plethodontids (Feder 1976), yet few studies simultaneously consider body mass and temperature in metabolic relationships (Petruzzi et al. 2006). Furthermore, some plethodontid species are high elevation specialists that have been shown to follow Bergmann's rule (Peterman et al. 2016), increasing in body size with the cooler temperatures that accompany elevational gain. However, these body size-elevation relationships have yet to be incorporated into physiological models, potentially disregarding an important driver of variation of energetic requirements across spatiotemporal scales. Accounting for biophysical processes at appropriate microclimatological scales may result in considerable spatiotemporal variation in salamander energetics and generate valuable information for improving predictions of habitat suitability.

Integrating physiological variation at microclimatic scales with commonly used approaches for modeling species' distributions is imperative for characterizing differences

between mechanistic and correlative models (Kearney and Porter 2009; Evans et al. 2015; Lembrechts et al. 2018). Comparing these different approaches can provide independent results that strengthen predictions in areas of agreement or provide insights on model disagreement, generating valuable information on spatiotemporal mismatches (Kearney and Porter 2009; Morin and Thuiller 2009). Here, we combined microclimate datasets that account for the buffering effects of forest vegetation structure with a physiological model predicting standard metabolic rate (SMR) to assess spatiotemporal patterns in the bioenergetics of three plethodontid salamander species in Great Smoky Mountains National Park (GSMNP; North Carolina and Tennessee, US). Because lower energetic demand suggest better performance for plethodontids (Feder and Pough 1975; Pough 1980; Sears 2005; DuRant et al. 2007), we evaluated the agreement between low SMR with predictions from SDMs. We also integrated body-mass elevation relationships into our physiological models using three plethodontid species of differing sizes, all of which have been shown to increase in body length at higher elevations (Peterman et al. 2016).

Materials and Methods

Study area and species

The study area consisted of the area within GSMNP plus a 150-meter buffer around the park boundary, for a total area of 2,430 km^2 (Fig. 3.1). Great Smoky Mountains National Park straddles the North Carolina and Tennessee border and ranges in elevation from ~265 to 2,025 m above sea level (Fig. 3.1; Fig. 3.2d). Topographical variation and vegetative diversity within the mostly deciduous forests of GSMNP (Whittaker et al. 2007) creates the cool, moist microclimates that lungless, plethodontid salamanders require for exchanging gases across their

skin without risking desiccation and providing suitable habitat (Petranka, 1998). The GSMNP is considered the "Salamander Capital of the World" because of the vast species richness and endemism of plethodontid salamanders (Kozak and Wiens 2010; Gifford and Kozak 2012).

We focused on three plethodontid species that vary in body size. *Desmognathus wrighti* (pygmy salamander) is the smallest species ranging from ~37-51 mm in total length (TL) at an adult stage. *Desmognathus ocoee* (Ocoee salamander) is a medium-sized speces ranging from ~70-110 mm in TL at an adult stage. *Plethodon jordani* (Jordan's or red-cheeked salamander) is a larger species ranging from ~85-185 mm in TL at an adult stage and is endemic to the GSMNP (Dodd 2004). These three species are high elevation specialists occuring between ~750-2,025 m and widely distributed throughout forested habitats of the GSMNP (Dodd 2004). *D. wrighti* and *P. jordani* are fully terrestrial species, but *D. ocoee* have a much more complicated life history, laying eggs in seepage areas and springs or near small streams but dispersing throughout the forests post-larval stage, especially at higher elevations (~1,460-1,830 m; Dodd 2004).

Plethodontid mass and elevation

We obtained body mass measurements for each plethodontid species from Peterman et al. (2016). Surveys were conducted in July 2012 at night and within one day of rain events using visual encounter to sample surface-active plethodontids (Peterman et al. 2016). Body mass measurements were recorded at site locations ranging from 669-2,019 m in elevation (Fig. 3.2d). To determine how body mass changed with elevation, we fit multiple linear regression models to salamander body mass as a function of elevation and species sex or stage class (Table 3.1; i.e., female, male or juvenile). We used a square root transformation of the response variable for the *D. ocoee* and *D. wrighti* adult models to meet the assumptions of linear regression. Including a

quadratic term improved model fit for predicting body mass of *D. wrighti* juveniles; therefore, we modeled juveniles separately from adults. For *P. jordani*, we included a cubic polynomial term to improve model fit for body mass predictions of females, males, and juveniles. We evaluated models using 10-fold cross validation in order to use the breadth of the dataset and to reduce variance. We assessed predictive accuracy by calculating mean absolute error and root-mean-square error. Model estimates from the *D. wrighti* adult, *D. wrighti* juvenile, *D. ocoee*, and *P. jordani* models were used to predict body mass for each sex and stage class of the study species across a 3 m^2 digital elevation model (DEM) raster.

Modeling standard metabolic rate

We modeled SMR (volume of oxygen consumption, VO_2 µl g^{-1} hr^{-1}) by combining the body mass predictions developed for the sex and stage class of each species with highly spatially resolved maps of microclimatic temperature for GSMNP. The microclimate maps were developed with an approach that incorporated vegetation buffering across the entire vertical profile of forest vegetation, thereby estimating the near-surface, sub-canopy temperatures that ground-dwelling organisms, like plethodontid salamanders, rely upon for surface activity in their microhabitat (Stickley and Fraterrigo 2021). Microclimate data consisted of monthly minimum, maximum, and average temperatures for March through November of 2006–2010 at a 3 m^2 spatial resolution. These months were chosen to coincide with periods of increased surface activity for terrestrial salamanders in GSMNP. Standard metabolic rate was calculated for the sex and stage class of each species using two equations from Feder (1976, 1983), which predict SMR for temperate plethodontid species as a function of temperature and body mass, respectively. For *P. jordani*, we also calculated SMR using a species-specific formula developed by Gifford and

Kozak (2012) and averaged those estimates with the Feder (1976,1983) predictions for *P. jordani* to account for both approaches to SMR prediction and limit uncertainty.

Overall, we developed 54 gridded maps of seasonal minimum and maximum SMR (3 species x 3 sex/stage classes x 3 seasons x 2 temperature estimates) by applying the SMR formulas described above to the microclimatic maps. Because we used average monthly minimum and maximum temperature (i.e., average monthly value during 2006-2010) for our microclimatic maps, we refer to spring, summer, and fall as the monthly averages of March-May, June-August, and September-November, respectively. Minimum SMR reflects the energy requirements during nighttime minimum temperatures and maximum SMR during daytime maximum temperatures. We also determined monthly average, minimum and maximum SMR (9 months x 3 sex/stage classes x 3 species x 3 temperature estimates = 243 values). To calculate SMR on a monthly time step, we randomly selected 50,000 points distributed throughout the study area and, for each point, applied the physiological formulas discussed above using the average, minimum, and maximum temperature values from the monthly microclimatic temperature maps (Stickley and Fraterrigo, 2021) as well as predicted body mass values from the maps for each species and sex/stage class. Further details can be found in the Appendix B.

Species distribution modeling

We developed coarse-resolution (1 km^2) SDMs to predict suitable climatic habitat for each study species with historical presence data and bioclimatic variables. We obtained historical presence-only data for each study species from Peterman et al. (2016), the Illinois Natural History Survey (https://herpetology.inhs.illinois.edu/databases/), the Smithsonian National Museum of Natural History (https://collections.nmnh.si.edu/search/), and the Hands on the Land

Network (https://handsontheland.org/). We also obtained data from Milanovich et al. (2010) via HerpNET (www.herpnet.org) and Global Biodiversity Information Facility (www.gbif.org). Presence locations were compiled into one spatial dataset and duplicate points were removed. The final dataset included 205, 158, and 316 presence locations for *D. wrighti*, *D. ocoee*, and *P. jordani*, respectively. We downloaded 11 WorldClim (1 km^2 spatial scale; https://www.worldclim.org/) bioclimatic variables previously shown to be biologically relevant and interpretable for plethodontid salamanders (Appendix B Table B.1; Rissler and Apodaca 2007; Milanovich et al. 2010).

Using the 11 bioclimatic variables and presence-only dataset, we calculated suitable climatic habitat at ~1 km^2 resolution for each study species (*D. wrighti*, *D. ocoee*, and *P. jordani*) across the GSMNP. We used a maximum entropy (MaxEnt) method as our modeling approach because MaxEnt (Elith et al. 2006) is the most popular and widely-used program for species distribution modeling due to high accuracy with presence-only data (Hernandez et al. 2006; Elith et al. 2011; Merow et al. 2013). We followed methodologies for data preparation, model fitting, model prediction, and model evaluation as recommended by Hijmans and Elith (2017). Model goodness of fit was assessed using the average area under the curve (AUC) value, calculated during model evaluation with *k*-fold cross validation. Further details can be found in the Appendix B.

Statistical analyses for model comparisons

To summarize SMR for each species, sex, and stage class, we calculated bootstrapped statistics (mean, standard deviation of mean, coefficient of variation, median and confidence interval of the median) using the 50,000 randomly selected points. Because SMR is strongly

influenced by body mass, we also calculated bootstrapped statistics for the percent change in SMR between each month of the study period, calculated as

$$(SMR_{t+1} - SMR_t) / SMR_t$$

where $_t$ is the initial month and $_{t+1}$ is the following month. This allowed us to compare patterns of spatiotemporal variation of SMR for each species, sex and stage class while accounting for allometry.

To evaluate the level of agreement and disagreement between estimated metabolic rate and predicted habitat suitability, we calculated the mean value of seasonal (spring, summer, and fall) SMR (minimum and maximum) for each sex and stage class of each species from the gridded maps (3 m^2 spatial resolution) within each pixel of the 1 km^2 SDM maps. Calculations were performed within the projected distributional range of each species as determined by the SDM threshold value (i.e., the lowest predicted habitat suitability value for an occurrence point). We determined the relationship between the mean SMR values and SDM-predicted habitat suitability using correlation coefficients from the modified t-test, based on the work of Clifford et al. (1989). The modified t-test creates an appropriate sample size to account for spatial autocorrelation and corrects correlation coefficients between two spatially correlated variables. Because low SMR values suggest higher performance for plethodontids (Feder and Pough 1975; Pough 1980; Sears 2005; DuRant et al. 2007), significant negative correlations ($\leq$ -0.7) indicated agreement among predictions, while significant positive correlations ($\geq$ 0.7) indicated disagreement.

To characterize spatial patterns of concordance between estimated salamander energetics and predicted habitat suitability, we identified areas with both low energetic costs of maintenance (defined as SMR values $\leq$ median) and high habitat suitability (SDM probability of

suitable habitat ≥ 0.7) for the sex and stage class of each species at minimum and maximum SMR and among seasons. To compare how concordance changed across space, we quantified the number of cells with low energetic cost of maintenance divided by the number of cells with high suitable climatic habitat at minimum and maximum SMR and among seasons. All statistical modeling was performed using R statistical software v. 3.50 (R Core Team 2020) and spatial modeling was conducted using ArcGIS® software versions 10.4.1–10.6.1 (Esri inc. 2020) and R statistical software v. 3.50 (R Core Team 2020). All data will be stored and available for download from a public repository when this manuscript is accepted for publication.

Results

Modeling salamander body mass

Overall, females were the larger sex for *D. wrighti* and *P. jordani*, whereas males exhibited larger body mass than females for *D. ocoee* (Table 3.1; Fig. 3.2). While body mass increased significantly with elevation for all plethodontid species, the rate of increase varied with sex and age (Table 3.1; Fig. 3.2). For every 100 m gain in elevation, model estimates indicated body mass increased by an average of 4.7% for *D. wrighti*, 12.8% for *D. ocoee*, and 4.8% for *P. jordani* (Appendix B Table B.2). For *D. wrighti*, juvenile body mass increased less at lower elevations (< 1,400 m) compared to higher elevations of the park (Fig. 3.2; > 1,400 m). *Desmognathus ocoee* adults showed a higher rate of increase in body mass across all elevations compared to juveniles (Fig. 3.2). For *P. jordani*, the estimated rate of body mass increase for all sex and stage classes was highest at elevations below 1,000 m (Δmass = 0.50g per 100 m) and above 1,600 m (Δmass = 0.43g per 100 m), with smaller increases in mass at mid-elevations (Fig. 3.2; Δmass = 0.01g per 100 m).

Standard metabolic rate

From 2006-2010, the average SMR was 34.0 VO_2 µl g^{-1} hr^{-1} for *D. wrighti* (female = 37.6, male = 34.8, juvenile = 29.7), 57.6 VO_2 µl g^{-1} hr^{-1} for *D. ocoee* (female = 65.0, male = 66.8, juvenile = 41.2) and 100.5 VO_2 µl g^{-1} hr^{-1} for *P. jordani* (Appendix B Fig. B.1, B.2, B.3, Table A3; female = 114.8, male = 101.2, juvenile = 85.4). Spatial variation in SMR over this period was greatest for *D. ocoee* (CV = 0.11) and P. *jordani* (CV = 0.10), with *D. wrighti* demonstrating the lowest variation overall (CV = 0.05). For all species, spatial variation in SMR was higher for juveniles than adults (Appendix B Table B.3; *D. wrighti* CV: female = 0.05, male = 0.05, juvenile = 0.08; *D. ocoee* CV: female = 0.11, male = 0.11, juvenile = 0.14; *P. jordani* CV: female = 0.8, male = 0.10, juvenile = 0.15) and generally higher in spring and autumn than in summer. For *D. ocoee* spatial variation was greater for minimum SMR compared to maximum SMR (Appendix B Fig. B.1-B.3, Table B.3).

Energetic requirements changed at different rates for each species as indicated by the monthly and seasonal differences in percent change of SMR (Fig. 3.3; Appendix B Fig. B.4-B.6). *Desmognathus wrighti* exhibited the largest increase in SMR from spring to summer and the largest decrease in SMR from summer to autumn (Fig. 3.3), while *D. ocoee* demonstrated the lowest rates of change. Juveniles for all species consistently exhibited the largest monthly and seasonal changes in SMR, with *D. wrighti* and *D. ocoee* exhibiting significant differences between adults and juveniles (Fig. 3.3). Variation in the percent change of SMR was consistently higher for minimum SMR than maximum SMR (Appendix B Fig. B.4-B.6).

Comparing physiology and suitable climatic habitat

The mean AUC for plethodontid salamander distribution models was 0.91 indicating high levels of model accuracy (Fig. 3.4; *D. wrighti* = 0.92; *D. ocoee* = 0.89; *P. jordani* = 0.90). For all three species, the most influential predictor variables were precipitation seasonality, followed by either annual mean temperature or mean monthly temperature diurnal range (Appendix B Table B.1). Approximately 10.3% (249.2 km^2), 8.0% (194.8 km^2), and 11.8% (286.5 km^2) of the 2,430 km^2 study area were considered highly suitable habitat (≥ 0.7) for *D. wrighti*, *D. ocoee*, and *P. jordani*, respectively (Fig. 3.4).

Correlation coefficients from modified t-tests indicated that the level of agreement between estimated standard metabolic rate and predicted habitat suitability varied among species and, in some cases, within species among season, sex or stage class, and between minimum or maximum SMR (Table 3.2; Fig. 3.5; Appendix B Fig. B.7-B.9). Overall, there was strong agreement for *P. jordani* ($\bar{x}$ = -0.71, range = -0.76 to -0.58) and *D. wrighti* ($\bar{x}$ = -0.65, range = -0.91 to 0.03) and weak agreement for *D. ocoee* ($\bar{x}$ = 0.81, range = 0.31 to 0.90). For *D. wrighti*, we found strong agreement between maximum SMR and habitat suitability across all seasons. However, agreement between minimum SMR and habitat suitability was inconsistent, with stronger agreement in spring than fall and for adults compared to juveniles (Table 3.2; Fig. 3.5). For *P. jordani*, agreement was strongest in summer and weakest in fall with higher model agreement for maximum SMR. There was minimal variation among sex or stage class for *P. Jordani*. For *D. ocoee*, SMR and habitat suitability generally disagreed for each sex and stage class, with greater disagreement for minimum SMR (Table 3.2; Fig. 3.5).

Spatial patterns of concordance between high habitat suitability (SDM probability ≥ 0.7) and areas with low energetic cost of maintenance (SMR ≤ median) varied seasonally, among

species' sex or stage class, and minimum and maximum SMR (Fig. 3.6). For *D. wrighti*, we found high levels of spatial concordance among all seasons at maximum SMR, with high concordance in summer (female, male, and juvenile = 0.99) and lower concordance during spring and autumn for juveniles (spring = 0.52, autumn = 0.41) and adults (female: spring = 0.72, autumn = 0.61; male: spring = 0.75, autumn =0.61). *Desmognathus ocoee* exhibited spatial discordance for minimum SMR for all sex and stage classes (all values < 3%), and for maximum SMR in spring and summer (0-7%). However, there was weak spatial concordance for adults at maximum SMR in autumn (female = 0.32, male = 0.34, juvenile = 0.08). We observed the opposite pattern for *P. jordani*, which demonstrated high levels of spatial concordance at minimum and maximum SMR, among seasons, and among each sex and stage class (average among sex and stage class for minimum SMR: spring = 0.85, summer = 0.88, autumn = 0.79; maximum SMR: spring, summer and fall = 0.89). Spatial concordance varied for each species, yet we found examples of spatial discordance within each species when comparing minimum and maximum SMR, adults and juveniles, and seasonal differences (Fig. 3.6; Appendix B Fig. B.7-B.9).

Discussion

Metabolic rate is a central component of amphibian energetics, and spatiotemporal patterns in energetic requirements have important implications for understanding habitat use and distributions of plethodontids (Gifford 2016). However, climate data are typically developed at broad spatiotemporal scales and neglect the dynamic buffering of near-surface, sub-canopy temperatures by forest vegetation, potentially disregarding information relevant to the prediction of salamander energetics (Cushman 2006; Kearney and Porter 2009; Lembrechts et al. 2018).

Furthermore, physiological models have not accounted for body size clines in plethodontid species following Bergmann's rule. To our knowledge, the physiological models we developed in this study are the first to integrate body mass-elevation relationships into metabolic rate formulas for plethodontid salamanders. By combining these models with microclimatic predictions that reflect seasonal and diurnal variation in sub-canopy, near-surface temperatures, we revealed large temporal discrepancies between energetic demand and static predictions of climatically suitable habitat. Our results therefore highlight novel challenges associated with relying solely on coarse resolution species distribution models for assessing habitat suitability.

Previous studies have indicated spatial mismatches between SDMs, developed from free-air temperature data at a coarse resolution, and mechanistic models, based on fine resolution microclimatic data (Kearney and Porter 2009; Bramer et al. 2018; Lembrechts et al. 2018), but our results also expose the potential for temporal misalignments between daily (i.e., minimum and maximum SMR) and seasonal variations in metabolic demands with static modeling approaches like those of SDM. It is the variability in body mass-elevation relationships, along with spatiotemporal variability in diurnal and seasonal temperatures, that contributed to the physiological variation and model mismatches found in this study. These findings reinforce the need to increase efforts in plethodontid sampling and research (Gifford 2016) to better estimate physiological responses, an important step in understanding physiological acclimatization to changing climate patterns. It may be critical to integrate temporally robust predictions of energetic demand for ectothermic species to use in conjunction with the commonly used correlative approaches in species distribution modeling.

Agreement between bioclimatic modeling approaches and mechanistically focused approaches that incorporate physiology for terrestrial salamanders has been found in previous

research (Arif et al 2007; Gifford and Kozak 2012). However, the spatiotemporal mismatches we observed between areas with low energetic cost of maintenance and suitable climatic habitat based on coarse resolution SDMs (Table 3.2; Fig. 3.5; Fig. 3.6) indicate that agreement between these approaches and spatial concordance may be species dependent, may fluctuate temporally, and may vary among stage classes within species (Table 3.2; Fig. 3.5; Fig. 3.6). Furthermore, we found that in cases of spatial discordance (Fig. 3.6), areas with low energetic cost of maintenance occurred towards the edges of a species' range, where climate-driven SDMs predicted low habitat suitability. Therefore, habitat suitability may not be generalizable across species or even within a species, a problem for developing conservation plans at desired levels, such as community- or taxa-levels (Mokany and Ferrier 2011; Jones et al. 2016). Further understanding the variation in body-mass elevation relationships for plethodontids will be important for future attempts at modeling physiologically suitable habitat.

There has been some debate on whether plethodontid salamanders follow Bergmann's rule, as body size clines may be dependent upon species' life history traits and regional location (Olalla-Tárraga et al. 2006; Adams and Church 2008; Peterman et al. 2016). We found that body mass increased with elevation for three species that were previously shown to clearly follow Bergmann's rule (Peterman et al. 2016). Our results suggest that the rate of increase in body mass differs for each species and for the sex or stage class within the species. Given that metabolism is directly influenced by body mass, investigating the effect that differing body mass clines have on the energetic demands of plethodontid salamanders, or other ectotherms following Bergmann's rule, is important for developing more accurate physiological models (Feder 1976).

Indeed, we found that the inclusion of body mass-elevation relationships in our physiological models resulted in substantial spatiotemporal variation of SMR among our study

species and among sex or stage classes within each study species. We also found temporal variation in these patterns, both seasonally and when comparing nighttime and daytime energetic demands (i.e., minimum and maximum SMR). For *D. ocoee*, juvenile body mass increased at a much lower rate than adults (Fig. 3.2). This was not the case for either *D. wrighti*, which demonstrated lower body cline rates at lower elevations and increased rates at higher elevations for juveniles, or *P. jordani*, which demonstrated relatively consistent body mass clines across all sex and stage classes (Fig. 3.2). Previous studies show that *D. ocoee* has slower development time to maturity (Tilley 1973, 1980), and *D. ocoee* has a much more complicated life history in comparison to the other species in this study with suitable habitat varying across ontogeny as shown in other organisms (Dodd 2004; Carscadden et al. 2020). Therefore, body cline rates for juveniles may be different depending upon the time of the year and level of maturation. Nevertheless, if body mass cline rates vary among species and among the sex or stage class for a species, then the result is variation in SMR along the heterogeneous, montane environment of GSMNP. There can be considerable disparities in microclimatic temperatures and lapse rates (i.e., the rate at which temperature changes with elevation) across seasons and between minimum and maximum temperatures within the GSMNP study area (Fridley 2009), especially when vegetation buffering is considered (Stickley and Fraterrigo 2021). It is these temporal variations in microclimatic temperatures along elevational gradients, combined with the different rates in body mass clines for each species, that drove the observed spatiotemporal variations of SMR.

Although there is limited understanding of how temperature or other environmental factors affect metabolic variation in closely related species (Gifford 2016), previous studies have indicated variation in metabolic rates among plethodontids (Feder 1976; Whitford and Hutchinson 1965, 1967; Withers 1980; Bernardo et al. 2007). It has also been suggested that

physiology may constrain some plethodontid species to certain elevational ranges while other species may experience greater or further constraint by other confounding biotic factors, such as competition (Gifford and Kozak 2012). Therefore, characterizing metabolic variation may be important for understanding plethodontid distributions and dispersal, yet how salamander bioenergetics vary across space and time is not well established. We found differences in the temporal patterns of metabolic requirement between daytime and nighttime (i.e., maximum and minimum SMR) temperatures. We also found that the observed monthly and seasonal differences in the percent change of metabolic rate suggest broader temporal variation in salamander energetics with the potential of physiological stress to shift at differing rates during seasonal transitions (Appendix B Fig. B.1-B.6). Riddell et al. (2018a) demonstrate seasonal acclimatization for a *Plethodon metcalfi*, a close relative to *P. jordani,* in which metabolic rate is lowered during increased summer temperatures. This finding potentially minimizes the magnitude of seasonal variation found in our physiological models. However, it is unknown whether acclimatization factors hold true among all plethodontids or whether acclimatization may occur over shorter temporal periods. The patterns we found across daily (i.e., daytime and nighttime SMR) and seasonal time periods are important to consider for plethodontid distributions and surface activity within the microhabitat.

High elevation, southern Appalachian salamanders, such as the three in this study, spend much of their time underground with some surface activity during the day, typically under leaf litter or downed woody debris, but are mostly surface-active during nighttime with variation in peak surface activity among different seasons (Petranka 1998; Dodd 2003; Connette et al. 2015). However, behavioral traits (e.g., timing of egg deposition, mating, dispersal, etc.) for each species differ or are poorly understood (Petranka 1998; Dodd 2004; Amphibiaweb 2020).

Increased energetic demand or variation in energetic demand during nighttime when temperatures are lowest or across broader seasonal patterns could constrain important nocturnal or phenological surface activities related to dispersal, food acquisition, mating, and other life history aspects (Fig. 3.3; Petranka 1998; Dodd 2004; Amphibiaweb 2020). Likewise, the higher variation in maximum SMR during summer suggests the potential for increased physiological stress during daytime temperatures at the hottest time of the year, potentially constraining the already limited daytime surface activity summer (Petranka 1998; Dodd 2003; Connette et al. 2015). For instance, the timing of surface activities is modified by increased burrowing under warmer or drier conditions (Fielding et al. 1999; Tingley 2012; Muñoz et al. 2016; Riddell et al. 2021); it is currently unclear how plethodontids of different life stages vary in their use of surface and vertical space (Dodd 2003). If different species, sexes or stage classes experience temporally different rates of physiological stress, behavioral and morphological constraints may result in different ecological trade-offs, such as low metabolic rate or resistance to water loss (Addo-Bediako et al. 2001; Riddell et al. 2018; Riddell et al. 2021), that limit access to suitable microclimatic conditions.

Taken together, the variation found in our physiological models and the resulting spatiotemporal mismatches with suitable climatic habitat may be of great importance to understanding patterns in salamander movement or habitat suitability. However, we do note that there are limitations with our physiological and suitable habitat models that should be taken into consideration. Most importantly, we focus on SMR, based on microclimatic temperatures, but do not include a water component, such as vapor pressure deficit or soil moisture, into these analyses, an integral part of predicting salamander surface activity (Riddell and Sears 2015; Riddell et al. 2017; Riddell et al. 2018b). Our goal here was to assess agreement between

salamander physiology and suitable habitat, but a water component will be an important aspect of future work that aims to locate physiologically suitable habitat for conservation purposes. Another limitation to this study is that *D. ocoee* has a different life history compared to the other two study species that involves a larval stage in or near seepages or small streams, and *D. ocoee* occurrence data have historically been misidentified due to close resemblance to *Desmognathus imitator* (Dodd 2004; Peterman et al. 2016). These differences may result in suitable habitat predictions based on *D. imitator* data, and therefore, should be considered more conservative estimates than the *D. wrighti* and *P. jordani* suitable habitat predictions. It should be noted that these issues could explain some of the variation in model disagreement for *D. ocoee*. Also, we relied on SMR formulas developed for all temperate plethodontid species to model *D. wrighti* and *D. ocoee* physiology (Feder 1976, 1983). These models do not account for the species-specific variation that may be found from SMR formulas developed from *in situ* body mass and oxygen consumption data. Because the variation in SMR predictions is driven by mass-elevation relationships and microclimatic patterns, we believe our predictions do account for key dimensions of variation in energetic demands for these species. However, the body mass-elevation models were generated from body mass data collected over a relatively short time period, and from surface-active salamanders, which could bias the results. Nonetheless, sampling effort was equitable and adequate under ideal survey conditions (Peterman et al. 2016), which should minimize bias. Lastly, plethodontid species can show physiological plasticity, acclimatizing to warmer temperatures during summer months by decreasing their metabolic rates (Wells 2007; Riddell et al. 2018a). Given these issues of potential uncertainty, the estimates of SMR presented here should also be considered conservative.

This study highlights the importance of including microclimatic data that account for forest vegetation buffering of near-surface temperatures and the integration of body mass-elevation relationships for modeling the physiological responses of ectothermic species that follow Bergmann's rule. Spatial discordance between SDM predictions of suitable habitat and areas of low energetic cost of maintenance implies that research or conservation efforts based solely on SDMs may be less effective than expected for important indicator species, like plethodontid salamanders. These findings thus demonstrate the challenges inherent in relying on SDMs to predict suitable habitat, and suggest the need for integrating multiple model types (correlative, mechanistic, agent-based, etc.) together to provide robust conservation outcomes (Kearney and Porter 2009; Keppel et al. 2012; Evans et al. 2015). The integration of microclimate data and mechanistic responses at appropriate spatial and temporal scales is an important consideration for future research. The data, information, and techniques we used in this study could be used in conjunction with vapor pressure deficit (Riddell and Sears 2015) to strengthen predictions of physiologically suitable habitat and incorporated into future climate projections to better understand potential responses to climate change. Including temporal variation in locations of low energetic cost of maintenance, based on SMR and vapor pressure deficit, could help in targeting microclimatic refugia, areas for translocation or reintroduction, and areas of functional connectivity during surface active periods within transient connectivity windows (Zeigler and Fagan 2014; Jones et al. 2016). We support calls to accrue more physiological data for plethodontids to better understand physiological variation and plasticity from the individual level up to broader taxonomic levels (Gifford 2016). Doing so could generate more accurate models to help conservation management for one of the biggest threats to plethodontids, anthropogenic climate change.

Figures

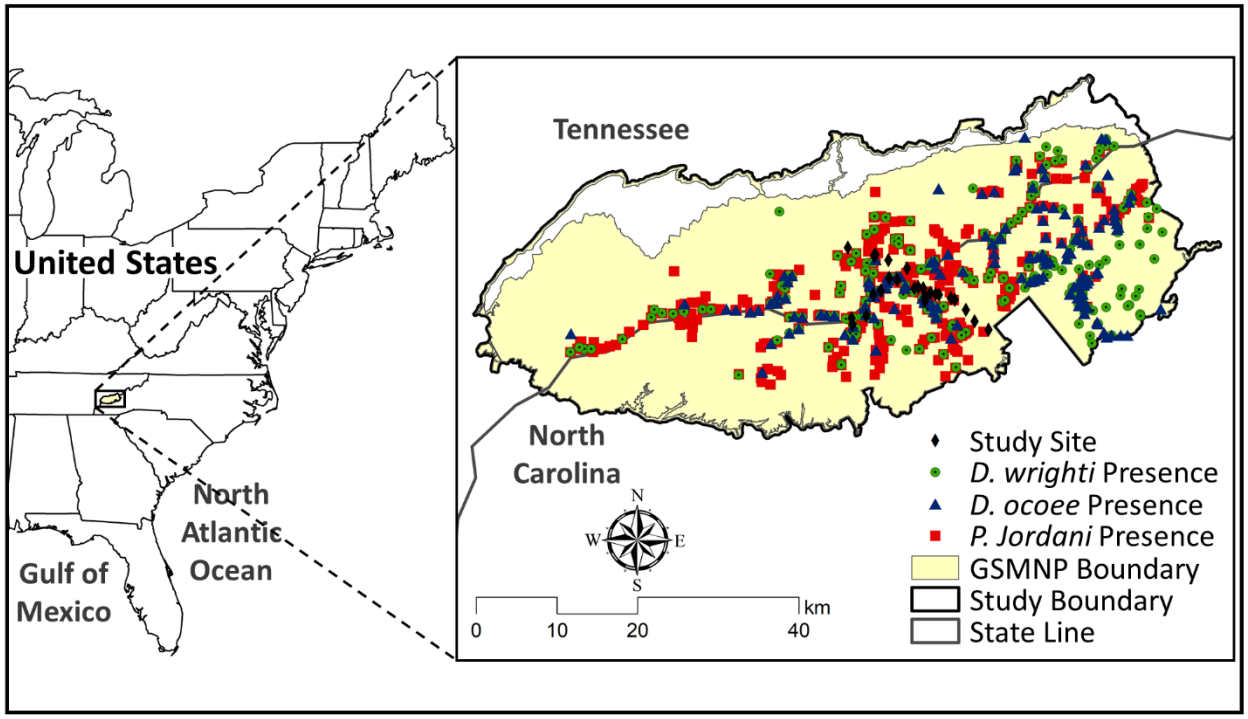

Figure 3.1. Location of Great Smoky Mountains National Park (GSMNP) and study area on the border of North Carolina and Tennessee in the southern Appalachian Mountains. The symbols indicate the presence locations used to model suitable climatic habitat for each species

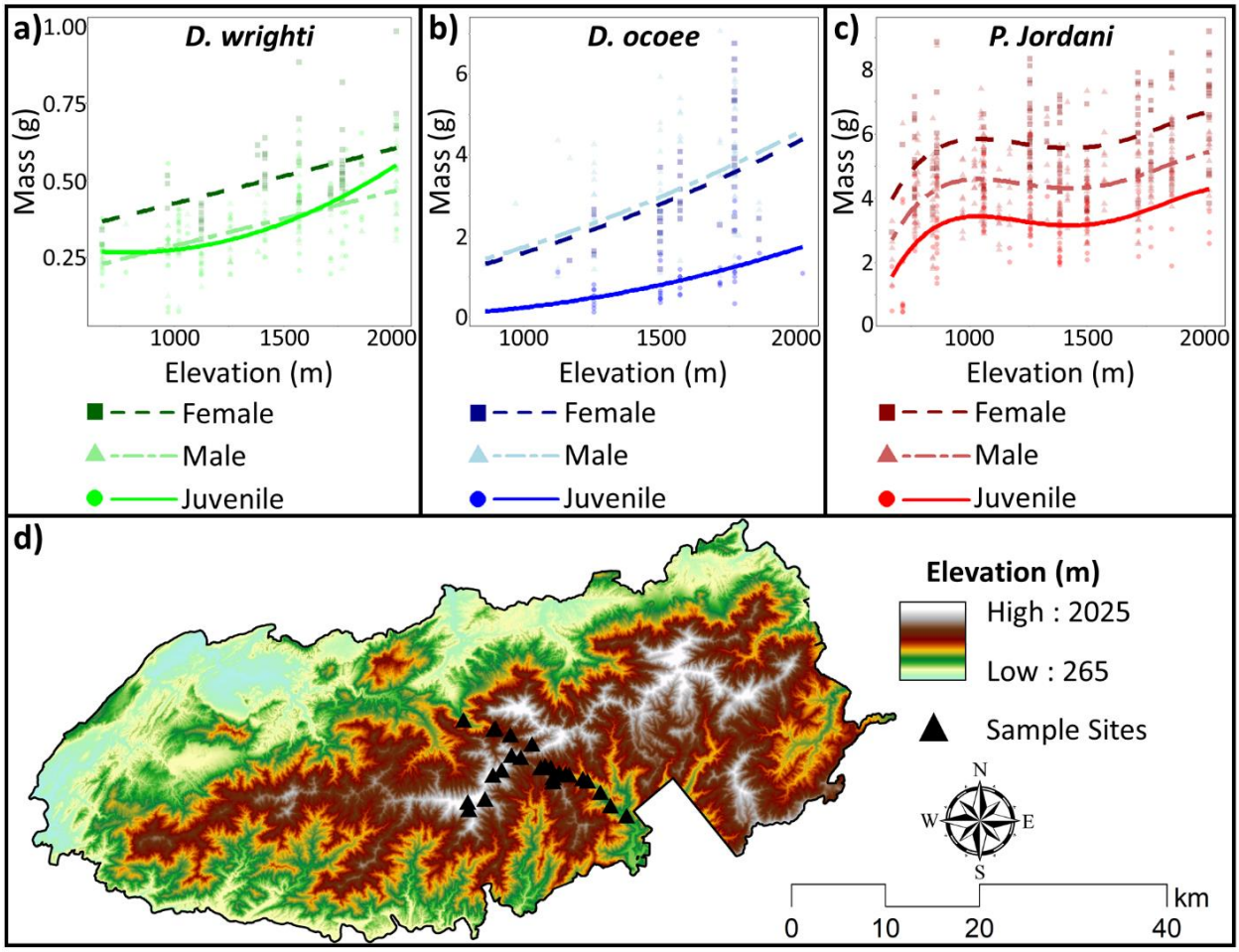

Figure 3.2. Relationship between body mass and elevation for (a) *Desmognathus wrighti*, (b) *Desmognathus ocoee*, and (c) *Plethodon jordani* by sex and age class. (d) Elevation of Great Smoky Mountains National Park study area and salamander sampling locations of Peterman et al. (2016)

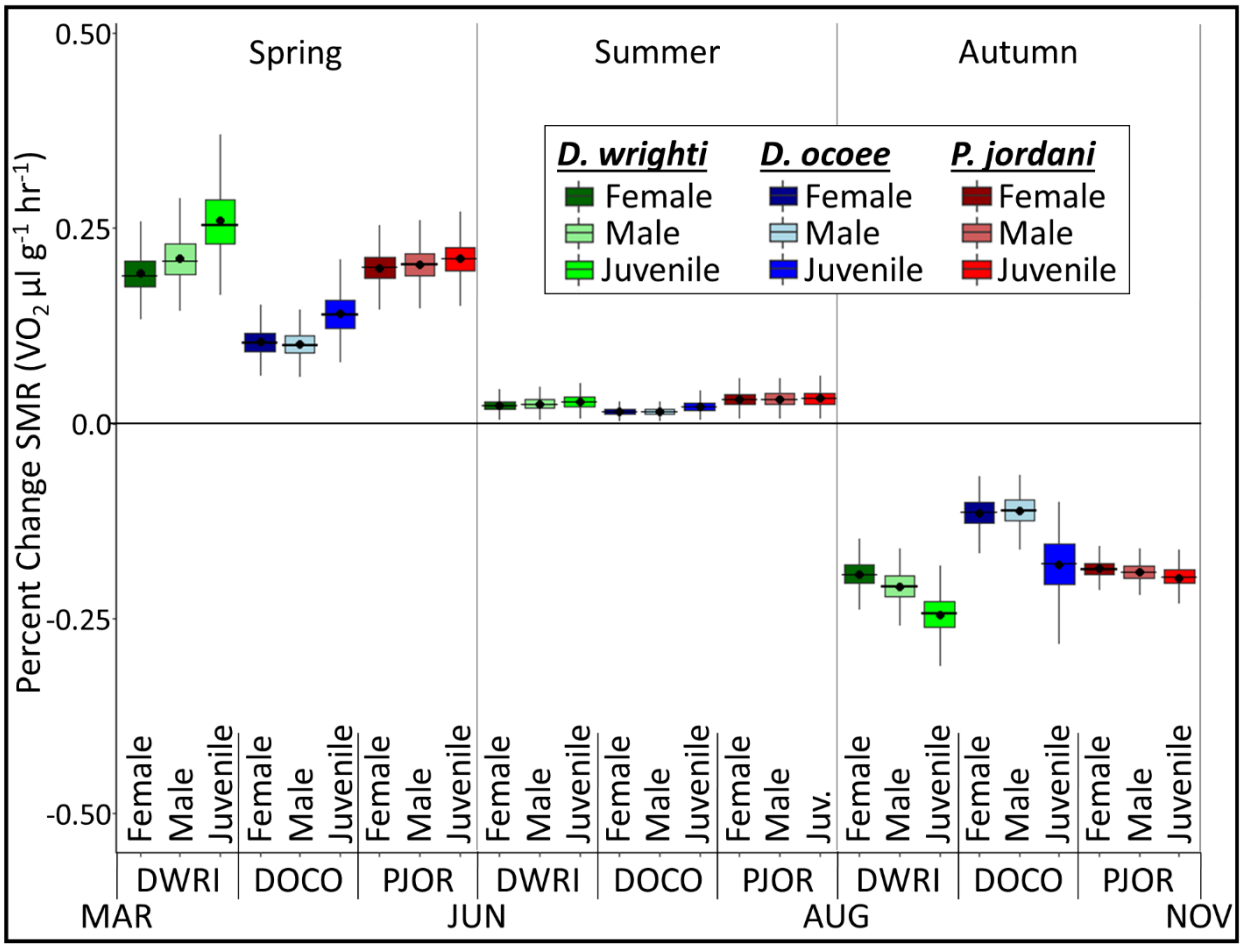

Figure 3.3. Percent change (increase from 0 to 50% and decrease from 0 to -50%) in average standard metabolic rate (SMR) from March to June, June to August, and August to November for each species (*Desmognathus wrighti*, *Desmognathus ocoee*, and *Plethodon jordani*), sex and stage class (male, female, and juvenile) across the study period (2006-2010). Percent change calculated as: $(SMR_{t+1} - SMR_t)/SMR_t$, where $_t$ is the initial time period and $_{t+1}$ is the following time period. Points indicate the bootstrapped mean and central error bar lines indicate the confidence interval for the bootstrapped median. Vertical lines indicate the error bar for standard deviation of mean

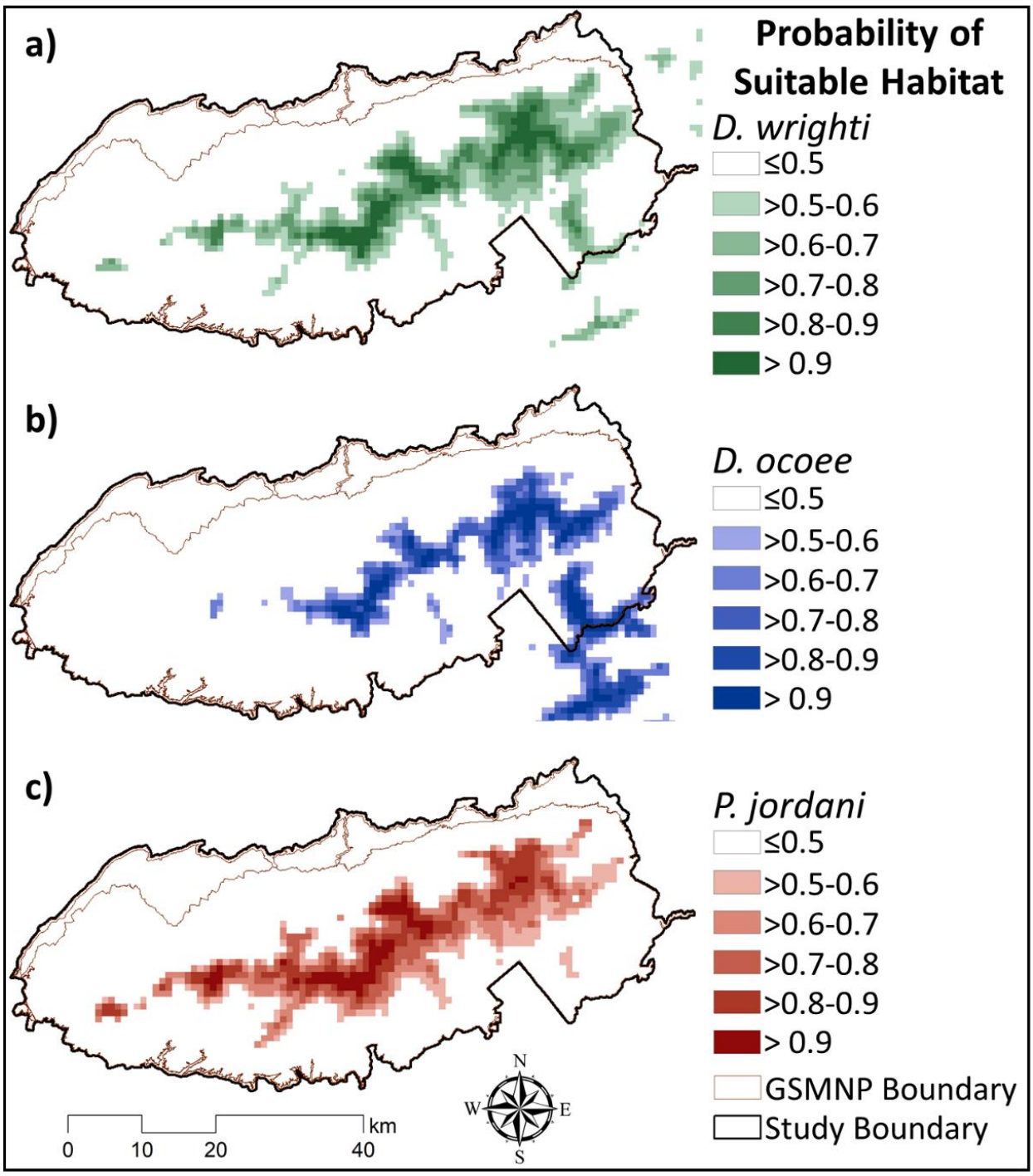

Figure 3.4. Species distribution models for (a) *Desmognathus wrighti*, (b) *Desmognathus ocoee*, and (c) *Plethodon jordani*. Suitable climatic habitat predictions are based on modeling presence-only data using maximum entropy and values represent the probability of suitable habitat

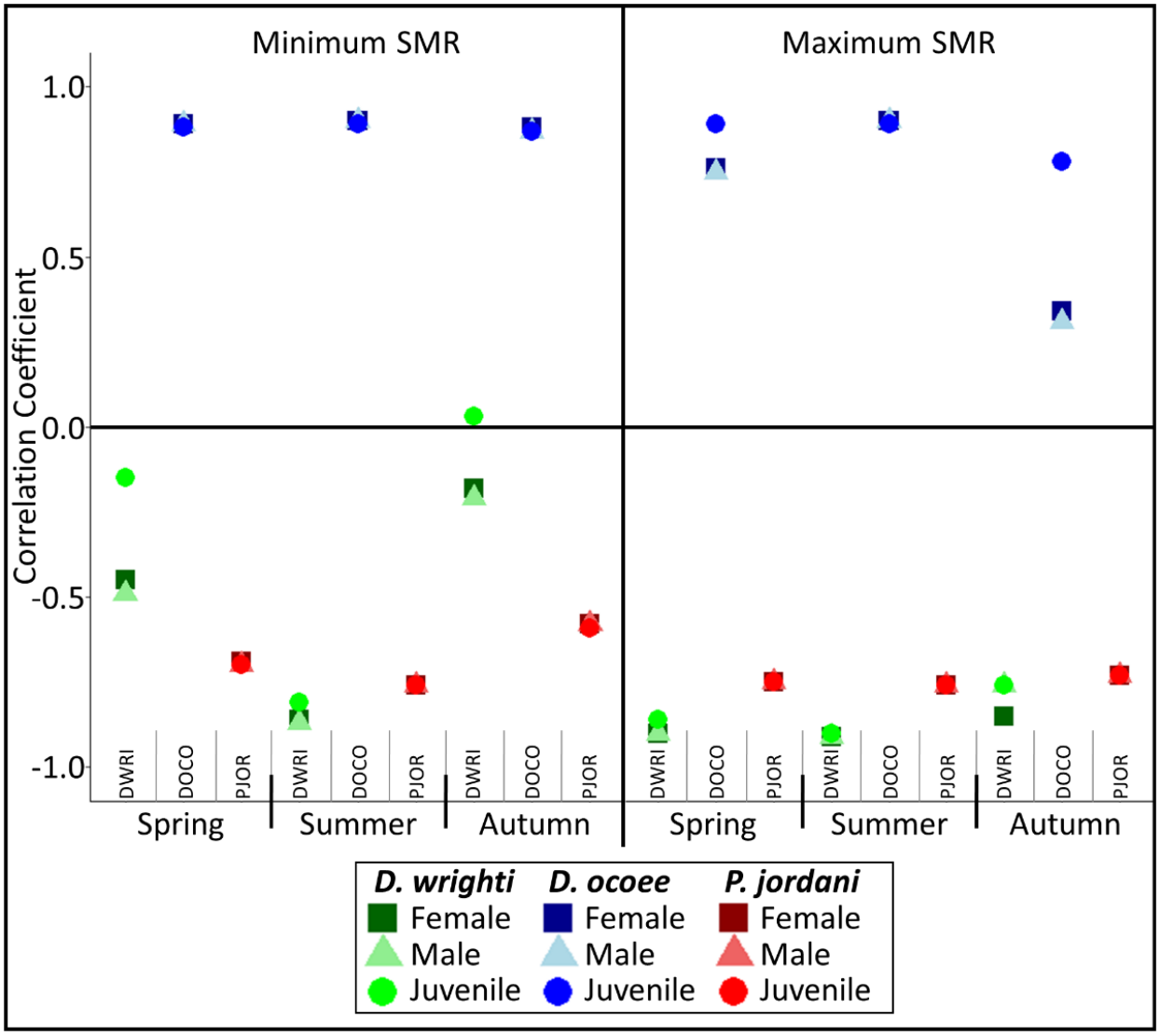

Figure 3.5. Correlation between predicted habitat suitability from maximum entropy species distribution models and minimum and maximum standard metabolic rate (SMR) from physiological models. Correlation coefficients based on modified t-tests to account for spatial autocorrelation. Values are seasonal averages of SMR for *Desmognathus wright* (DWRI), *Desmognathus ocoee* (DOCO), and *Plethodon jordani* (PJOR) by sex or stage class. High negative values indicate strong agreement between SDM and SMR predictions; high positive values indicate disagreement

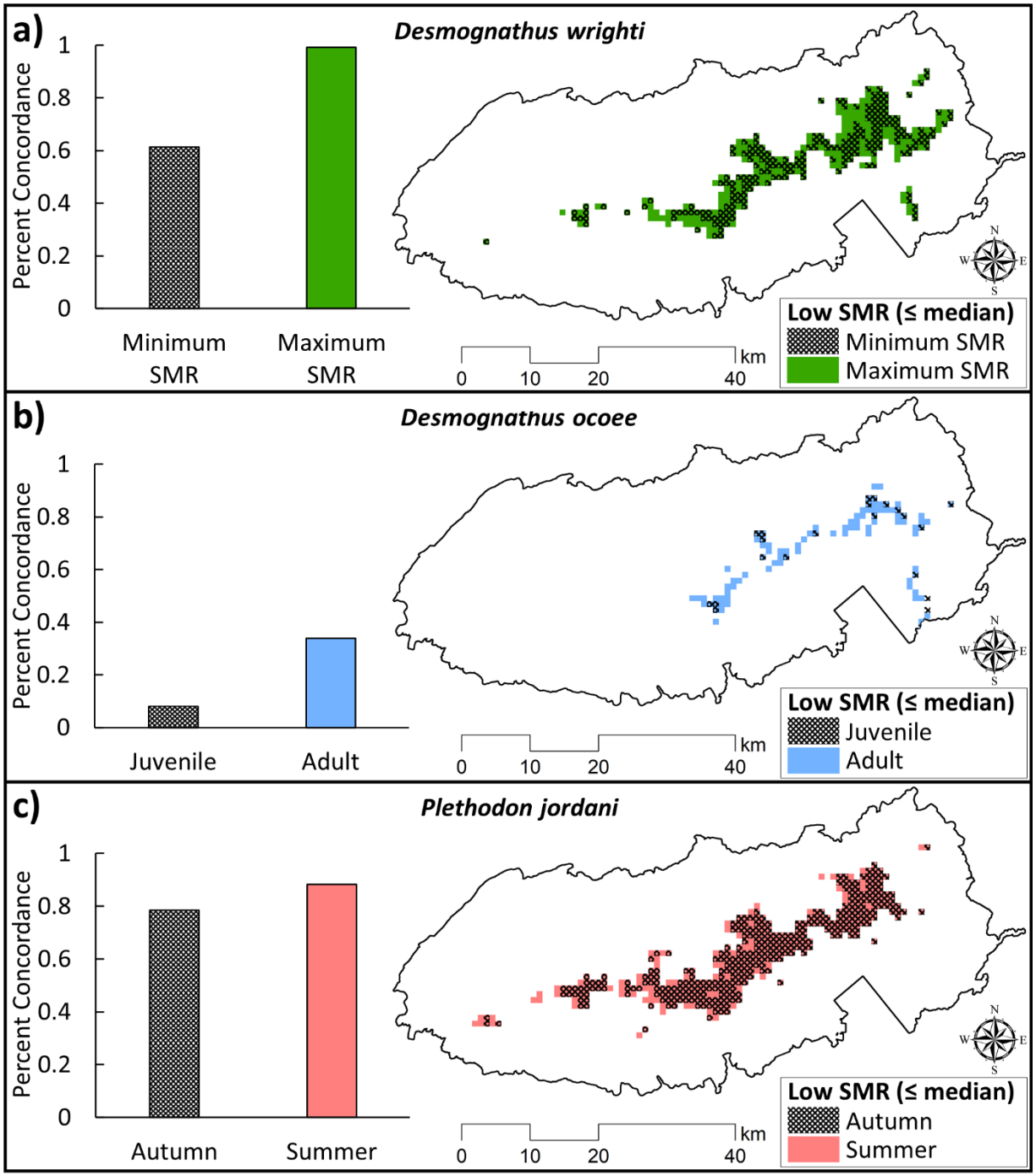

Figure 3.6. Concordance between locations with high suitable climatic habitat (probability ≥ 0.7) and areas with low energetic cost of maintenance (standard metabolic rate ≤ median) for each study species. Graphs show the total percent concordance across the study area and maps represent spatial patterns in concordance for (a) *Desmognathus wrighti* females during autumn demonstrating variation in concordance among minimum and maximum temperature, (b) *Desmogntahus ocoee* during autumn maximum temperatures demonstrating variation in concordance among adults and juveniles, and (c) *Plethodon jordani* males during minimum temperature demonstrating variation in concordance among season

Tables

Table 3.1. Results from multiple linear regression models predicting salamander body mass changes in relation to elevation and sex/stage. Goodness of fit measures shown are the coefficient of determination (R^2), mean absolute error (MAE), and root-mean-square error (RMSE) calculated with repeated *k*-fold cross validation. Also shown are variable names, final parameter estimates with square root transformations for *D. wrighti* adults and *D. ocoee*), the standard error of estimates (SE), 95% confidence intervals (df), *t*-values and *p*-values (**p*-value < 0.05, ** *p*-value < 0.01, and *** *p*-value < 0.001).

Variable	Parameter estimate	SE	95% CI	*t*-value	*p*-value
***Desmognathus wrighti* – Male and Female** n = 209, R^2 = 0.55, MAE = 0.07, RMSE = 0.10					
(Intercept)	0.250	0.0303	0.19–0.31	8.234	***
Elevation (m)	0.000176	0.0000182	0.00014–0.00021	9.705	***
Sex - male	-0.138	0.0151	-0.17 to -0.11	-9.123	***
***Desmognathus wrighti* – Juvenile** n = 82, R^2 = 0.40, MAE = 0.09, RMSE = 0.11					
(Intercept)	0.380	0.0127	0.0060–0.17	2.993	**
Elevation (m)	-0.000291	0.000205	0.00015–0.00026	-1.423	
Elevation^2	0.000000186	0.00000007643	0.00015–0.00026	2.436	*
Desmognathus ocoee n = 161, R^2 = 0.54, MAE = 0.28, RMSE = 0.37					
(Intercept)	0.442	0.219	0.0087–0.87	2.015	*
Elevation (m)	0.000819	0.000132	0.00056–0.0011	6.210	***
Sex - juvenile	-0.777	0.0801	-0.94 to -0.62	-9.699	***
Sex - male	0.0530	0.0719	-0.09–0.19	0.738	
Plethodon jordani n = 611, R^2 = 0.42, MAE = 0.89, RMSE = 1.12					
(Intercept)	-6.112	2.093	-10.22 to -2.00	-2.920	**
Elevation (m)	0.02731	0.00508	0.017–0.037	5.374	***
Elevation^2	-0.0000207	0.00000391	-0.000028 to -0.000013	-5.281	***
Elevation^3	0.00000000511	0.000000000962	0.0000000032 - 0.0000000070	5.317	***
Sex - juvenile	-2.439	-2.439	-2.73 to -2.15	-16.690	***
Sex - male	-1.206	-1.206	-1.42 to -0.99	-10.839	***

Table 3.2. Results from modified t-tests (Clifford et al. 1989) indicating the association between standard metabolic rate (SMR) and estimates for the probability of suitable habitat from species distribution models. Model results are displayed for minimum SMR and maximum SMR in () for each sex or stage class (i.e., male, female or juvenile) across each season (i.e., spring, summer or fall), and include the correlation coefficient, F-statistic, degrees of freedom (df), and *p*-values (**p*-value < 0.05, ** *p*-value < 0.01, and *** *p*-value < 0.001).

Sex/Stage Class	Season	Correlation Coefficient	F-statistic	df	*p*-value
Desmognathus wrighti		SMR Minimum (Maximum)			
Female	Spring	-0.45 (-0.90)	44.9 (448.8)	173 (107)	*** (***)
	Summer	-0.86 (-0.91)	226.7 (500.4)	87 (102)	*** (***)
	Fall	-0.18 (-0.85)	15.2 (320.2)	443 (123)	*** (***)
Male	Spring	-0.49 (-0.90)	51.6 (440.6)	164 (108)	*** (***)
	Summer	-0.87 (-0.91)	255.8 (502.5)	84 (102)	*** (***)
	Fall	-0.21 (-0.76)	19.7 (217.6)	419 (162)	*** (***)
Juvenile	Spring	-0.15 (-0.87)	9.0 (351.6)	377 (118)	** (***)
	Summer	-0.81 (-0.90)	185.0 (459.0)	97 (107)	*** (***)
	Fall	0.03 (-0.76)	0.5 (217.6)	661 (162)	0.47 (***)
Desmognathus ocoee		SMR Minimum (Maximum)			
Female	Spring	0.89 (0.76)	535.8 (326.7)	145 (241)	*** (***)
	Summer	0.90 (0.90)	579.8 (573.0)	143 (140)	*** (***)
	Fall	0.88 (0.34)	480.1 (59.3)	145 (462)	*** (***)
Male	Spring	0.89 (0.75)	536.5 (313.6)	144 (250)	*** (***)
	Summer	0.90 (0.90)	580.8 (573.7)	143 (140)	*** (***)
	Fall	0.88 (0.31)	481.3 (49.5)	145 (483)	*** (***)
Juvenile	Spring	0.88 (0.89)	519.3 (588.6)	146 (163)	*** (***)
	Summer	0.89 (0.89)	547.3 (537.8)	149 (143)	*** (***)
	Fall	0.87 (0.78)	453.7 (286.4)	147 (189)	*** (***)
Plethodon jordani		SMR Minimum (Maximum)			
Female	Spring	-0.69 (-0.75)	145.8 (208.2)	156 (159)	*** (***)
	Summer	-0.76 (-0.76)	178.7 (213.2)	130 (153)	*** (***)
	Fall	-0.58 (-0.73)	112.9 (195.7)	224 (170)	*** (***)
Male	Spring	-0.70 (-0.75)	146.5 (159.1)	157 (159)	*** (***)
	Summer	-0.76 (-0.76)	178.4 (212.8)	130 (154)	*** (***)
	Fall	-0.58 (-0.73)	114.2 (195.7)	223 (170)	*** (***)
Juvenile	Spring	-0.70(-0.75)	147.4 (207.3)	158 (160)	*** (***)
	Summer	-0.76 (-0.76)	177.5 (212.0)	132 (154)	*** (***)
	Fall	-0.59 (-0.73)	116.0 (195.6)	222 (170)	*** (***)

CHAPTER 4: TARGETING AREAS OF HIGH CONSERVATION VALUE FOR PLETHODONTID SALAMANDERS THREATENED FROM CLIMATE-INDUCED RANGE LOSS

Introduction

Global biodiversity is declining at an unparalleled rate (Hoffmann et al. 2010; WWF 2020), and climate change is expected to drive future losses (Thomas et al. 2004; Maclean and Wilson 2011; Urban 2015). Climate change is causing the distributions of many species to shift towards higher latitudes or higher elevations (Chen et al. 2011; Tingley et al. 2012; Lenoir and Svenning 2015), and extinction risk has been linked to increased levels of range loss for many species (Urban 2015). Conservation planning has the potential to mitigate climate change effects on biodiversity; however, there are several impediments to developing robust plans. Notably, accurate predictions of organismal responses to future climatic conditions are still lacking and often fail to address uncertainty in climate change forecasts (Hoegh-Guldberg et al. 2008; Clusella-Trullas et al. 2011; Urban 2016). Additionally, common approaches to spatially targeting areas for conservation are typically neither resolved nor extensive enough (Kearney and Porter 2009; Potter et al. 2013; Lenoir et al. 2017) to allow for habitat connectivity planning and protection of microclimatic refugia (Groves et al. 2012; Schmitz et al. 2015; Jones et al. 2016). There remains a need to incorporate microclimate into habitat suitability analysis to predict organismal responses to climate change with high levels of accuracy for conservation management (Lembrechts et al. 2018).

Species distribution models (SDMs) are widely used to map future suitable habit for spatial conservation planning (Elith et al. 2008; Lentini and Wintle 2015; Araújo et al. 2019), and are typically based on climate data developed from free-air temperature predictions at coarse spatial resolutions (Lenoir et al. 2017; Lembrechts et al. 2018). However, free-air temperature

predictions disregard the important buffering effects that vegetation and plant-water interactions have on near-surface (i.e., microclimatic) temperatures (Davis et al. 2018; De Frenne et al. 2019; Zellweger et al. 2019a; Stickley and Fraterrigo 2021). These biophysical and spatial mismatches between free-air temperatures and buffered microclimatic temperatures are amplified in montane environments because localized climate can vary only a few meters apart due to topographic and vegetation heterogeneity (Fridley 2009; Geiger et al. 2009; Stickley and Fraterrigo 2021). Therefore, coarse resolution climate predictions may neglect the localized climatic regimes that small, ground-dwelling organisms experience within their microhabitat (Kearney and Porter 2009; Helmuth et al. 2010). The use of coarse-resolution, free-air climate data for modeling future species distributions may result in regional overestimations and local underestimations of suitable habitat (Trivedi et al. 2008; Gillingham et al. 2012a, b; Franklin et al. 2013). This "spatial resolution paradox" demonstrates the potential importance of developing SDMs at microclimatological scales, an essential step for improving predictions of species responses to climate change (Lenoir et al. 2017).

However, SDMs are also typically unable to capture fine-scale variation in biological and physiological processes that affect the performance and fitness of organisms (Barton and Terblanche 2014; Evans et al. 2015). Species distribution models either do not account for physiological processes at all or they predict physiological responses with climate information at spatial scales much greater than the study species and averaged across temporal periods irrelevant to the fine-scale variation in energetic demand (see Chapter 3; Kearney and Porter 2009; Bramer et al. 2018). Predicting physiological responses of organisms at biologically relevant scales is imperative for ectotherms, because areas estimated to provide low standard metabolic rate (SMR) may provide highly suitable habitat or important connectivity pathways

due the low energetic costs of maintenance to survive in those areas (Cushman 2006; Kearney and Porter 2009). Furthermore, because warmer air increases the magnitude of drying, high vapor pressure deficits (VPD) may limit foraging activity of plethodontids (Riddell and Sears 2015; Riddell et al. 2017) and low VPDs may enhance breeding activities for ectotherms (Bellis 1962). Therefore, locating physiologically suitable microhabitat, where low VPDs and low SMR co-occur, may be a critical mechanistic component to plethodontid suitable habitat analysis. While there have been substantial advancements in the development of physiological models at microclimatic scales, there remains a need to further enhance physiological models that account for vegetation and other relevant buffers to sub-canopy, near-surface forest climates to provide more accurate estimates (Kearney and Porter 2009, 2016).

There has been a call to develop SDMs with microclimatic data at biologically relevant scales and broad spatial extents (Lembrechts et al. 2018). This is a critical step for conservation management of small or dispersal-limited, ground-dwelling species that may be vulnerable to climate change (Cushman 2006; Hoegh-Guldberg et al. 2008; Kearney and Porter 2009; Clusella-Trullas et al. 2011). Plethodontid salamanders are lungless ectotherms vulnerable to climate change because they thrive in the cool, moist microclimates of montane ecosystems, disperse short distances during limited surface active periods (Feder 1983; Lutterschmidt and Hutchison 1997; Bernardo and Spotila 2006; Connette et al. 2015), and increases in temperature can affect their overall fitness (Sears 2005; DuRant et al. 2007). Plethodontid distributions and range extents are largely determined by climate and have been projected to drastically shrink in area or be completely lost under mid-century climate projections (Milanovich et al. 2010; Gifford and Kozak 2012).

Here, we used highly spatially resolved maps (3 m^2 resolution) of near-surface, microclimatic temperature (Stickley and Fraterrigo 2021) to model current and future distributions, VPD, and SMR during periods of increased surface activity (March-November) for three terrestrial salamander species in Great Smoky Mountains National Park (GSMNP; Tennessee and North Carolina, US). Because lower energetic demand and increased moisture suggest higher surface activity and performance for plethodontids (Feder and Pough 1975; Pough 1980; Sears 2005; DuRant et al. 2007; Riddell and Sears 2015), we evaluated the agreement between suitable habitat from species distribution models with VPD and SMR. Furthermore, we integrated model predictions to identify areas of low energetic cost of maintenance (i.e., where low VPD and low SMR coincide) in suitable microclimatic habitat and areas that enhance functional connectivity between fragmented areas of suitable habitat. We also quantified future changes in surface activity area, suitable habitat, and salamander physiology at the microscale. Additionally, we tested the "spatial resolution paradox" by evaluating spatial discrepancies between microclimatic and coarse resolution predictions of suitable habitat and predictions from models of salamander metabolic rate.

Materials and Methods

Study area and species

This study was conducted in GSMNP which straddles the North Carolina and Tennessee border (Fig. 4.1). The study area included the entirety of the park plus a 150-meter buffer for a total area of 2,430 km^2 (Fig. 4.1). Great Smoky Mountains National Park ranges in elevation from 265 to 2,025 m above sea level. This topographical variation and the accompanying diversity of vegetation within the mostly deciduous forests (Whittaker et al. 2007) create the

cool, moist microclimates that lungless, plethodontid salamanders require for exchanging gases across their skin without risking desiccation (Petranka, 1998). The GSMNP, nicknamed the "Salamander Capital of the World", is known to shelter very high levels of species richness and endemism of plethodontid salamanders (Kozak and Wiens 2010; Gifford and Kozak 2012).

We studied three plethodontid salamander species that vary in body size across different sex and stage classes. The smallest species, *Desmognathus wrighti* (pygmy salamander), ranges from 37-51 mm in total length (TL) at an adult stage. A medium sized species, *Desmognathus ocoee* (Ocoee salamander), ranges from 70-110 mm in TL at an adult. The largest of our study species, *Plethodon jordani* (Jordan's or red-cheeked salamander), ranges from 85-185 mm in TL at an adult stage. All three species are high elevation specialists occuring between 750-2,025 m and widely distributed throughout the GSMNP forests (Dodd 2004). *Desmognathus wrighti* and *P. jordani* are fully terrestrial species and *P. jordani* is endemic to the GSMNP region (Dodd 2004). *Desmognathus ocoee* is also terrestrial in the higher elevations of the GSMNP but is a streamside salamander with a more complicated life history and larval stage, laying eggs in small streams or seepages, especially at lower elevations (Dodd 2004). However, all three study species have been shown to follow Bergmann's rule, increasing in length and body mass at higher elevations (see Chapter 3; Peterman et al. 2016).

Modeling current and future physiology

We modeled current and future SMR (volume of oxygen consumption, VO_2 $\mu l\ g^{-1}\ hr^{-1}$) for each sex and stage class (male, female, and juvenile) of the three study species. Following the approach in Chapter 3, we combined species specific body mass predictions that account for body mass-elevation relationships with seasonal maps of minimum and maximum microclimatic

temperature (Stickley and Fraterrigo 2021). Because we used monthly climate data as inputs, we refer to spring, summer, and fall as the monthly averages of March-May, June-August, and September-November, respectively. Minimum and maximum SMR (i.e., SMR during nighttime minimum and daytime maximum temperatures) were calculated for each sex and stage class of the study species separately using the equations of Feder (1976, 1983), which predict SMR for temperate plethodontid species as a function of temperature and body mass. For *P. jordani*, we also estimated SMR using a formula that incorporated body mass measurements to obtain more accurate estimates of percent change in SMR (Gifford and Kozak 2012) and averaged those predictions with the Feder (1976, 1983) predictions to reduce uncertainty. Detailed information about the modeling approach are available in Stickley and Fraterrigo (2021). Overall, we developed 162 gridded maps of seasonal minimum and maximum SMR (3 species x 3 sex/stage classes x 3 seasons x 2 temperature estimates x 3 time periods) by applying the SMR formulas described above to the maps of microclimatic temperature and body mass.

Because the microclimatic maps are computationally expensive, we randomly selected 50,000 points across GSMNP, extracted SMR values from the seasonal SMR maps, and calculated bootstrapped statistics from the extracted points. We also calculated the percent change in SMR across time periods (i.e., 2006-2010 average, 2030, and 2050) as

$$(SMR_{t+1} - SMR_t)/SMR_t,$$

where $_t$ is the initial time period and $_{t+1}$ is the following time period. This allowed us to compare changes in SMR while accounting for allometric differences among species, and sex and stage classes. Further details can be found in the Appendix C.

Modeling current and future vapor pressure deficit

Because plethodontid salamanders increase surface and foraging activity under low VPD conditions (Riddell and Sears 2015), and plethodontids are mostly surface active at night, we estimated minimum VPD to include in our analysis. To model monthly and seasonal minimum VPD (kPa), we used our microclimatic temperature dataset as input temperature maps and followed similar methodologies to Allen et al. (1998). Here, VPD is measured as the difference between the amount of water vapor the air is capable of holding at saturation less the actual water vapor in the air, which is calculated as

$$VPD_{Min} = e_{sMin} - e_{aMin}$$

where (e_{sMin}) is saturation water vapor pressure (kPa) during minimum temperatures and (e_a) is actual water vapor pressure (kPa) during minimum temperatures. We used the microclimatic minimum temperature maps to estimate e_{sMin} as

$$e_{sMin} = 0.611 * \exp(17.3 * T_{min} / T_{min} + 237.3)$$

where T_{min} is minimum temperature (^{o}C). We estimate e_{aMin} as

$$e_{aMin} = RH * e_{sMin} / 100$$

where RH is relative humidity (%) and calculated as

$$RH = 100 * (SH * p) / e_{sMin} * 0.622$$

where SH is specific humidity (kg/kg) and p is atmospheric pressure. Atmospheric pressure is corrected for elevation as

$$p = p_{sea\ level} * (293\text{-}0.0065 * Elevation / 293)^{5.26}$$

where $p_{sea\ level}$ is atmospheric pressure at sea level (101.3 kPa) and Elevation is elevation in meters above sea level. Specific humidity was extracted from the Multivariate Adaptive Constructed Analogs (MACA) dataset (Abatzoglou and Brown 2012). We downloaded NetCDF

files of monthly specific humidity estimates at a 4 km^2 spatial resolution for the months of March through April during 2006-2010, 2030, and 2050. Monthly specific humidity estimates from 20 climate projections (Abatzoglou and Brown 2012; http://www.climatologylab.org/) were averaged into ensemble models for each month of these study years. We used projections estimated under Representative Concentration Pathway (RCP) 8.5 because this highly aggressive emissions scenario shows close agreement to current trends and is recommended for future climate projections through the mid-century (Schwalm et al. 2020). The 4 km^2 rasters were resampled to a ~3m^2 grid size to match the spatial resolution of the other raster datasets used for the VPD calculation. Because we used monthly data, we refer to spring, summer, and fall as the monthly averages of March-May, June-August, and September-November, respectively.

Modeling current and future suitable habitat

To develop climate inputs for SDMs at differing spatial resolutions, we used microclimatic temperature maps (3m^2 spatial resolution) from Stickley and Fraterrigo (2021) and coarse resolution climate maps (30 arc-second resolution was ~0.85 km^2 after projection) from the National Aeronautics and Space Administration Earth Exchange Downscaled Climate Projections (Thrasher et al. 2013; NEX-DCP30) dataset. The microclimatic temperature maps consisted of monthly minimum and maximum temperature predictions during the growing season (March-November) from 2006 to 2010. We downloaded monthly temperature and precipitation maps during the same months (March-November) from NEX-DCP30 from 2006-2010, 2030, and 2050. For future climate predictions, we used projections from an ensemble model produced with Representative Concentration Pathway (RCP) 8.5 because this emissions scenario shows close agreement to current trends and is recommended for future climate

projections through the mid-century (Schwalm et al. 2020). For future microclimatic temperature predictions, we calculated spatially explicit temperature anomalies with the NASA NEX-DCP30 dataset by subtracting the monthly temperature estimates for the current period (monthly average from 2006-2010) from the temperature estimates for the future period (2030 and 2050). The monthly temperature anomaly maps were resampled to match the spatial resolution of the microclimatic maps, then added to the current monthly microclimatic maps to develop fine resolution predictions of future temperature. We used current and future temperature predictions to estimate changes in future microclimatic temperature and surface active area (i.e., area in km^2 that falls within the preferred temperature range 12-26 ^oC; Brattstrom 1979; Farallo and Miles 2016) across GSMNP. Precipitation maps from NASA NEX-DCP30 were resampled to match the spatial resolution of the microclimatic maps for use in microclimatic modeling of suitable habitat.

We modeled the probability of suitable habitat and the range extent for each study species (*D. wrighti*, *D. ocoee*, and *P. jordani*) across the GSMNP for the 2006-2010, 2030, and 2050 time periods using bioclimatic variables and species occurrence data. Current and future monthly temperature predictions and precipitation predictions were used to calculate 11 bioclimatic variables demonstrated to be biologically relevant and interpretable for plethodontid salamanders (Rissler and Apodaca 2007; Milanovich et al. 2010; Supplementary Table C.1). We calculated all bioclimatic variables specifically during the growing season months to develop predictions during periods of increased surface activity for plethodontid salamanders (March-November). We obtained historical presence-only data for each study species from Peterman et al. (2016), the Illinois Natural History Survey (https://herpetology.inhs.illinois.edu/databases/), the Smithsonian National Museum of Natural History (https://collections.nmnh.si.edu/search/), the Hands on the

Land Network (https://handsontheland.org/), and from Milanovich et al. (2010) via HerpNET (www.herpnet.org) and Global Biodiversity Information Facility (www.gbif.org). After compilation and removal of duplicate points, presence locations included 205, 158, and 316 points for *D. wrighti*, *D. ocoee*, and *P. jordani*, respectively (Fig. 4.1).

We used a maximum entropy (MaxEnt) approach to estimate suitable habitat for each species because MaxEnt (Elith et al. 2006) is the most widely-used program for species distribution modeling due to accuracy with presence-only occurrence data (Hernandez et al. 2006; Elith et al. 2011; Merow et al. 2013). We followed methodologies for data preparation, model fitting, model prediction, and model evaluation as recommended by Hijmans and Elith (2017). Model goodness of fit was assessed using the average area under the curve (AUC) and we considered model fit with AUC ≥ 0.7 to be valid for estimating current and future habitat suitability. We evaluated models using *k*-fold cross validation to ensure the use of all data points while reducing variance. The models and threshold values produced for the 2006-2010 time period were used to predict the future range and suitable habitat with the bioclimate estimates for 2030 and 2050. Overall, we produced 18 species distribution models at microclimatic and coarse resolutions (3 species x 3 time periods x 2 model approaches). We also characterized changes in fragmentation of suitable habitat for each microclimatic model by calculating patch density (PD) as the number of individual patches of the species' range divided by the area of the range.

To assess the spatiotemporal differences between microclimatic and coarse resolution predictions of suitable habitat, we calculated the differences between model outputs as NASA NEX-DCP30 prediction less the microclimatic predictions for each time period (2006-2010, 2030, and 2050). Using these values, we determined the average difference in suitability within the predicted species' ranges and in areas within and outside of highly suitable habitat

(probability of suitable habitat ≥ 0.7). We also compared the extent (km^2) of predicted species' ranges and highly suitable habitat for each species and each model and calculated percent change in area from current (2006-2010 average) predictions to 2030 and 2050 projections. Further details can be found in the Appendix C.

Integrating physiology and suitable habitat

To evaluate the agreement between physiological variables and suitable habitat predictions across spatial scales, we used correlation coefficients, estimated from the modified t-test (Clifford et al. 1989), between SMR (minimum and maximum) or VPD and the probability of suitable habitat within the predicted species' range. We used the modified t-test, based on the work of Clifford et al. (1989), because this method creates an appropriate sample size to account for spatial autocorrelation and corrects correlation coefficients between two spatially correlated sequences. To evaluate the association between variables, we extracted values for each variable and location (i.e., latitude and longitude) at 50,000 randomly selected points within each species' predicted range extent within GSMNP. Negative correlations ≤ -0.7 indicated model agreement and positive correlations ≥ 0.7 indicated model disagreement. We conducted separate analyses for each season during the 2006-2010 and 2050 time periods and for microclimatic and coarse resolution, aggregated predictions. We previously examined the agreement between physiological and suitable habitat predictions for these plethodontid species using aggregated SMR data and SDM-predicted habitat suitability at coarse resolutions for the current time period (see Chapter 3). We used a similar approach here to evaluate the agreement between future microclimatic predictions of suitable habitat and SMR to compare microclimatic model agreement and aggregated model agreement under future climate conditions. To develop

aggregated predictions of future habitat suitability, VPD and SMR, we used our microclimatic maps to calculate the mean value for probability of suitable habitat, mean VPD, and mean SMR at the same coarse-resolution (~0.85 km^2). Points were extracted from every raster grid within each species' predicted range for statistical analyses.

To locate suitable habitat and evaluate potential conservation approaches, we integrated predictions of suitable habitat with areas of low energetic cost of maintenance. Here, areas of low energetic cost of maintenance are defined as areas within the species' predicted range where low SMR and VPD co-occur. We grouped areas with low energetic cost of maintenance into high priority areas (HPA) indicated as the SMR and VPD ≤ first quartile (Q_1) and secondary priority areas (SPA) as the SMR between Q_1 and the median. Our previous research indicates that SMR of the three study species varies among seasons and between adults and juveniles (see Chapter 3). We incorporate this variation into the SMR estimates by spatially intersecting SMR for juveniles and adults and across seasons. We also account for temporal connectivity across each time period (i.e., 2010, 2030, 2050), by calculating the average SMR and VPD across time periods, then producing final mapped HPAs and SPAs for each season. After classifying VPD and SMR into priority areas, we spatially intersected seasonal HPAs to locate where the lowest VPD and lowest SMR coincide during spring, summer and fall, thus indicating areas where plethodontids would, on average, experience increased ability for surface activity.

To identify areas of high conservation value, we spatially located areas of overlap between microclimatic predictions of highly suitable habitat (≥ 0.7) with locations of low energetic cost of maintenance based on HPAs. We also used a multiscale approach to target areas of agreement between the aggregated predictions of habitat suitability and VPD by locating the raster grids from broad-resolution maps (~0.85 km^2) that indicated the highest levels of

agreement (i.e., grids where the lowest VPD and highest habitat suitability estimates co-occur). Then, we targeted areas of high conservation value from our microscale (3 m^2) maps that fell within the broad-resolution grids of high predictive agreement. Furthermore, we identified areas of low energetic cost of maintenance (i.e., HPAs or SPAs) outside of each species' range to identify potential pathways of functional connectivity between fragmented suitable habitat patches. We evaluated the strength of habitat connectivity by comparing the change in a habitat fragmentation metric, patch density (PD = patch per km^2), between sole habitat suitability maps and maps that account for both habitat suitability and areas with low energetic cost of maintenance. For connectivity metrics, we only included HPAs and SPAs within dispersal distances between time periods. Although home range size has been shown to typically be < 7.5 m for a plethodontid species, it is accepted that the dispersal ability could be up to a few hundred meters (Welsh and Lind 1992; NatureServe 2021), Therefore, we use a conservative approach and estimate a possible dispersal distance of 300 m per year or 6,000 m between time periods (i.e., from 2010–2030 and 2030-2050). For all spatial and statistical modeling, we used R statistical software v. 3.50 (R Core Team 2020) and ArcGIS® software versions 10.4.1–10.6.1 (Esri 2020). Further details can be found in the Appendix C. All data will be stored and available for download from a public repository when this manuscript is accepted for publication.

Results

Future climate and suitable habitat

From the initial time period (2006-2010) to 2050, average microclimatic temperatures within GSMNP are projected to increase by 2.2 ºC for minimum temperatures (2006-2010 average: spring = 10.8 ºC, summer = 18.4 ºC, autumn = 10.3 ºC; 2050: spring = 12.9 ºC, summer

= 20.5 ºC, autumn = 12.5 ºC) and 2.2 ºC for maximum temperatures (2006-2010 average: spring = 19.6 ºC, summer = 26.0 ºC, autumn = 18.9 ºC; 2050: spring = 21.8 ºC, summer = 28.0 ºC, autumn = 21.4 ºC). The area of potential surface activity (i.e., temperature between 12-26 ºC) is projected to decline 16% and 27% at summer maximum temperatures through 2030 and 2050, respectively (total area of surface activity in 2030 = 712 km^2, 2050 = 446 km^2). However, area of potential surface activity is predicted to increase during the spring (18% by 2030, 53% by 2050) and fall (18% by 2030, 34% by 2050) at nighttime minimum temperatures (total area of surface activity during spring 2030 = 930 km^2, fall 2030 = 707 km^2; spring 2050 = 1,771 km^2, fall 2050 = 1,540 km^2). We found no significant change in area of surface activity during other time periods as roughly 96% of the park area (2,334-2,336 km^2) fell within the surface active temperature range.

Microclimatic SDMs had an average area under the curve (AUC) of 0.80 for the three study species, indicating moderate to high model accuracy (Fig. 4.2; Appendix C Fig. C.1; *D. wrighti* =0.74; *D. ocoee* = 0.86; *P. jordani* = 0.81). The most influential predictor variables were mean temperature of the wettest quarter (WorldClim BIO8) and precipitation of the driest quarter (WorldClim BIO17) for all three species (Appendix C Table C.1). Species distribution models developed with NASA NEX-DCP30 data had an average AUC of 0.90 indicating high model accuracy (Appendix C Fig. C.2; *D. wrighti* = 0.92; *D. ocoee* = 0.91; *P. jordani* = 0.92). The most influential predictor variables varied among each species (Appendix C Table C.1; *D. wrighti* = BIO1, BIO17; *D. ocoee* = BIO7, BIO17, BIO8; *P. jordani* = BIO17, BIO18).

Compared to the initial time period (2006-2010), microclimate-based predictions of species' ranges are projected to shift an average of 0.94 km north and 2.75 km east through 2050 (Fig. 4.3; Appendix C Fig. C.1; *D. wrighti* = 0.21 km north, 0.23 km east; *D. ocoee* = 0.52 km

north, 5.43 km east; *P. jordani* = 2.10 km north, 2.59 km east). By 2050, species' ranges are projected to decline by 74%, 55%, and 80% for *D. wrighti*, *D. ocoee*, and *P. jordani*, respectively (Table 4.1; Fig. 4.3; Appendix C Fig. C.1). Areas of highly suitable habitat (probability ≥ 0.7) are projected to decline by 91%, 92%, and 71% for *D. wrighti*, *D. ocoee*, and *P. jordani*, respectively (Table 4.1; Fig. 4.2). However, we also found some gain in areas of highly suitable habitat under future microclimatic projections for each species with the majority of gain occurring through 2030 and minimal gain from 2030 to 2050 (Fig. 4.2). In total, *D. wrighti* and *D. ocoee* are estimated to gain 9 km^2 and 3 km^2, respectively, in area of highly suitable habitat. *Plethodon jordani* is estimated to gain 39 km^2 of highly suitable habitat under future SDM projections. For *P. jordani* and *D. ocoee*, average elevation for area of gain in highly suitable habitat is estimated to be at higher elevations (*P. jordani* = 1,481 m, *D. ocoee* = 1,836 m) compared to areas of loss in highly suitable habitat (*P. jordani* = 1,357 m, *D. ocoee* = 1,574 m). The opposite pattern was found for D. wrighti (gain = 1,426 m, loss = 1,538 m). For all species, gain in highly suitable habitat is estimated at increasingly southwestern aspects (D. *wrighti* = 189, *D. ocoee* = 176, *P. jordani* = 189) compared to losses in highly suitable habitat at southeastern aspects (D. *wrighti* = 179, *D. ocoee* = 159, *P. jordani* = 165). Fragmentation of suitable habitat is projected to increase for all species by an average of 265 patches/km^2, more than doubling for *D. wrighti* and *P. jordani* by 2050 (Appendix C Table C.2).

Compared to microclimate-based predictions, predicted suitable habitat and range extents based on coarse-resolution, free-air temperatures were larger for all species during the 2006-2010 time period. However, the estimated amount of future range loss and loss of highly suitable habitat varied among species and models (Table 4.1; Appendix C Fig. C.1, C.2). For the 2006-2010 time period, species' ranges predicted from coarse-resolution, free-air temperatures were

13.7% larger than those predicted from microclimate temperatures (*D. wrighti* = 19%, *D. ocoee* = 10%, and *P. jordani* = 12%), and area of highly suitable habitat was 40.3% larger than microclimatic predictions (Table 4.1; *D. wrighti* = 20%, *D. ocoee* = 45%, and *P. jordani* = 56%). The coarse-resolution models predict a larger 2050 range but lower area of highly suitable habitat for *D. wrighti*, and a larger 2050 range and larger area of highly suitable habitat for *D. ocoee* (Table 4.1). By 2050, *P. jordani* is projected to lose 99% of its range extent and 100% of highly suitable habitat based on coarse-resolution predictions, a considerably larger loss of habitat compared to the microclimatic estimates of 80% and 71% declines, respectively (Table 4.1; Appendix C Fig. C.2).

For the 2006-2010 time period, the coarse-resolution predictions indicated a higher probability of suitable habitat for all species compared to microclimatic projections, but the probability of suitable habitat was lower within areas of highly suitable habitat (Fig. 4.3; Appendix C Table C.3). By 2050, coarse-resolution predictions project lower probability of suitable habitat for each species' range, except for *D. ocoee* (Fig. 4.3). Under current and future conditions, coarse-resolution predictions for the probability of suitable habitat were found to be consistently lower within areas of highly suitable habitat as compared to microclimatic predictions (Fig. 4.3; Appendix C Table C.3).

Physiological changes under future climate

The rate at which SMR increases under future temperature projections varied among each species, between nighttime and daytime temperatures (i.e., minimum and maximum SMR), and among season (Fig. 4.4; Appendix C Fig. C.3-C.6). By 2050, SMR is estimated to increase by an average of 13.5%, 6.5%, and 13.2% for *D. wrighti*, *D. ocoee*, and *P. jordani*, respectively.

Percent change in SMR from the 2006-2010 time period to 2030 and to 2050 is estimated to be greater during nighttime minimum temperatures for *D. wrighti* and *D. ocoee*, but marginally higher during daytime maximum temperatures for *P. jordani* (Fig. 4.4; Appendix C Fig. C.6). For *D. wrighti* and *D. ocoee*, juvenile stage classes exhibited significantly higher SMR increases during minimum temperatures with the highest rates and highest variation during spring and autumn (Fig. 4.4). Juvenile estimates for *P. jordani* did not differ significantly, and seasonal variation was minimal for all sex and stage classes of *P. jordani* (Fig. 4.4).

Integrating physiology and suitable habitat

Results from modified t-tests indicated negative correlations between fine resolution SMR and suitable habitat within *D. wrighti* and *P. jordani* ranges during the 2006-2010 period, but the relationships were weak to moderate on average (Appendix C Table C.4; *D. wrighti*, $\bar{x}$ = -0.14$\pm$ 0.13; *P. jordani*, $\bar{x}$ = -0.49$\pm$ 0.13). However, within the *D. ocoee* range correlations were strong and positive on average (Appendix C Table C.4; $\bar{x}$ = 0.67$\pm$ 0.03). Correlations between fine resolution suitable habitat and VPD were moderate in strength and negative (Appendix C Table C.4; *D. wrighti*, $\bar{x}$ = -0.47$\pm$ 0.08; *P. jordani*, $\bar{x}$ = -0.38$\pm$ 0.07; *P. jordani*, $\bar{x}$ = -0.36$\pm$ 0.08). In general, predictions based on coarse-resolution, aggregated data indicated a higher magnitude in correlation between the probability of suitable habitat with SMR and VPD compared to fine resolution data (Appendix C Table C.5). Under future climate projections for 2050, we found no substantial correlation between predictions of fine resolution SMR and suitable habitat (Appendix C Table C.4; *D. wrighti*, $\bar{x}$ = -0.02$\pm$ 0.04; *D. ocoee*, $\bar{x}$ = 0.28$\pm$ 0.04; *P. jordani*, $\bar{x}$ = -0.01$\pm$ 0.05). Correlations between fine resolution suitable habitat and VPD were weak to moderate under future climate projections for 2050 (Appendix C Table C.4; *D. wrighti*, $\bar{x}$ = -

0.20± 0.04; *D. ocoee*, $\bar{x}$ = -0.38± 0.04; *P. jordani*, $\bar{x}$ = 0.09± 0.03). However, aggregating future microclimatic habitat estimates, SMR, and VPD to coarser resolutions (~0.85 km^2) increased correlation magnitudes (Appendix C Table C.5; *D. wrighti*, Δ*SMR* r = -0.24, ΔVPD r = -0.25; *D. ocoee*, Δ*SMR* r = 0.22, ΔVPD r = 0.02; *P. jordani*, Δ*SMR* r = -0.26, ΔVPD r = -0.15).

In total, we located large extents of high conservation value (i.e., agreement between areas of highly suitable habitat with HPAs) for *D. wrighti* and *P. jordani* but considerably less area was located for *D. ocoee* (Fig. 4.5; Appendix C Fig. C.7). For the 2006-2010 period, area of high conservation value was greater for *P. jordani* (84 km^2, 33% of highly suitable habitat) compared to *D. wrighti* (48 km^2, 20% of highly suitable habitat) and *D. ocoee* (2 km^2, 1% of highly suitable habitat). By 2050, area of agreement is estimated to be considerably larger for *P. jordani* (32 km^2, 43% of highly suitable habitat) compared to *D. wrighti* (2 km^2, 9% of highly suitable habitat) and *D. ocoee* (< 1 km^2, < 1% of highly suitable habitat area). Using the multiscale approach to first target broad-scale agreement between habitat suitability and low SMR resulted in the ability to narrow down targets of high conservation value with an average of 0.14 km^2 and 0.13 km^2 in area of high conservation value per coarse-resolution grid cell for 2010 and 2050 estimates, respectively (*D. wrighti* 2010 = 0.16 km^2, 2050 = 0.09 km^2; *D. ocoee* 2010 = < 0.01 km^2, 2050 = < 0.01 km^2: *P. jordani* 2010 = 0.26 km^2, 2050 = 0.30 km^2).

Integration of functional pathways (i.e., HPAs and SPAs between fragmented areas of suitable habitat) with projected range extents enhanced connectivity by reducing fragmentation of habitat for each species (Fig. 4.5; Appendix C Table C.2, Fig. C.8). When functional pathways are integrated with species' ranges, fragmentation is estimated to decrease by 36%, 47%, and 26% in 2050 for D. wrighti, D. ocoee, and P. jordani, respectively (Appendix C Table C.2, Fig. C.8).

Discussion

It is critically important to protect areas where species may persist under future climate conditions (Faleiro and Machado 2013; Jones et al. 2016a; Elsen et al. 2020). However, conservation approaches commonly disregard microclimatic regimes and biophysical responses to microclimatic conditions at spatiotemporal scales relevant to a multitude of species threatened from climate change (Kearney and Porter 2009; Potter et al. 2013; Lenoir et al. 2017; Ripple et al. 2017). Here, we answer the call to incorporate microclimate into SDMs at broad extents (Lembrechts et al. 2018) by developing microclimatic SDMs at a 3 m^2 spatial resolution across GSMNP (2,430 km^2 spatial extent). By comparing microclimatic models of suitable habitat, which account for the buffering effect of forest vegetation on near-surface temperatures, to coarse resolution SDMs, we found potential mismatches across spatial scales. Furthermore, we demonstrate approaches to integrating mechanistic and correlative models for locating areas of high conservation value (i.e., where suitable habitat, low VPD, and low SMR co-occur), which may increase efficiency and flexibility in spatial conservation planning and increase habitat connectivity.

Using a multiscale approach to locate areas of high conservation value may have multiple benefits. We found large extents of high conservation value for *D. wrighti* and *P. jordani*, but substantially less area of high conservation value for *D. ocoee* due to increased levels of model disagreement between predictions of suitable habitat and metabolic rate (Appendix C Table C.4, C.5). For *D. wrighti* and *P. jordani*, a multiscale approach is beneficial because it allows for prioritizing the vast extent of potentially important microscale habitat by first locating broad-scale areas of co-occurrence between models, then targeting the microscale areas of co-occurrence between suitable habitat and areas of high conservation value among a choice of

assets (Fig. 4.5; Appendix C Fig. C.7). However, a multiscale approach may also be useful for *D. ocoee* because it allows for flexibility in targeting the broad extents that contain the vast majority of high conservation value. For example, targeting areas of high conservation value for *D. ocoee* required a backwards approach by first assessing locations with the highest model agreement between suitable habitat and vapor pressure deficit, then moving backwards to areas that may exhibit less model agreement but spatially higher levels of conservation value (Appendix C Fig. C.7). In both examples, the multiscale approach gives more options for choosing areas to target for conservation and allows for prioritizing large extents into smaller, more manageable assets. This is the type of efficiency, flexibility, and risk spreading that is called for in systematic conservation planning (Possingham et al. 2006).

We also found that targeting areas of low energetic cost of maintenance (i.e., where low VPD and low SMR co-occur) between fragmented patches of suitable habitat may provide conservation targets of potential functional connectivity under future projections of suitable habitat (Fig. 4.5; Appendix C Fig. C.8). Including these areas of low energetic cost of maintenance as potentially suitable habitat could reduce fragmentation estimates under future climate scenarios (Appendix C Table C.2). Furthermore, the incorporation of temporal differences into estimates of low energetic cost of maintenance may reduce uncertainty in these connectivity pathways under future climate conditions, an important aspect for developing robust conservation plans (Groves et al. 2012; Schmitz et al. 2015; Jones et al. 2016).

Our results also demonstrate other types of flexibility that could benefit spatial prioritization of future conservation assets under climate change. For instance, we found that future predictions of energetic demand vary among species, between adults and juveniles, and temporally among daily or seasonal temperatures (Fig. 4.4; Appendix C C.3-C.6). These

variations in energetic demand were incorporated into conservation plans by targeting intersected locations of low VPD with low SMR across future time periods (i.e., through 2030 and 2050) for different stage classes of the study species and across multiple seasons of potential surface activity. This may help enhance species' protection at different life stages and during critical temporal periods. For example, the high elevation plethodontid salamanders of GSMNP are typically surface active at night during the summer (Petranka 1998; Dodd 2004; Connette et al. 2015). However, temperature projections indicated large increases in surface activity area during spring and autumn minimum temperatures. Intersecting areas with low SMR and low VPD during these time periods of increased surface activity (e.g., summer nighttime) may allow for the identification of spatiotemporally explicit conservation targets (Fig. 4.5; Appendix C Fig. C.7, C.8).

Similarly, this integrative approach supports the development of conservation plans at different levels of taxonomic organization. Targeting locations of low energetic cost of maintenance for entire taxa could greatly reduce uncertainty in spatial prioritization should these species have closely related niche requirements (i.e., phylogenetic niche conservatism; Mokany and Ferrier 2011; Jones et al. 2016; Wiens et al. 2009; Evans et al. 2015). Alternatively, targeting locations for specific species or stage classes may be important should more robust demographic analyses be needed. For example, population connectivity among amphibians is often dependent upon juvenile dispersal (Cushman 2006), so the use of connectivity maps that account for juvenile variation in physiology may be desired over species-level estimates. These approaches could allow for very specific conservation targets or intersected targets that reduce uncertainty by accounting for variations in SMR, a necessity for small or dispersal-limited species that may

need to move across the landscape as suitable habitat areas decline or become more fragmented (Fahrig 2003; Cushman 2006).

Indeed, we found substantial fragmentation and loss of suitable habitat by mid-century for our three study species (Table 4.1; Fig. 4.2; Appendix C Fig. C.1, C.2). These results are similar to the findings of other studies that assessed future habitat suitability of high elevation plethodontid species (Parra-Olea et al. 2005; Milanovich et al. 2010; Sutton et al. 2015; Jacobsen et al. 2020). However, the losses estimated using microclimatic SDMs were not as severe as projections from some of these previous studies. For example, Milanovich et al. (2010) projected loss of habitat to be much greater by 2050 for the same species we studied, with an average loss 25.5% greater than our microclimatic estimates. Similar to our estimates from the coarse resolution NASA NEX-DCP30 model, Milanovich et al. (2010) estimated over a 99% reduction in *P. jordani* suitable habitat by 2050, indicating near extinction for this species. Our microclimatic models indicated a roughly 80% loss in suitable habitat. Differences in spatial resolution may be a factor, but we found mixed results that indicated our microclimatic estimates projected decreased and increased range losses compared to coarse-resolution predictions depending upon the species (Table 4.1). Because the only differences among our SDMs were the temperature inputs (i.e., microclimatic and NASA NEX-DCP30), these results indicate large potential for over- or underestimation of species' ranges with free-air, coarse resolution climate data.

We also found that coarse resolution SDMs consistently overestimated the probability of suitable habitat in each species range, but underestimated within areas of highly suitable habitat (Fig. 4.3). These underestimations were amplified under future climate projections, indicating that the most important areas to target for conservation may be undervalued by coarse resolution

climate models (Fig. 4.3). The “spatial resolution paradox” suggests that coarse resolution SDMs may simultaneously overestimate suitable habitat regionally but underestimate suitable habitat locally (Lenoir et al. 2017). For instance, bias from coarse resolution SDMs has been shown to overestimate thermal tolerances and suitable habitat regionally (Trivedi et al. 2008; Franklin et al. 2013) while underestimating locations of climatically stable locations of potential microrefugia (Franklin et al. 2013). Our findings of over- and underestimation across spatial scales agree with this paradox in terms of valuing suitable habitat and highlight an important disparity between SDMs developed from fine resolution, microclimatic and coarse resolution, free-air temperature data. Because finer resolution climate data are likely to produce more accurate predictions of species distributions compared to broader model inputs (Gillingham et al. 2012a), we believe the use of more robust climate inputs, that account for the effects of vegetation and biophysical interactions of forest microclimate, will be imperative for developing robust conservation targets at an appropriate biological level for many species vulnerable to climate change (Lembrechts et al. 2018; Stickley and Fraterrigo 2021).

Our results also demonstrate the value of bottom-up scaling for assessing model agreement between suitable habitat and salamander bioenergetics, because the aggregated data resulted in increased correlations between model predictions (Fig. 4.5; Appendix C Fig. C.7). Finding these broad scale trends in model agreement or disagreement allows for more precise targeting of locations with low energetic cost of maintenance within projected suitable habitat at the microscale (Fig. 4.5; Appendix C Fig. C.7). It has been shown that correlations are likely to increase between spatial variables at aggregated scales, but the use of scaling approaches has long been controversial due to potential problems in interpreting ecological processes (Turner et

al. 1989; Marceau 1999; Perveen and James 2012). However, our results show this can be a useful tactic for locating future suitable habitat.

We note that this study has limitations that should be considered. First, we specifically use a common, maximum entropy approach to modeling suitable habitat with bioclimatic variables shown to be important to our study species (Elith et al. 2006, 2011; Rissler and Apodaca 2007; Milanovich et al. 2010). There is likely an array of other types of data or abiotic and biotic variables that have causal relationships to the distributions of our study species but were unable to be captured in our predictions (Araújo et al. 2019; Leitão and Santos 2019). Furthermore, using an ensemble approach to modeling species' distributions would help limit uncertainty. While our microclimatic temperature models account for vegetation buffering of near-surface temperatures and our physiological models account for the body mass-elevation relationships found for the three study species, the suitable habitat projections should be considered conservative because other biological processes that can influence organismal responses to climate change were not represented (e.g., behavioral changes). We also note that there are potential misidentifications of *D. ocoee* occurrence points due to similar appearance to *D. imitator*, and combined with the complicated life history of *D. ocoee*, estimates for areas of high conservation value with this species should be considered very conservative (see Chapter 3). Furthermore, the conservation strategies evaluated in this study are within the GSMNP region, an already protected area. However, the approach we developed should be useful for further research in the region or for park management and can certainly be applied to other forested environments globally as the availability of finer resolution data become available (Lefsky et al. 2002; Bramer et al. 2018; Zellweger et al. 2019b).

The findings from this study elucidate problems associated with relying on coarse resolution SDMs and demonstrate the potential for enhancing connectivity and targeting future suitable microclimatic habitat at a fine resolution. Additionally, the integration of physiological variability among stage classes of species and temporally among seasons can help reduce uncertainty under future climate conditions. This is an essential step in accurately predicting organismal responses to future climate change, especially for species like plethodontid salamanders that are reliant on the availability of physiologically and climatically suitable habitat for regional persistence (Milanovich et al. 2010; Gifford and Kozak 2012). Targeting locations in the microhabitat where species may find microclimatic refugia (Hannah et al. 2014; Lenoir et al. 2017) or functional connectivity (Groves et al. 2012; Nunez et al. 2013; Jones et al. 2016) to future suitable habitats is imperative for all species that need to outpace climate change (Loarie et al. 2009). The techniques we apply in this study may also be valuable in searching for potential sites of translocation or assisted migration (Hoegh-Guldberg et al. 2008; Jones et al. 2016). Because climate change is a major threat to the loss of species' ranges (Urban 2015), further approaches to integrating microclimatic inputs into SDMs, along with mechanistic approaches, are greatly needed. The conservation of a great portion of global biodiversity will be dependent on strengthening predictions of organismal responses to climate change at the microscale.

Figures

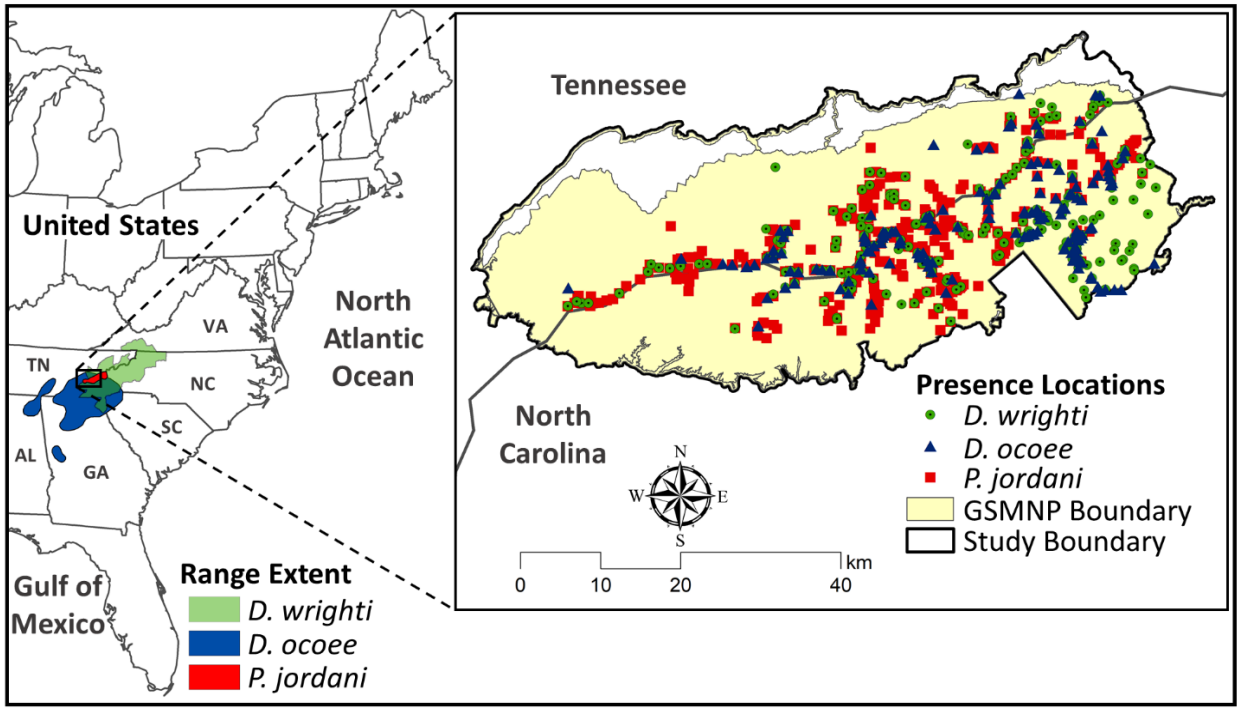

Figure 4.1. Location of Great Smoky Mountains National Park (GSMNP) and study area on the border of North Carolina and Tennessee in the southern Appalachian Mountains. The symbols indicate the presence locations used to model suitable habitat for each species. Also shown are the estimated range extents for each species (IUCN Red List 2021)

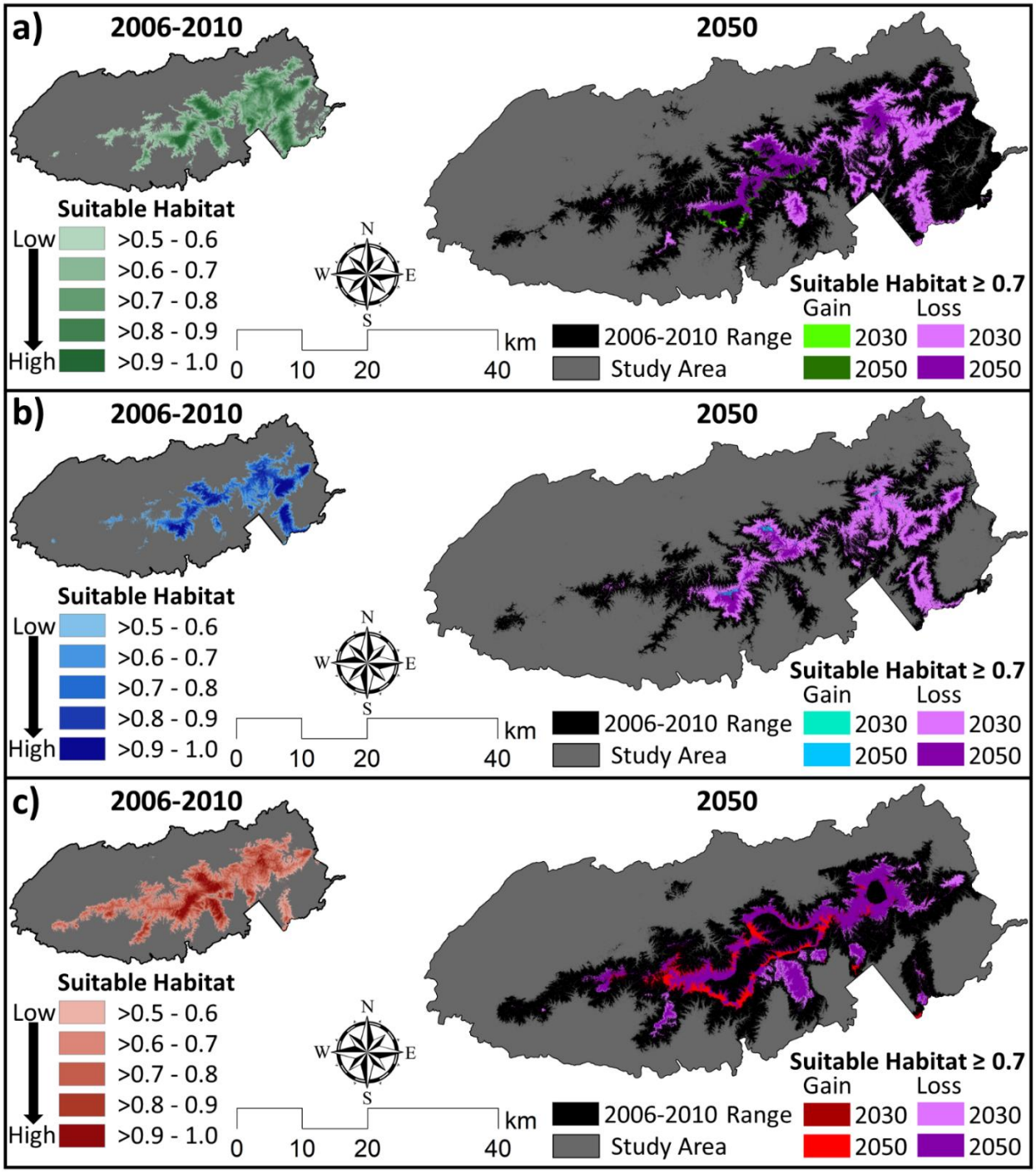

Figure 4.2. Microclimatic species distribution models displaying the probability of suitable habitat for the 2006-2010 time period (left) and loss or gain in highly suitable habitat (probability ≥ 0.7) in 2050 (right) for (a) *Desmognathus wrighti*, (b) *Desmognathus ocoee*, and (c) *Plethodon jordani*. Scale bar represents 2050 map

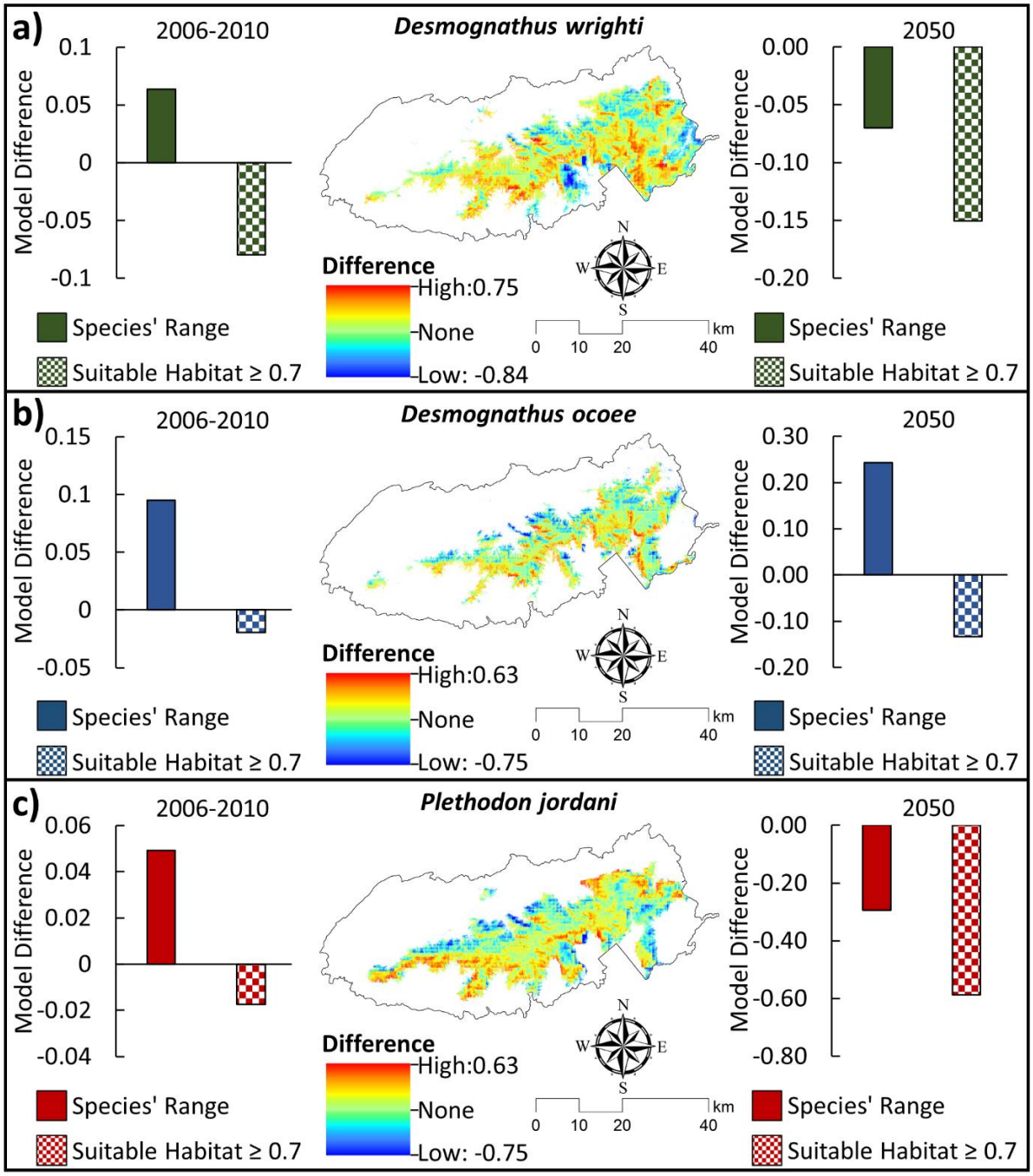

Figure 4.3. Graphs and heatmap showing the difference in the probability of suitable habitat between species distribution models derived from NASA NEX-DCP30 coarse-resolution, free-air temperature data and microclimatic temperature data. Bar graphs represent the mean difference within the predicted species' range and within predicted areas of highly suitable habitat (probability ≥ 0.7) during the 2006-2010 and 2050 periods for (a) *Desmognathus wrighti*, (b) *Desmognathus ocoee*, and (c) *Plethodon jordani*. Heat maps display the differences during the 2006-2010 period. Positive values indicate higher predictions by NASA NEX-DCP30 (overestimation) and negative values indicate lower predictions (underestimation) compared to microclimatic predictions

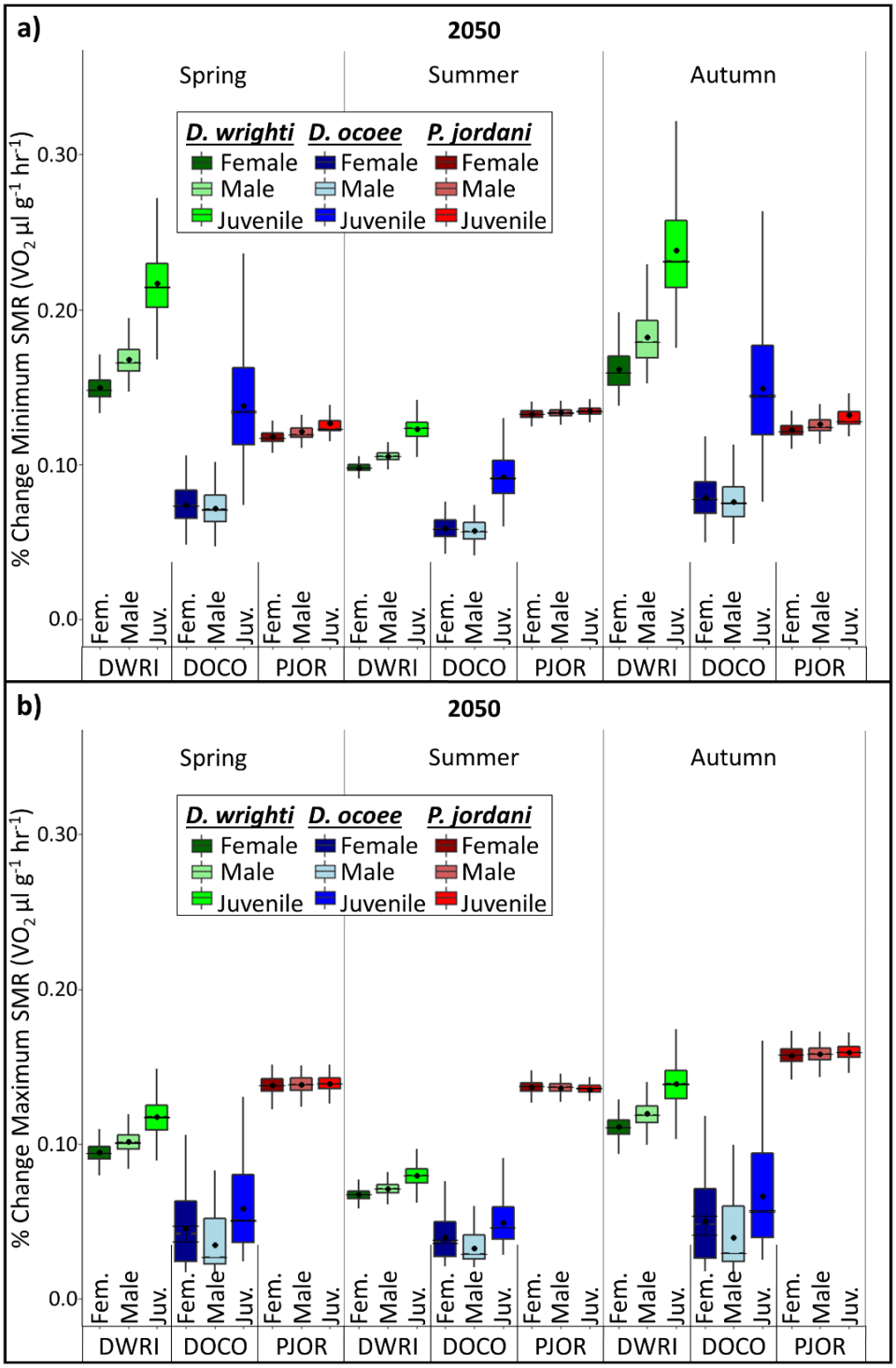

Figure 4.4. Percent change in minimum and maximum standard metabolic rate (SMR) between the 2006-2010 average and 2050 during spring, summer, and fall months. Shown are estimates for the sex and stage class (male, female, and juvenile) for *Desmognathus wrighti* (DWRI), *Desmognathus ocoee* (DOCO), and *Plethodon jordani* (PJOR). Points indicate the bootstrapped mean and central error bar lines indicate the confidence interval for the bootstrapped median. Vertical lines indicate the error bar for standard deviation of mean

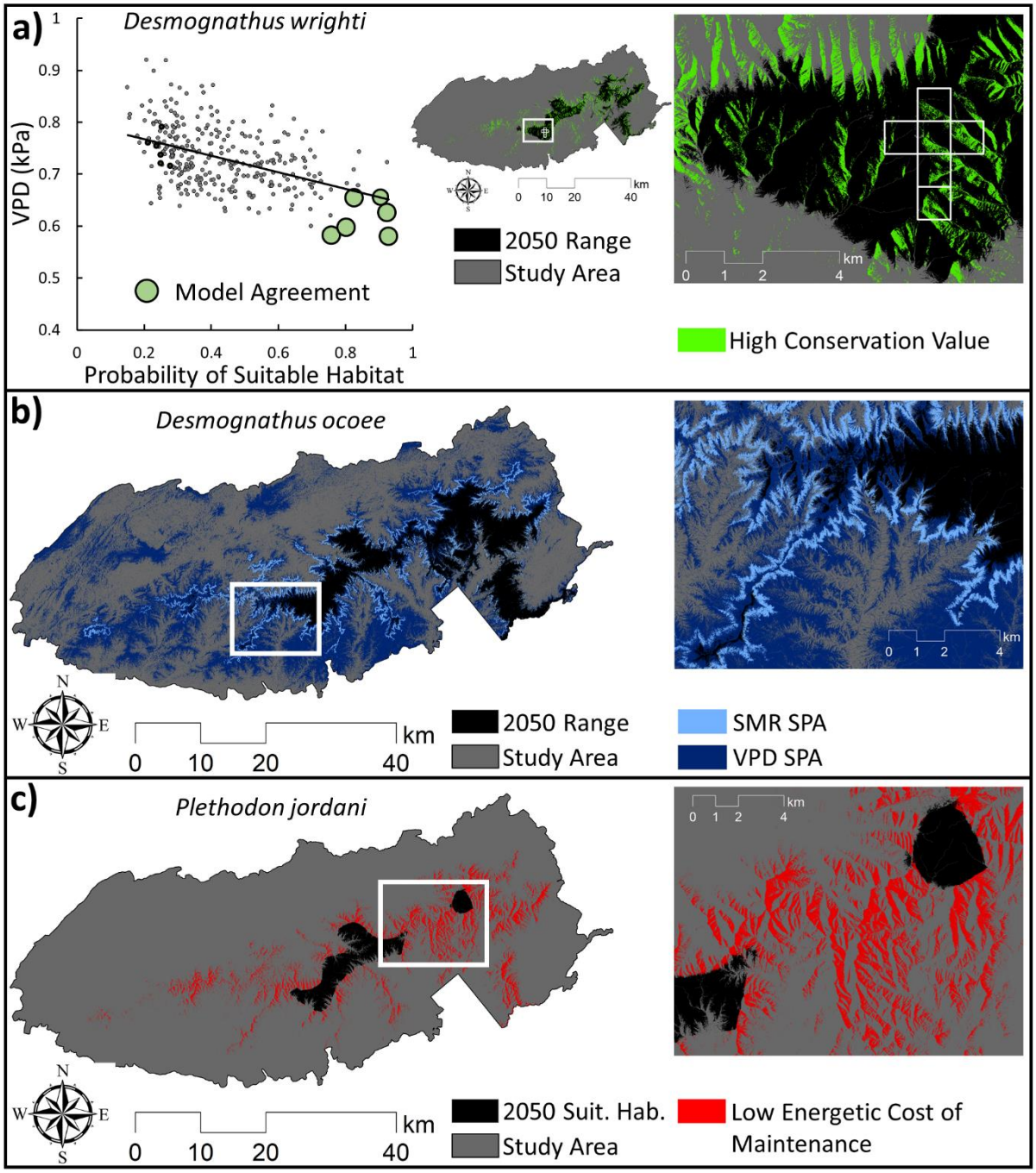

Figure 4.5. (a) Multi-scale conservation approach targeting areas with highest model agreement (large, colored points in graph) between low vapor pressure deficit (VPD) and high probability of suitable habitat to spatially target microscale areas of high conservation value within coarse resolution areas (white boxes in map inset). (b) Secondary priority areas (SPA) for microscale standard metabolic rate (SMR) and VPD may be useful for targeting functional connectivity between 2050 range projections for *Desmognathus ocoee*. (c) Low energetic cost of maintenance at the microscale may be useful in targeting functional connectivity between 2050 projections of highly suitable habitat (probability ≥ 0.7) for *Plethodon jordani*.

Table

Table 4.1. Predicted area of species' range and highly suitable habitat (probability ≥ 0.7) from species distribution models developed with bioclimatic variables calculated from microclimate and NASA NEX-DCP30 climate models. Suitable habitat was calculated for *Desmognathus wrighti*, *Desmognathus ocoee* and *Plethodon jordani* for the time periods of 2010 (average from 2006-2010), 2030 and 2050. Also shown is percent change between time periods.

			Area (km^2)		Percent Change		
Year	Species	Model	Range	Suitable Habitat ≥0.7	Years	Range	Suitable Habitat ≥0.7
2010	*Desmognathus wrighti*	Microclimate	920.1	243.7	2010-2030	-0.48	-0.60
2010	*Desmognathus wrighti*	NASA NEX-DCP30	1093.3	292.2	2010-2030	-0.49	-0.84
2010	*Desmognathus ocoee*	Microclimate	604.2	197.4	2010-2030	-0.60	-0.81
2010	*Desmognathus ocoee*	NASA NEX-DCP30	661.9	287.2	2010-2030	-0.42	-0.63
2010	*Plethodon jordani*	Microclimate	840.3	257.1	2010-2030	-0.14	-0.03
2010	*Plethodon jordani*	NASA NEX-DCP30	941.0	399.8	2010-2030	-0.45	-0.45
2030	*Desmognathus wrighti*	Microclimate	482.2	96.7	2030-2050	-0.51	-0.78
2030	*Desmognathus wrighti*	NASA NEX-DCP30	558.7	46.9	2030-2050	-0.28	-0.66
2030	*Desmognathus ocoee*	Microclimate	243.0	37.0	2030-2050	0.13	-0.56
2030	*Desmognathus ocoee*	NASA NEX-DCP30	384.7	106.4	2030-2050	0.22	0.70
2030	*Plethodon jordani*	Microclimate	722.0	249.4	2030-2050	-0.77	-0.70
2030	*Plethodon jordani*	NASA NEX-DCP30	514.1	220.4	2030-2050	-1.00	-1.00
2050	*Desmognathus wrighti*	Microclimate	235.4	21.6	2010-2050	-0.74	-0.91
2050	*Desmognathus wrighti*	NASA NEX-DCP30	402.0	16.1	2010-2050	-0.63	-0.94
2050	*Desmognathus ocoee*	Microclimate	273.8	16.3	2010-2050	-0.55	-0.92
2050	*Desmognathus ocoee*	NASA NEX-DCP30	467.8	180.8	2010-2050	-0.29	-0.37
2050	*Plethodon jordani*	Microclimate	164.4	73.9	2010-2050	-0.80	-0.71
2050	*Plethodon jordani*	NASA NEX-DCP30	0.7	0.0	2010-2050	-1.00	-1.00

CHAPTER 5: SUMMARY AND CONCLUSIONS

Predicting organismal responses to climate change is a difficult, but critically important, objective for conservation management, especially for species vulnerable to diminishing ranges. Currently, there is a large spatiotemporal gap between the modeling approaches most commonly used to assess species' distributions and the actual conditions many species vulnerable to climate change experience within their microhabitat. Our lack of understanding in the structural and biophysical effects that forest vegetation and topographical factors have on buffering microclimates must be resolved in order to produce accurate climate data for use in developing robust correlative and mechanistic habitat suitability predictions. Furthermore, integrating these modeling approaches in effective ways that reduce uncertainty in prioritizing suitable microclimatic habitat is crucial for the many organisms that rely on microclimatic regimes near the surface of the earth.

The findings from this dissertation research illustrate important spatiotemporal variations in mechanistic and correlative models and demonstrate approaches to integrating multiple model types for suitable habitat analysis that accounts for temporal variations in energetic demand. The results from Chapter 2 indicate that the inclusion of complex vegetation characteristics is important for developing robust predictions of microclimatic temperature at fine resolutions, an essential aspect of estimating the habitat component of small, ectothermic species, like plethodontid salamanders. By integrating robust predictions of microclimatic temperature into a physiological model, which also accounts for body-mass elevation relationships of the study species, the comparison of fine resolution salamander bioenergetics with commonly used, coarse resolution SDMs indicated spatial mismatches between model types. However, the results from this study highlight important temporal misalignments between diurnal and seasonal variations in

metabolic demand with static modeling approaches like SDMs. This dissertation research answers the call to incorporate microclimatic data into SDMs and establishes approaches to integrating mechanistic and correlative models for spatially targeting areas of high conservation value at relevant biological scales for plethodontid salamanders.

Multiple findings from this research suggest important considerations for future work in this field. In Chapter 2, the finding that sub-canopy vegetation is an important contributor to buffering near-surface temperatures and increasing predictive accuracy of microclimatic temperature estimates should greatly benefit future attempts at microclimate downscaling. There remains a need to enhance these approaches by incorporating more advanced remote sensing technologies across multiple temporal periods and collecting better information, like soil moisture data, to estimate accurate effects of plant-water interactions on near-surface temperatures. In Chapter 3 and Chapter 4, the demonstrated temporal misalignments between static, correlative models and mechanistic models will be important to account for habitat suitability analysis under projected climate change scenarios. Future studies should integrate multiple model approaches that account for spatiotemporal differences, as opposed to solely relying on correlative SDMs for analyzing the distributions of species. It will be important for future research to include increased efforts of in situ sampling to produce more robust estimates of energetic maintenance cost of plethodontids that account for spatiotemporal variation and acclimatization. Doing so will greatly benefit mechanistic models and enhance spatial targeting of suitable habitat.

Finally, the approaches used in this dissertation for estimating microclimatic temperature, and incorporating that microclimatic data into mechanistic and correlative models of habitat suitability, will be useful for spatially identifying areas of high conservation value.

Future studies could imitate and expand on these models as increased availability of LiDAR and other fine resolution datasets become available. Enhancing habitat suitability analyses in species' microhabitat could help in precisely targeting areas of microclimatic refugia and connectivity pathways between refugial areas. These approaches may also be useful for predicting areas appropriate for in situ sampling or for targeting areas for translocation or reintroduction of species that rely on microclimatic habitats. The continued development of more robust approaches to assessing suitable habitat in the microenvironment is necessary for truly understanding how species may respond to climate change.

APPENDIX A: CHAPTER 2 SUPPLEMENTARY MATERIAL

Modeling Vegetation Structure and Landscape Physiographic Characteristics

Vegetation structure was characterized using two LiDAR datasets, one on the Tennessee side and one on the North Carolina side of Great Smoky Mountains National Park. Both datasets were airborne-collected, represent leaf-off LiDAR, and LiDAR point clouds were classified using automated data classification methods with manual post-classification reviews, cleanup, and accuracy testing. The TN dataset was collected in 2011 and processed by The Center for Remote Sensing and Mapping Science at the University of Georgia and Photo Science, Inc. (Jordan et al 2011). At the time of this paper, information about the TN LiDAR dataset and LiDAR classification was available at http://www.cgr.uga.edu/index.php/projects/usgs-great-smoky-mountains-lidar-and-orthophotos/index.html and downloadable at https://www.data.gov/. The NC phase 3, airborne LiDAR dataset was collected in 2006 and processed by the North Carolina Floodplain and Mapping Program (OCM Partners 2019). At the time of this paper, information about the NC LiDAR dataset and LiDAR classification was available from https://flood.nc.gov/ncflood/ and downloadable from https://www.coast.noaa.gov/digitalcoast/data/.

Because the LiDAR datasets were collected from different organizations at different times, we tested the correlation between the two datasets to measure the strength of the association. We extracted vegetation height (VH) and vegetation structure (VS) from 5,000 points within the area of overlap on the TN and NC border, and we only used vegetation structure variables that had a Pearson correlation coefficient of ≥ 0.5 in our linear mixed-effects (LME) models. The final layers chosen between the two LiDAR datasets were vegetation height (VH; $r = 0.66$), and vegetation structure (VS) in the following layers: low-understory = VS

below 5 m (r = 0.63), high-understory = VS > 5 m to 10 m (r = 0.65), low-canopy = VS > 10 m to 15 m (r = 0.63), and mid-canopy VS = > 15 m to 20 m (r = 0.65). We also examined correlation and covariance among each vegetation layer chosen for this study (Table A.1).

Table A.1. Correlation coefficient and covariance (in parentheses) matrix for each vegetation structure and vegetation height class chosen for this study.

	Low-understory VS (< 5 m)	**High-understory VS (5 m-10 m)**	**Low-canopy VS (10 m-15 m**	**Mid-canopy VS (15 m-20 m)**	**Vegetation Height**
Low-understory VS (< 5 m)	1.00 (172.57)	0.05 (7.51)	-0.16 (-18.93)	-0.30 (-36.80)	-0.39 (-38.15)
High-understory VS (5 m-10 m)	0.05 (7.51)	1.00 (115.43)	0.18 (18.00)	-0.23 (-23.30)	-0.37 (-28.64)
Low-canopy VS (10 m-15 m	-0.16 (-18.93)	0.18 (18.00)	1.00 (83.15)	0.17 (14.13)	-0.27 (-17.70)
Mid-canopy VS (15 m-20 m)	-0.30 (-36.80)	-0.23 (23.30)	0.17 (14.13)	1.00 (85.86)	-0.01 (-0.52)
Vegetation Height	-0.39 (-38.15)	-0.37 (-28.64)	-0.27 (-17.70)	-0.01 (-0.52)	1.00 (52.87)

To develop the VS layers, LiDAR point data were filtered into different height classes and converted into raster data as point counts per each height class. Calculations were processed at a spatial resolution of 9 m^2 to allow for an average of 30 points per pixel. Vegetation height was calculated for each raster cell of the 3 m^2 digital elevation model (DEM). Vegetation structure percentages were calculated as the points within each vegetation class divided by the total above ground points for each 9 m^2 raster cell. We followed similar methodology as Lidar Analysis of Vegetation Structure (https://grasswiki.osgeo.org/wiki/Lidar_Analysis_of_Vegetation_Structure) for vegetation structure data and used r.inlidar to calculate vegetation height data and to develop vegetation point count rasters using GRASS GIS version 7.2.0.

ArcGIS® software versions 10.4.1–10.6.1 by Esri Inc. (2020) was used to calculate slope, aspect, distance-to-stream, and topographic convergence index (TCI). We developed the TCI layer by calculating the upslope catchment area of a site and correcting for local slope (Beven and Kirby, 1979). Landscape physiographic layers were derived using a DEM produced and distributed by the National Park Service, Great Smoky Mountains National Park and downloaded from the National Park Service, Integrated Resource Management Applications Data Store (Colson 2011; https://irma.nps.gov/Datastore/). Solar insolation was calculated using R.sun with GRASS GIS version 7.2.0 (https://grasswiki.osgeo.org/wiki/R.sun). We used the DEM, slope, and aspect as inputs keeping the default settings for orientation, slope, atmospheric turbidity, and albedo. We calculated solar insolation ($Wh/m^2/day^{-1}$), also known as solar irradiance, for the middle day of each week (i.e., estimating weekly average solar insolation) during the study period months of March–November. We did not incorporate shadowing effect of terrain due to the computational time of calculating solar insolation across such a fine-grain DEM and broad extent.

Linear Mixed-Effects Modeling and Results

The level one (L1) model was calculated to incorporate temperature predictions based solely on elevational lapse and regional weather station measurements. We followed a similar methodology in producing the L1 model as Fridley (2009) because of the importance in elevational lapse rates affecting temperatures in montane environments. The L1 model predictions were included as fixed effects in our LME models for the same reason (Fig. A.1). Our goal was to develop a final model that outcompeted this null model, which included the L1 model temperature predictions.

Temperature predictions from the level one (L1) model were highly correlated to the datalogger measurements for daily MaxT (r= 0.85) and MinT (r = 0.94). On average, MaxT and MinT decreased with elevation (ΔMaxT = -0.66 ^{o}C and ΔMinT = -0.38 ^{o}C with 100-m (hm) elevational increase), with the highest lapse rates occurring in summer (MaxT = -0.70 ^{o}C hm^{-1}, MinT = -0.42 ^{o}C hm^{-1}) and lowest lapse rates occurring in fall (MaxT = -0.61 ^{o}C hm^{-1}, MinT = -0.34 ^{o}C hm^{-1}). We fit our linear mixed effects models to daily MaxT and MinT data from the climate dataloggers as a function of the L1 model temperature predictions, vegetation structure, and landscape physiographic variables (Fig. A.1).

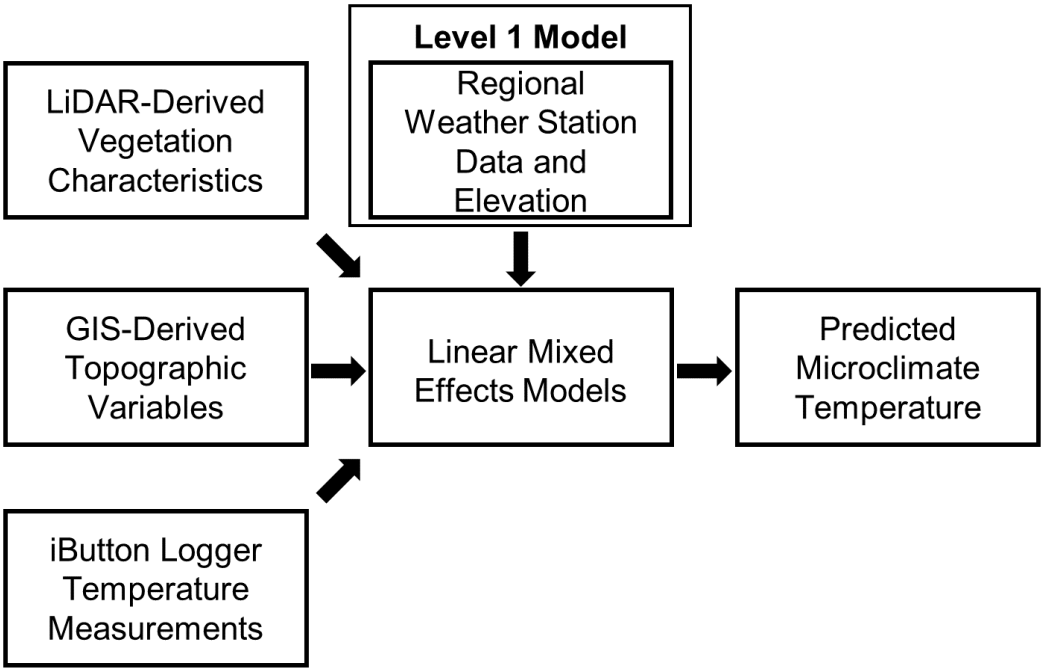

Figure A.1. Flow chart of microclimate temperature model predictions (3 m^2 spatial resolution) for daily minimum and maximum temperature from 2006–2010 for the months of March–November. The level one model was developed with daily temperature lapse rates produced using simple linear models with data from 11 regional weather stations and elevation data from a 3m^2 digital elevation model. We then combined LiDAR-derived vegetation structure and GIS-derived landscape physiography variables with daily temperature predictions from the level one model to predict daily microclimate temperatures using a linear mixed-effects models

We followed a top-down selection method for model fitting and evaluation as suggested by Zuur et al. (2009). We evaluated the predictions from each top-ranked model based on Akaike's Information Criterion (AICc) as seen in Table A.2. To validate the top ranked models,

Table A.2. Akaike's Information Criterion for minimum and maximum temperature models within a 95% confidence set. Final selected models (FSM) and candidate models are shown. Candidate models show the FSM plus (+) or less (-) the other variables included in the candidate model. DTS = Distance-to-Stream, TCI = Topographic Convergence Index, Solar = Solar Insolation, Veg. = vegetation.

Model	k	log $\mathcal{L}$	AICc	ΔAICc	w_i
Minimum Temperature					
Final Selected Model (FSM)	12	-257275.3	514574.7	0.00	0.37
FSM + TCI*Veg. Density Below 5 m	13	-257274.8	514575.7	0.98	0.23
FSM + DTS*Veg. Density 5 m to 10 m	14	-257274.2	514576.4	1.72	0.16
FSM + TCI*Veg. Density Below 5 m + DTS*Veg. Density 5 m to 10 m	15	-257273.6	514577.1	2.44	0.11
FSM - TCI - DTS	10	-257278.6	514577.2	2.47	0.11
Global Model	28	-257271.6	598700.0	15.64	0.00
Null Model	5	-257271.6	600194.3	1509.90	0.00
Maximum Temperature					
Final Selected Model (FSM)	12	-299330.2	598684.4	0.00	0.25
FSM + Solar*Veg. Density 5 m to 10 m	14	-299328.3	598684.7	0.29	0.21
FSM + Veg. Height	13	-299329.5	598684.9	0.53	0.19
FSM + Solar*Veg. Density 5 m to 10 m + Veg. Height	15	-299327.5	598684.9	0.54	0.19
FSM + DTS*Veg. Height	14	-299329.3	598686.6	2.23	0.08
FSM + Solar*Veg. Density 5 m to 10 m + DTS*Veg. Height	16	-299327.3	598686.7	2.27	0.08
Global Model	28	-299322.0	598700.0	15.64	0.00
Null Model	5	-300092.1	600194.3	1509.86	0.00

we randomly split the data into 70% training data for model fitting and used the remaining 30% as testing data for evaluation. This method was chosen because we had a very large dataset and found no significant variation in the descriptive statistics among the entire dataset, training

dataset, and testing dataset. We measured goodness-of-fit for each model using the coefficient of determination (R^2). Our aim was to maximize predictive accuracy, so we calculated mean absolute error (MAE) for each candidate model, selecting the model with the lowest MAE. For both MinT and MaxT, the models with the lowest MAE coincided with the best ranked models according to AICc (Table A.2).

Final selected models for MaxT and MinT were re-fit using restricted maximum likelihood to obtain parameter estimates (Zuur et al. 2009). Our final LME models resulted in conditional coefficient of determinations above 0.8 (Fig. A.2; MaxT $R^2 = 0.81$, MinT $R^2 = 0.92$).

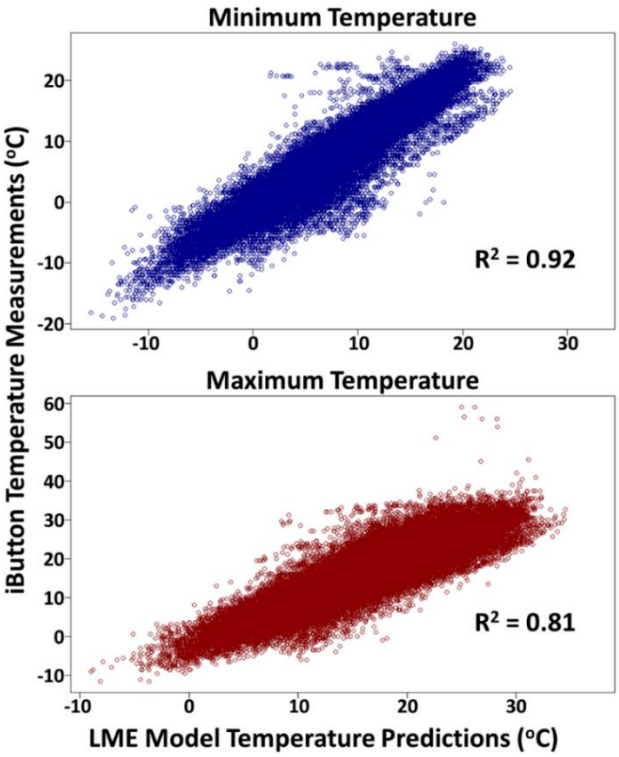

Figure A2. Relationship between daily temperature measurements from 159 iButton loggers and temperature predictions at each iButton logger location from our final linear mixed effects (LME) models. Daily minimum and maximum temperatures were estimated from March–November of 2006–2010 at each iButton logger location (N = 218,625). Data were split into 70 percent training data (N = 153,037) and 30 percent test data (N = 65,588) for model validation. Graphs and coefficient of determinations were produced with test data

Free-Air and Microclimatic Temperature Mismatches

The gridded, free-air temperature data from the Daymet (Thornton et al. 2016) and the Parameter–Elevation Regressions on Independent Slopes Model (PRISM; Daly et al 1994) datasets were downloaded at 1-km^2 and 4-km^2 spatial resolutions, respectively. Raster data and extracted point data were downloaded from https://daymet.ornl.gov/ for the Daymet dataset and http://www.prism.oregonstate.edu/ for the PRISM dataset.

We used ArcGIS® software versions 10.4.1–10.6.1 by Esri Inc. (2020) to extract 5,000 random points from each raster dataset of the climate variables, landscape physiographic variables and vegetation structure variables. These point data were used to quantify mismatches, based on temperature differences (absolute and real values) on a monthly and seasonal time scale, which equated to temperature predictions from the L1, Daymet or PRISM raster models less the temperature predictions of our final LME model. We also calculated these temperature differences for each raster dataset to develop heat maps of model differences (Fig. A.3; Fig. A.4; Fig. A.5; Fig. A.6).

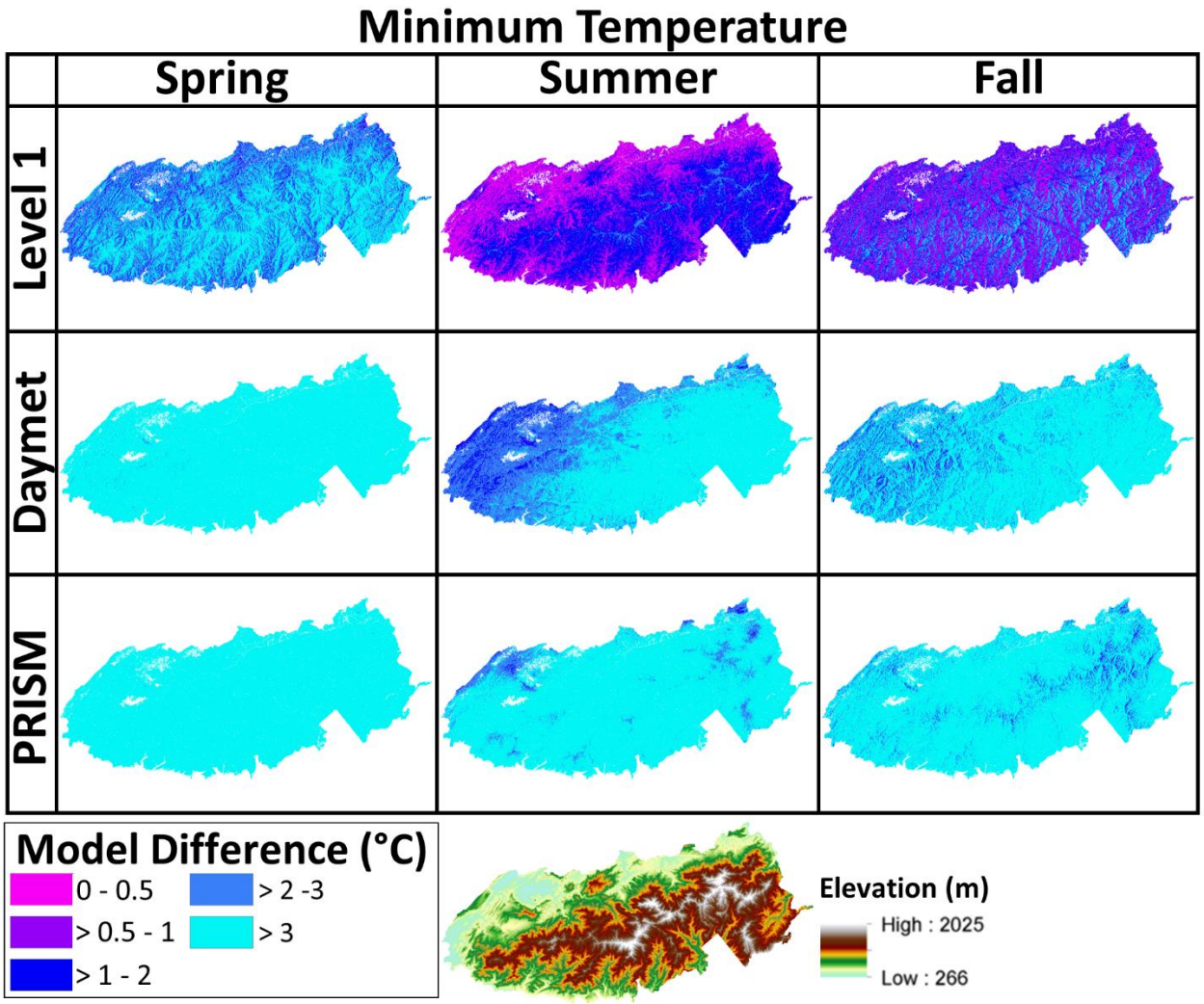

Figure A.3. Heat maps showing the mismatch for minimum temperature between the level one model (3 m^2), Daymet model (1 km^2), and Prism model (4 km^2) from our LME model predictions. Mismatches are calculated as follows: Comparison Model (i.e., level one or Daymet or Prism) – Final LME Model Predictions = Mismatch. Values are absolute to show the spatiotemporal locations of the largest temperature mismatches. An elevation map is included to show elevational patterns in some temperature mismatches

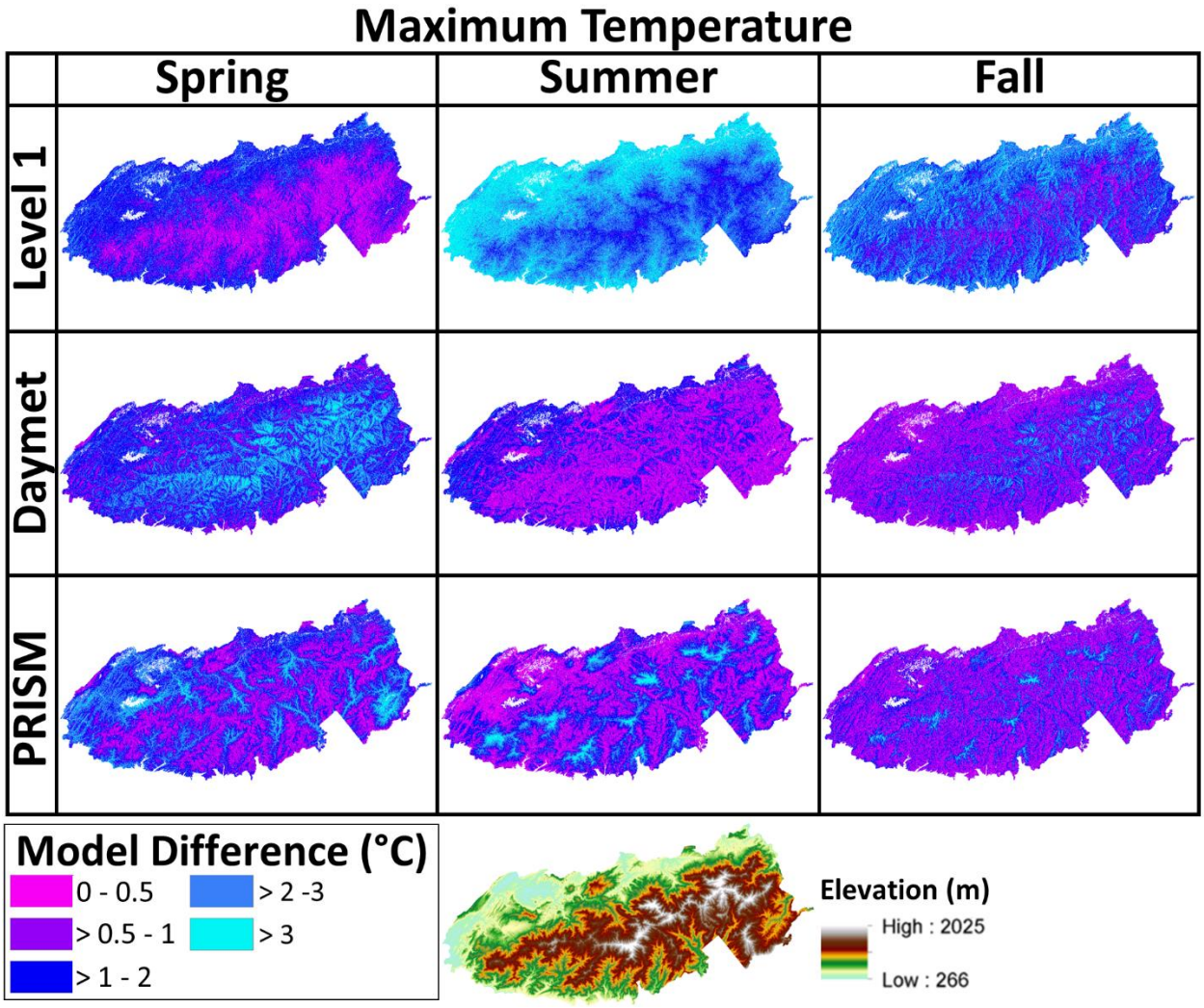

Figure A.4. Heat maps showing the mismatch for maximum temperature between the level one model (3 m^2), Daymet model (1 km^2), and Prism model (4 km^2) from our LME model predictions. Mismatches are calculated as follows: Comparison Model (i.e., level one or Dayment or Prism) – Final LME Model Predictions = Temperature Mismatch. Values are absolute to show the spatiotemporal locations of the largest temperature mismatches. An elevation map is included to show elevational patterns in some temperature mismatches

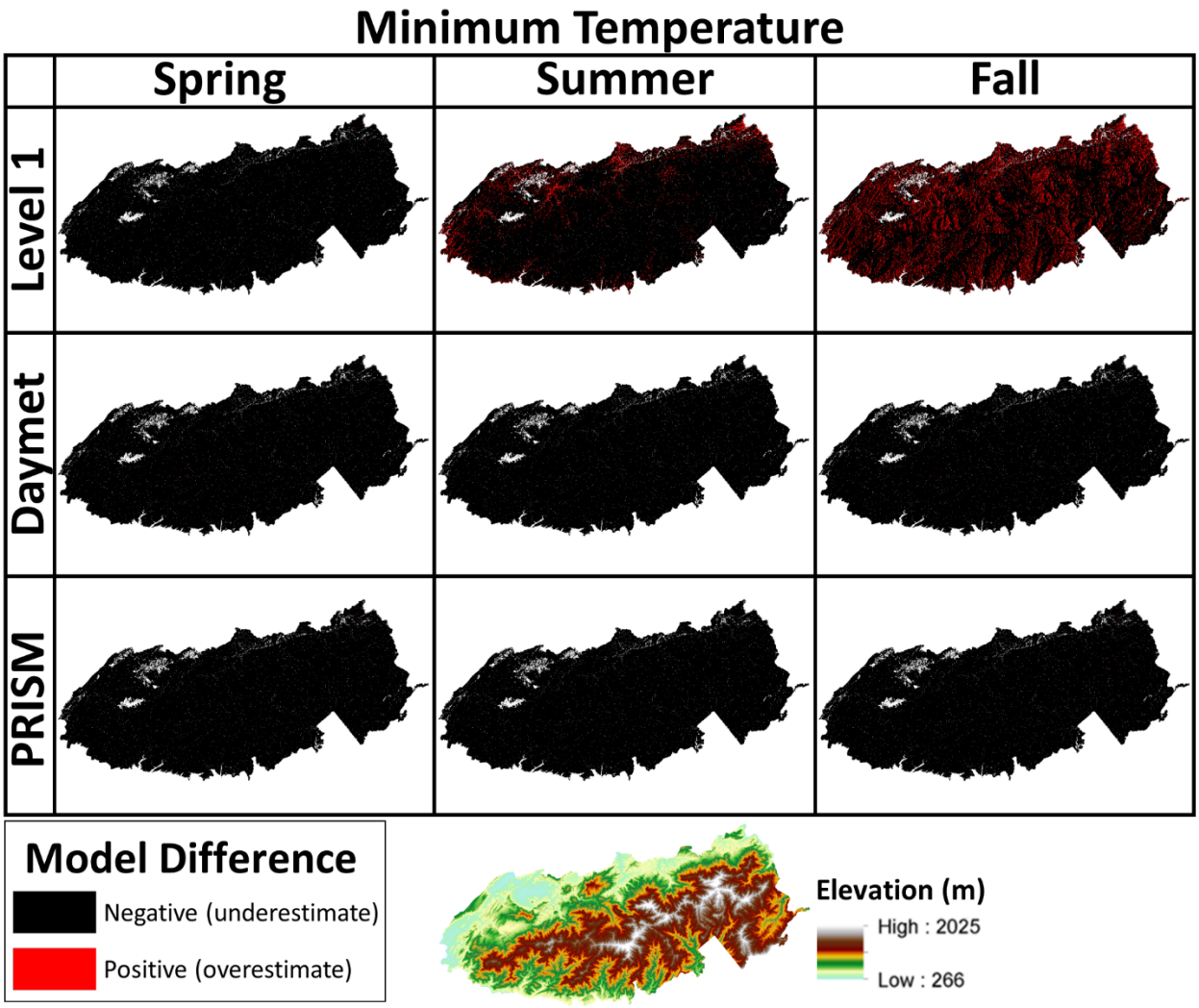

Figure A.5. Heat maps showing the mismatch for minimum temperature between the level one model (3 m^2), Daymet model (1 km^2), and Prism model (4 km^2) from our LME model predictions. Mismatches are calculated as follows: Comparison Model (i.e., level one or Dayment or Prism) – Final LME Model Predictions = Temperature Mismatch. Real values are re-classified to show areas of overestimation and underestimation. A negative value means the comparison model (i.e., level one, Daymet or Prism Model) is underestimating temperature in comparison to our final LME model predictions. An elevation map is included to show elevational patterns in some temperature mismatches

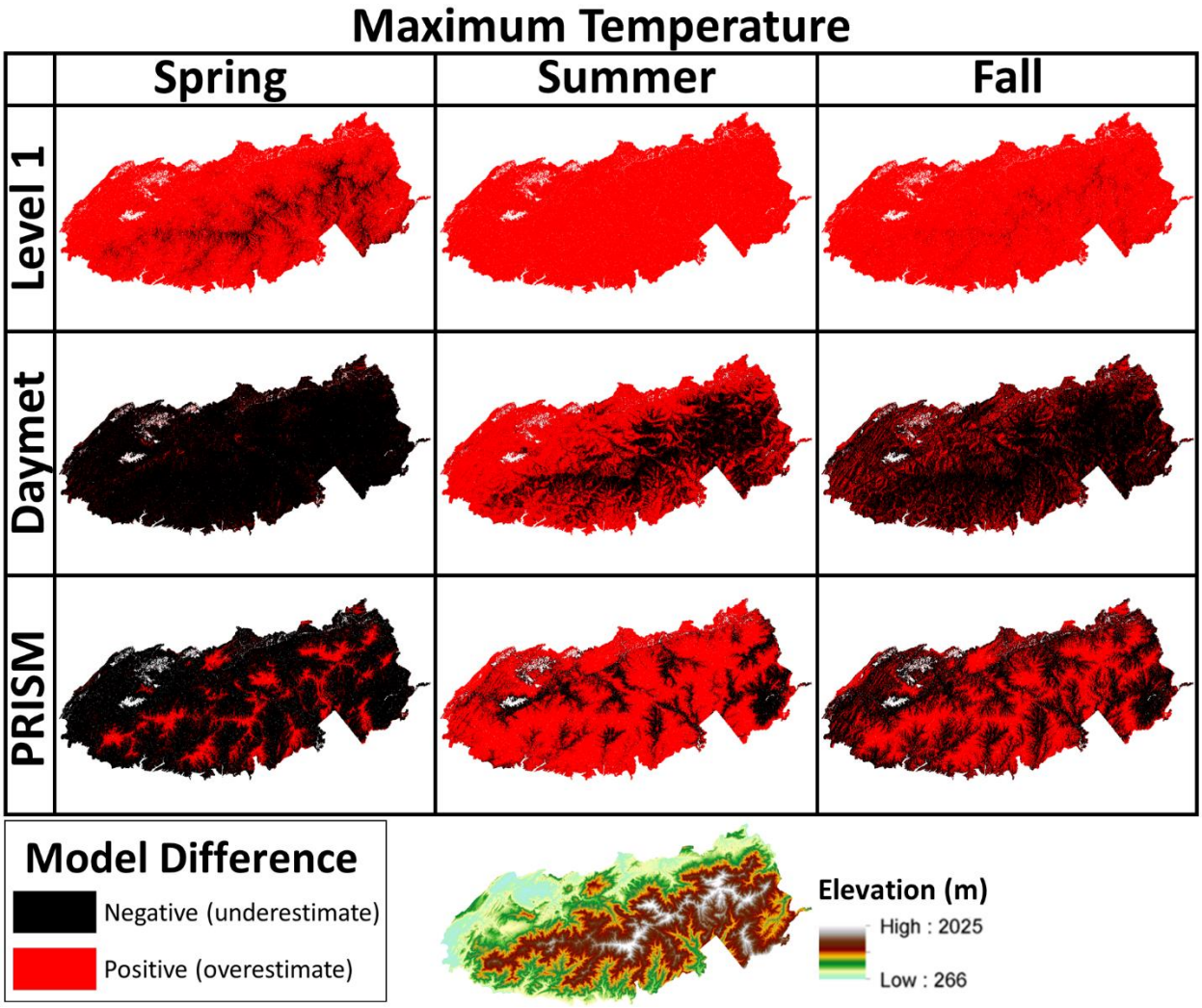

Figure A.6. Heat maps showing the mismatch for maximum temperature between the level one model (3 m^2), Daymet model (1 km^2), and Prism model (4 km^2) from our LME model predictions. Mismatches are calculated as follows: Comparison Model (i.e., level one or Dayment or Prism) – Final LME Model Predictions = Temperature Mismatch. Real values are re-classified to show areas of overestimation and underestimation. A negative value means the comparison model (i.e., level one, Daymet or Prism Model) is underestimating temperature in comparison to our final LME model predictions. An elevation map is included to show elevational patterns in some temperature mismatches

Contribution of Predictor Variables to Spatiotemporal Mismatches

We found that elevation and solar insolation heavily contributed to mismatches and, therefore, focused on those predictor variables in our results and discussion. Here, we also display

the results from each of the predictor variables from our final LME models to display the contribution of temperature mismatches from each predictor variable (Fig. A.7; Fig. A.8; Fig. A.9).

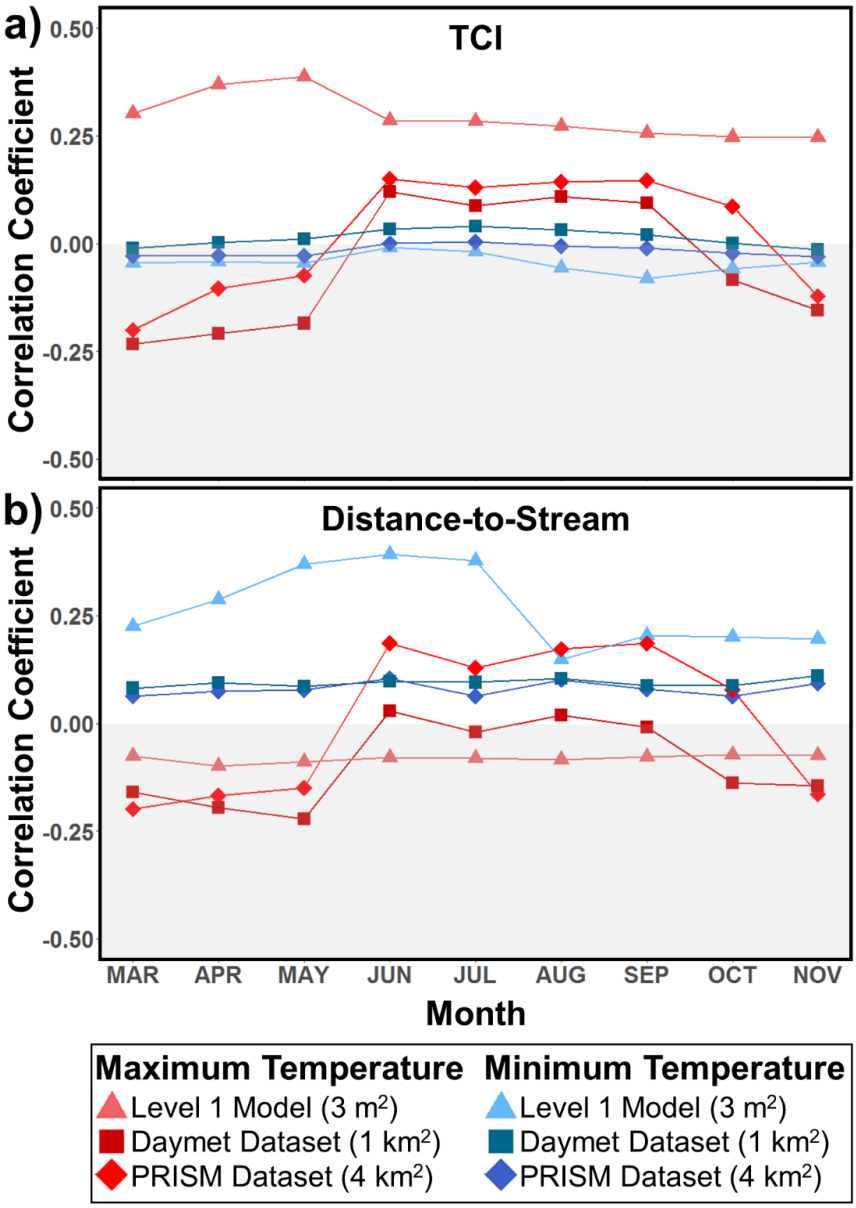

Figure A.7. Monthly average correlation coefficients between temperature mismatches (absolute values from 2006–2010) and the important landscape physiographic drivers of (a) topographic convergence index (TCI) and (b) distance-to-stream (m). Temperature mismatches are the difference between free-air temperature estimates and microclimatic predictions from our final LME models. Large positive or negative values for a given month indicate that the predictor variable substantially contributed to the mismatch between microclimatic and free-air temperatures

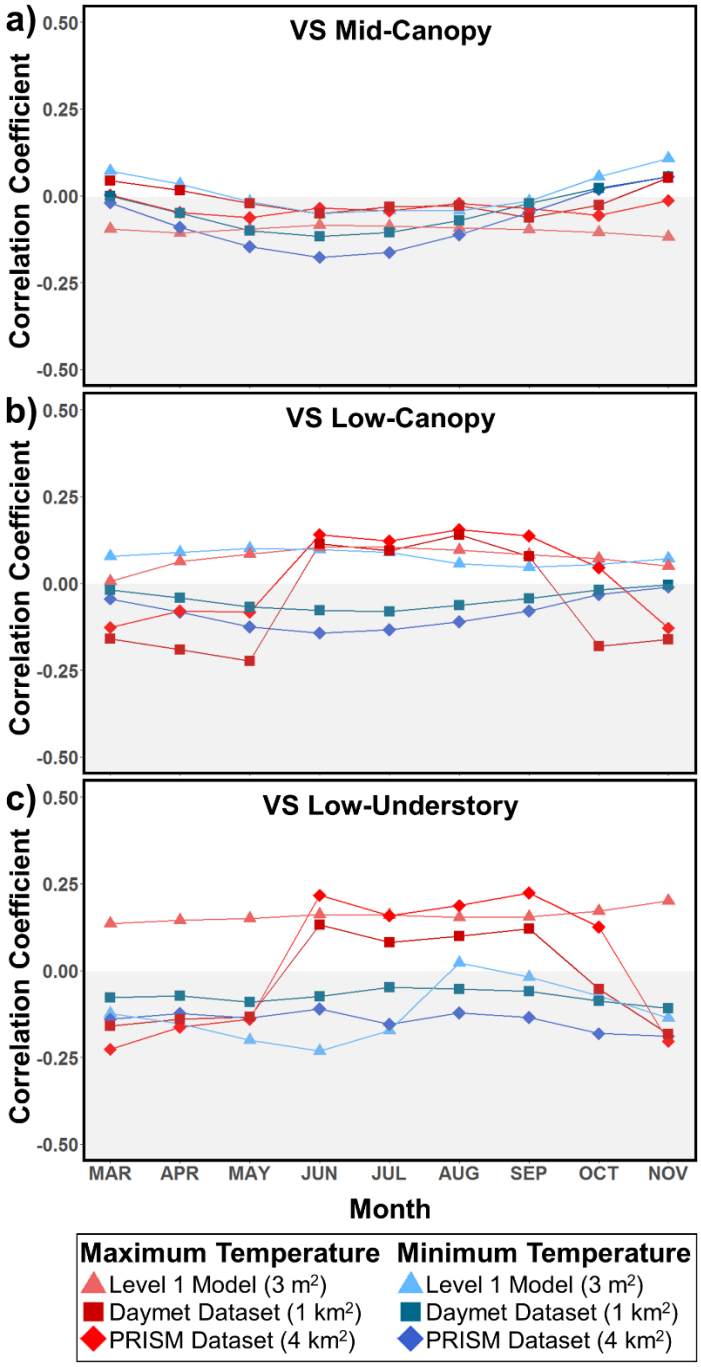

Figure A.8. Monthly average correlation coefficients between temperature mismatches (absolute values from 2006–2010) and the important vegetation structure (VS) drivers of (a) VS in the mid-canopy strata, (b) VS in the low-canopy strata and (c) VS in the low-understory strata. Temperature mismatches are the difference between free-air temperature estimates and microclimatic predictions from our final LME models. Large positive or negative values for a given month indicate that the predictor variable substantially contributed to the mismatch between microclimatic and free-air temperatures

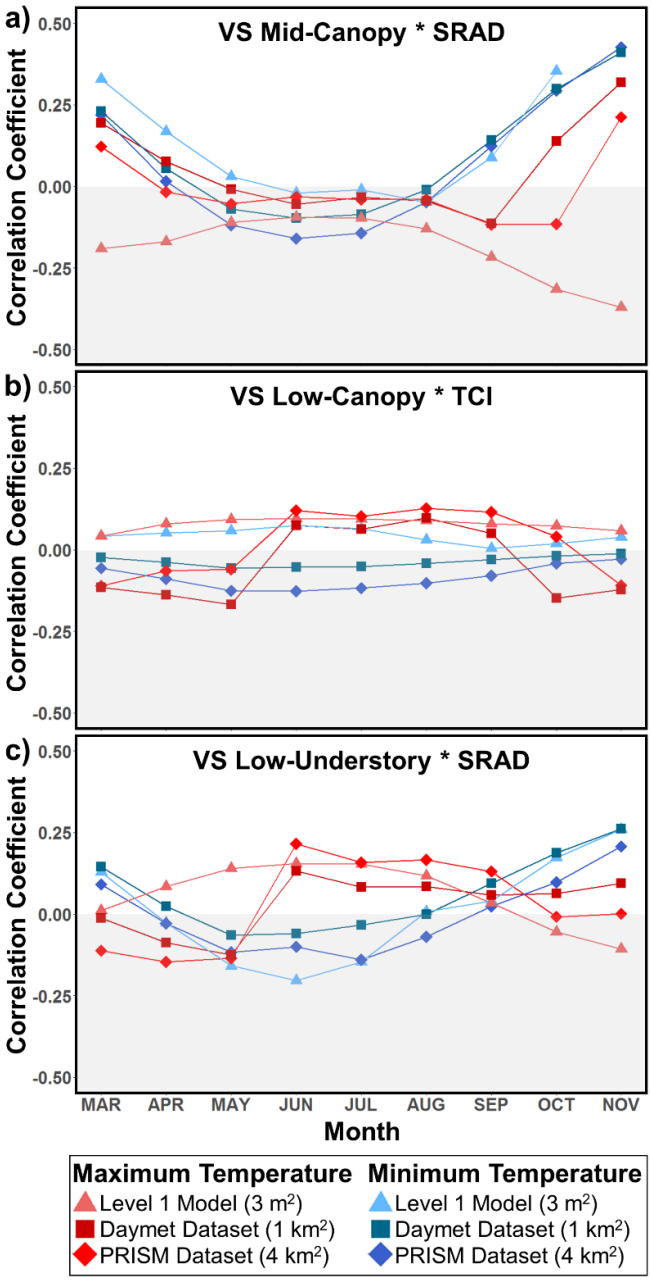

Figure A.9. Monthly average correlation coefficients between temperature mismatches (absolute values from 2006–2010) and the important interactions between vegetation structure (VS) and landscape physiographic drivers of (a) VS in the mid-canopy strata * solar insolation ($Wh/m^2/day^{-1}$), (b) VS in the low-canopy strata * topographic convergence index (TCI), and (c) VS in the low-understory strata * solar insolation ($Wh/m^2/day^{-1}$). Temperature mismatches are the difference between free-air temperature estimates and microclimatic predictions from our final LME models. Large positive or negative values for a given month indicate that the predictor variable substantially contributed to the mismatch between microclimatic and free-air temperatures

APPENDIX B: CHAPTER 3 SUPPLEMENTARY MATERIAL

Materials and Methods

Fine-grain standard metabolic rate

The standard metabolic rate (SMR) formulas we used for can be found in Feder (1976, 1983). We also used a species-specific formula for *P. jordani*, which can be found in Gifford and Kozak (2012). To produce the Feder SMR models, we used the relationship between body mass and SMR at different temperatures (Feder 1976; 5 ^{o}C, 15 ^{o}C, and 25^{o}C) to develop SMR estimates at those temperatures and produce SMR maps at a 3 m^2 spatial scale at those static temperatures. We then used the linear relationship from Feder (1983) to predict SMR for each species using the SMR maps at static temperatures as the initial input. We also calculated *P. jordani* SMR using the following Gifford and Kozak (2012) formula:

$$\log_{10} \text{SMR} = 0.036(\text{temperature}) + 0.57(\log_{10} \text{Body Mass}) - 1.95$$

For *P. jordani*, we model averaged our final outputs from both SMR predictions to limit uncertainty. All SMR models were converted to volume of oxygen consumption in microliters (VO_2 µl g^{-1} hr^{-1}). Spatial modeling was conducted using the raster calculator with ArcGIS® software versions 10.4.1–10.6.1 (Esri inc. 2020).

Species distribution modeling

Our objective was to develop climatically-derived species distribution models that are commonly used for predicting habitat suitability. The 11 WorldClim (https://www.worldclim.org/) bioclimatic variables used for our species distribution models had previously been shown to be biologically relevant and interpretable for plethodontid salamanders (Rissler and Apodaca 2007; Milanovich 2010). The 11 bioclimatic variables included annual

mean temperature (BIO1), mean diurnal range (BIO2), isothermality (BIO3), temperature annual range (BIO7), mean temperature of wettest (BIO8) and driest quarter (BIO9), precipitation seasonality (BIO15), precipitation of the wettest quarter (BIO16) and driest quarter (BIO17), and precipitation of the warmest (BIO18) and coldest quarter (BIO19; Table B.1).

To develop SDMs, we first produced raw outputs of suitable habitat at approximately 1 km^2 resolution for each plethodontid salamander species (*D. wrighti*, *D. ocoee*, and *P. jordani*) across GSMNP using the 11 bioclimatic variables and presence-only dataset. A maximum entropy method was chosen for our modeling approach because MaxEnt is one of the most popular and widely-used programs due to high accuracy with presence-only data (Elith et al. 2006; Hernandez et al. 2006). We followed methodologies for data preparation, model fitting, model prediction, and model evaluation as recommended by Hijmans and Elith (2017). For model fitting and prediction, we selected 500 random points across the study area and extracted the bioclimatic variables as background data points. We also extracted the bioclimatic variables at every presence location for each species. Data were partitioned into five groups and we fit and test our model five times using *k*-fold cross validation. Goodness of fit was assessed using the average area under the curve (AUC) value. We used the 'dismo' package in R statistical software v. 3.50 (R Core Team 2020) to estimate MaxEnt habitat suitability.

Figures

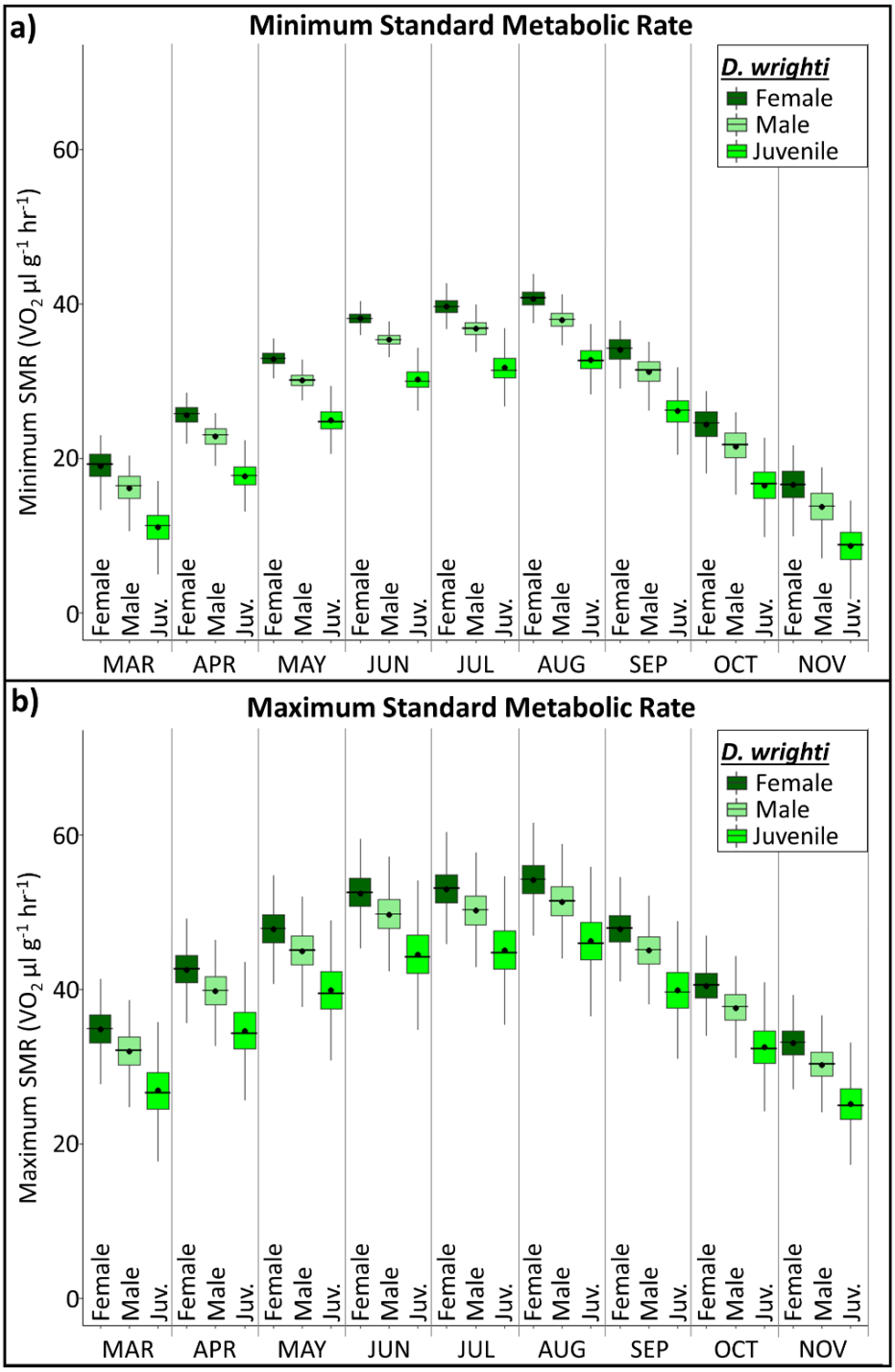

Figure B.1. Minimum and maximum standard metabolic rate (SMR) for *Desmognathus wrighti*. Shown are estimates for each sex and stage class (female, male, and juvenile) during each month of the study period. Points indicate the bootstrapped mean and central error bar lines indicate the confidence interval for the bootstrapped median. Vertical lines indicate the error bar for standard deviation of mean

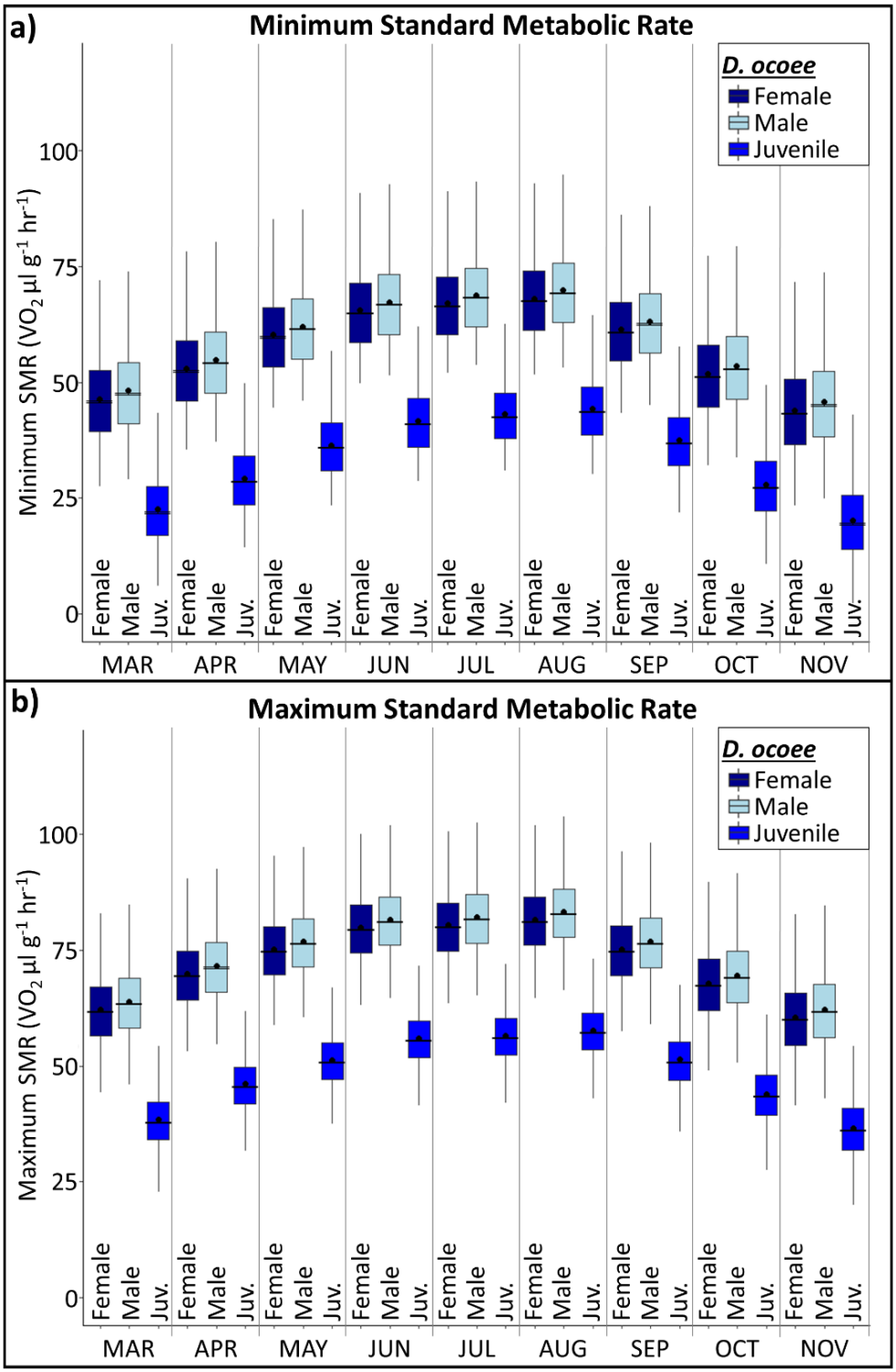

Figure B.2. Minimum and maximum standard metabolic rate (SMR) for *Desmognathus ocoee*. Shown are estimates for each sex and stage class (female, male, and juvenile) during each month of the study period. Points indicate the bootstrapped mean and central error bar lines indicate the confidence interval for the bootstrapped median. Vertical lines indicate the error bar for standard deviation of mean

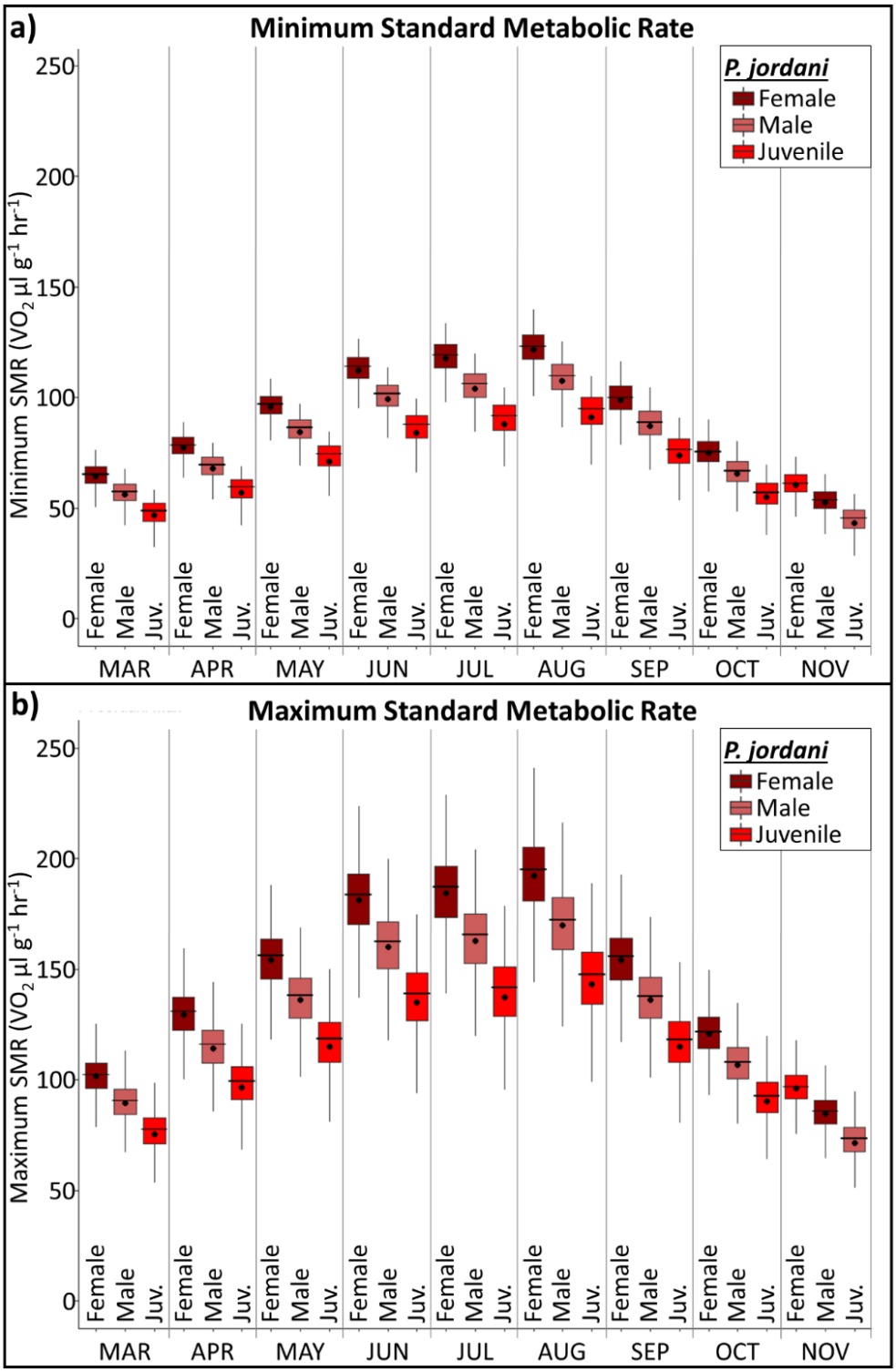

Figure B.3. Minimum and maximum standard metabolic rate (SMR) for *Plethodon jordani*. Shown are estimates for each sex and stage class (female, male, and juvenile) during each month of the study period. Points indicate the bootstrapped mean and central error bar lines indicate the confidence interval for the bootstrapped median. Vertical lines indicate the error bar for standard deviation of mean

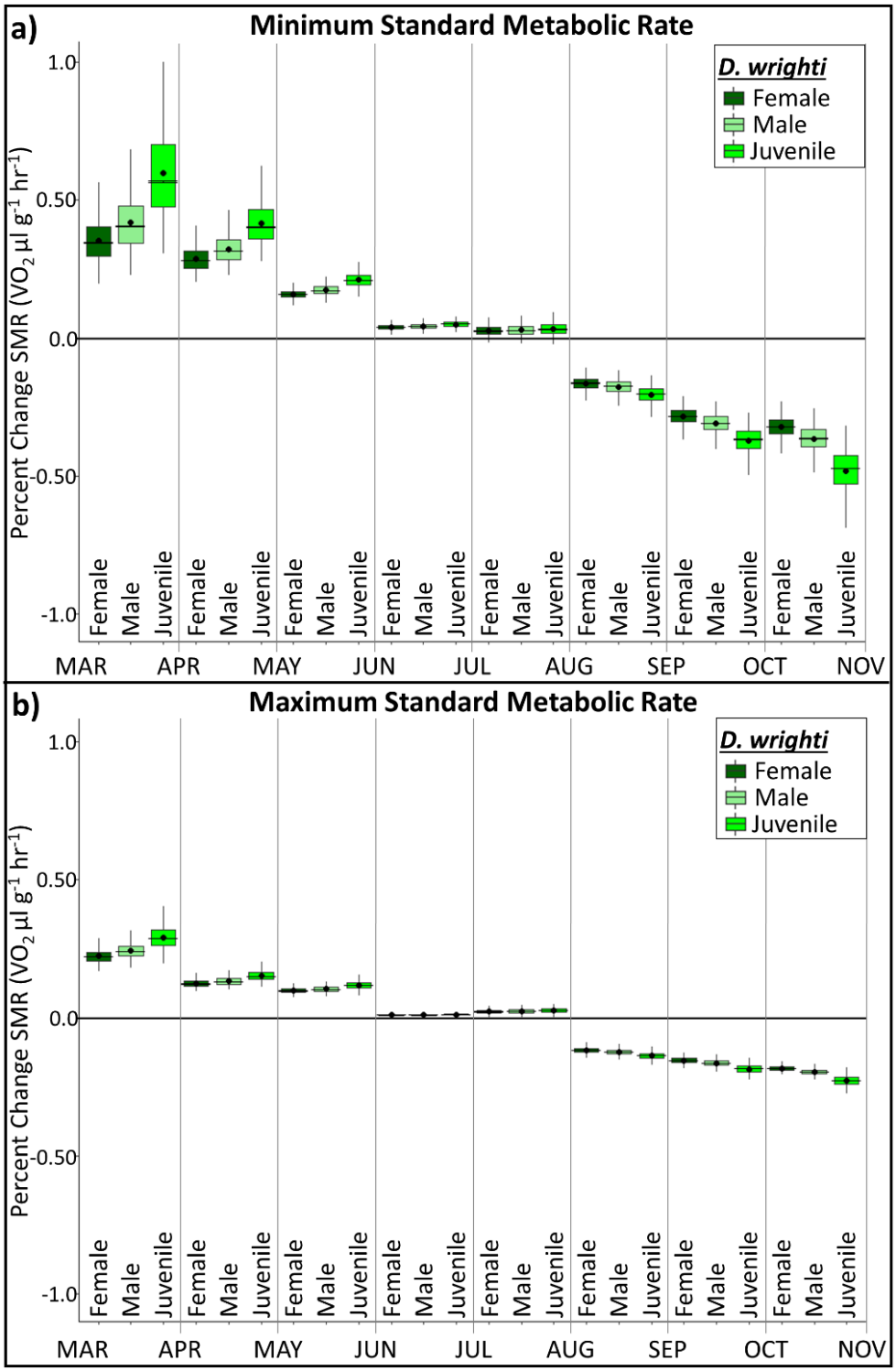

Figure B.4. Percent change in minimum and maximum standard metabolic rate (SMR) between each month of the study period (March-November). Shown are estimates for the sex and stage class (male, female, and juvenile) for *Desmognathus wrighti*. Points indicate the bootstrapped mean and central error bar lines indicate the confidence interval for the bootstrapped median. Vertical lines indicate the error bar for standard deviation of mean

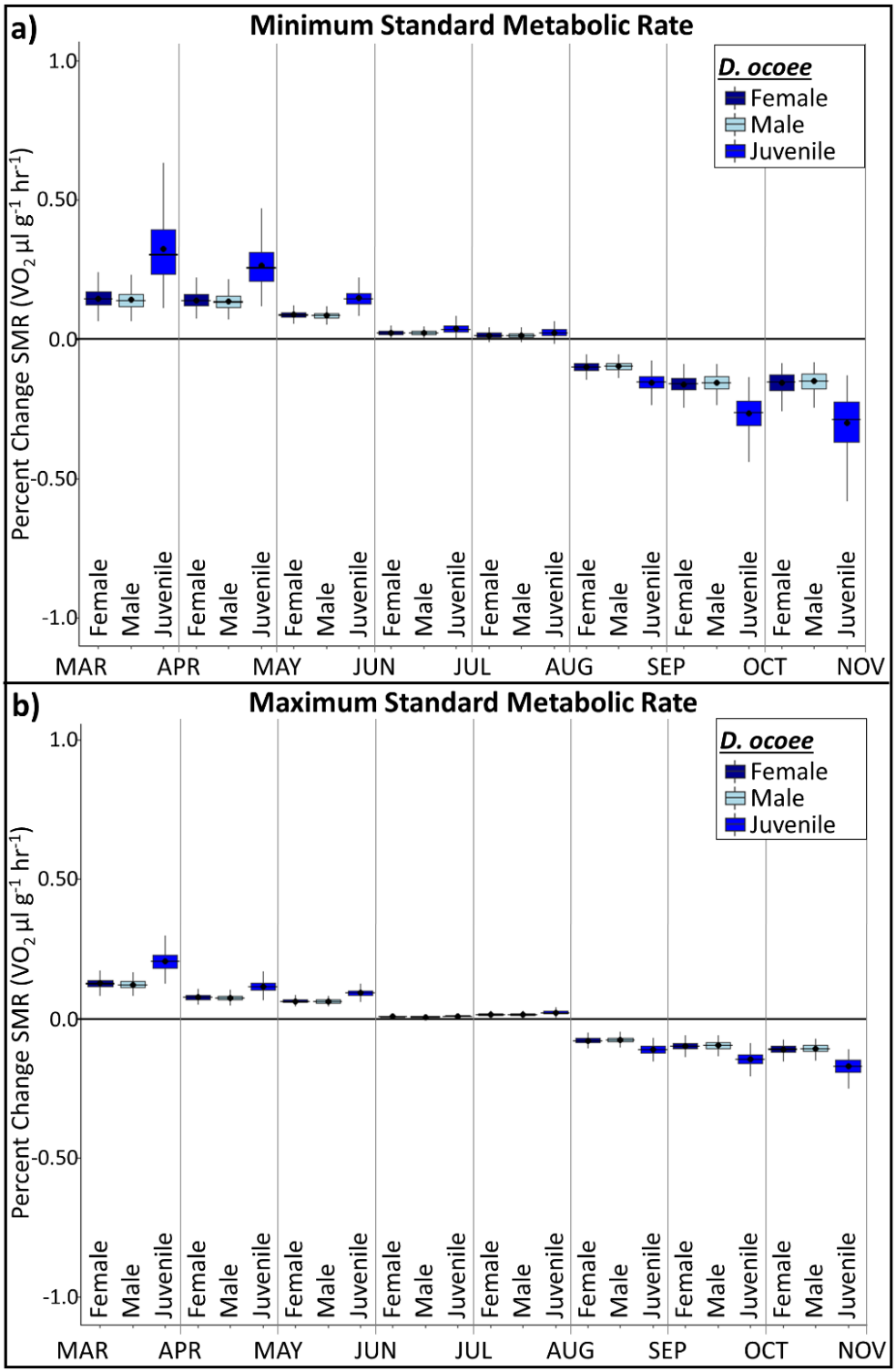

Figure B.5. Percent change in minimum and maximum standard metabolic rate (SMR) between each month of the study period (March-November). Shown are estimates for the sex and stage class (male, female, and juvenile) for *Desmognathus ocoee*. Points indicate the bootstrapped mean and central error bar lines indicate the confidence interval for the bootstrapped median. Vertical lines indicate the error bar for standard deviation of mean

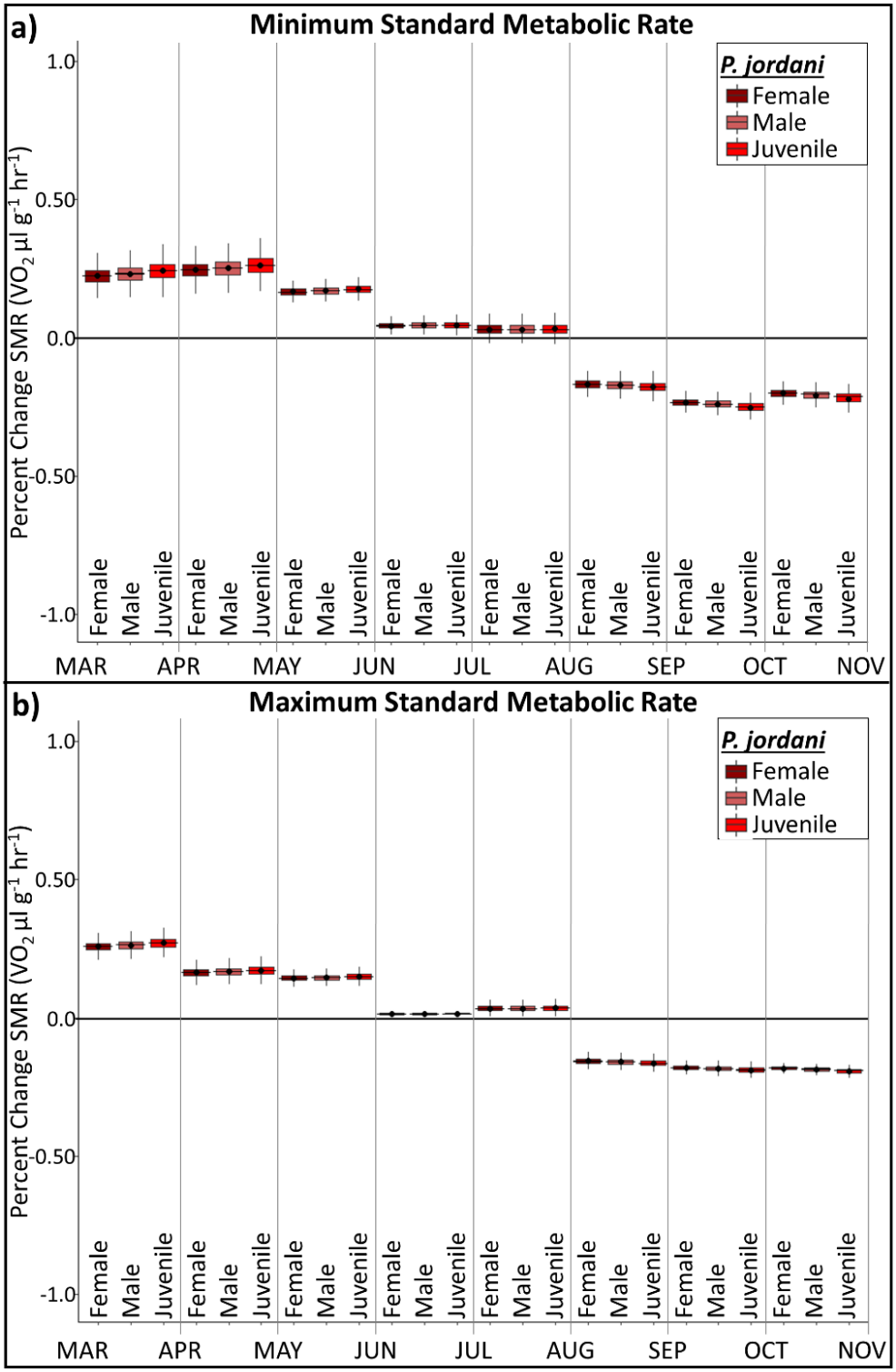

Figure B.6. Percent change in minimum and maximum standard metabolic rate (SMR) between each month of the study period (March-November). Shown are estimates for the sex and stage class (male, female, and juvenile) for *Plethodon jordani*. Points indicate the bootstrapped mean and central error bar lines indicate the confidence interval for the bootstrapped median. Vertical lines indicate the error bar for standard deviation of mean

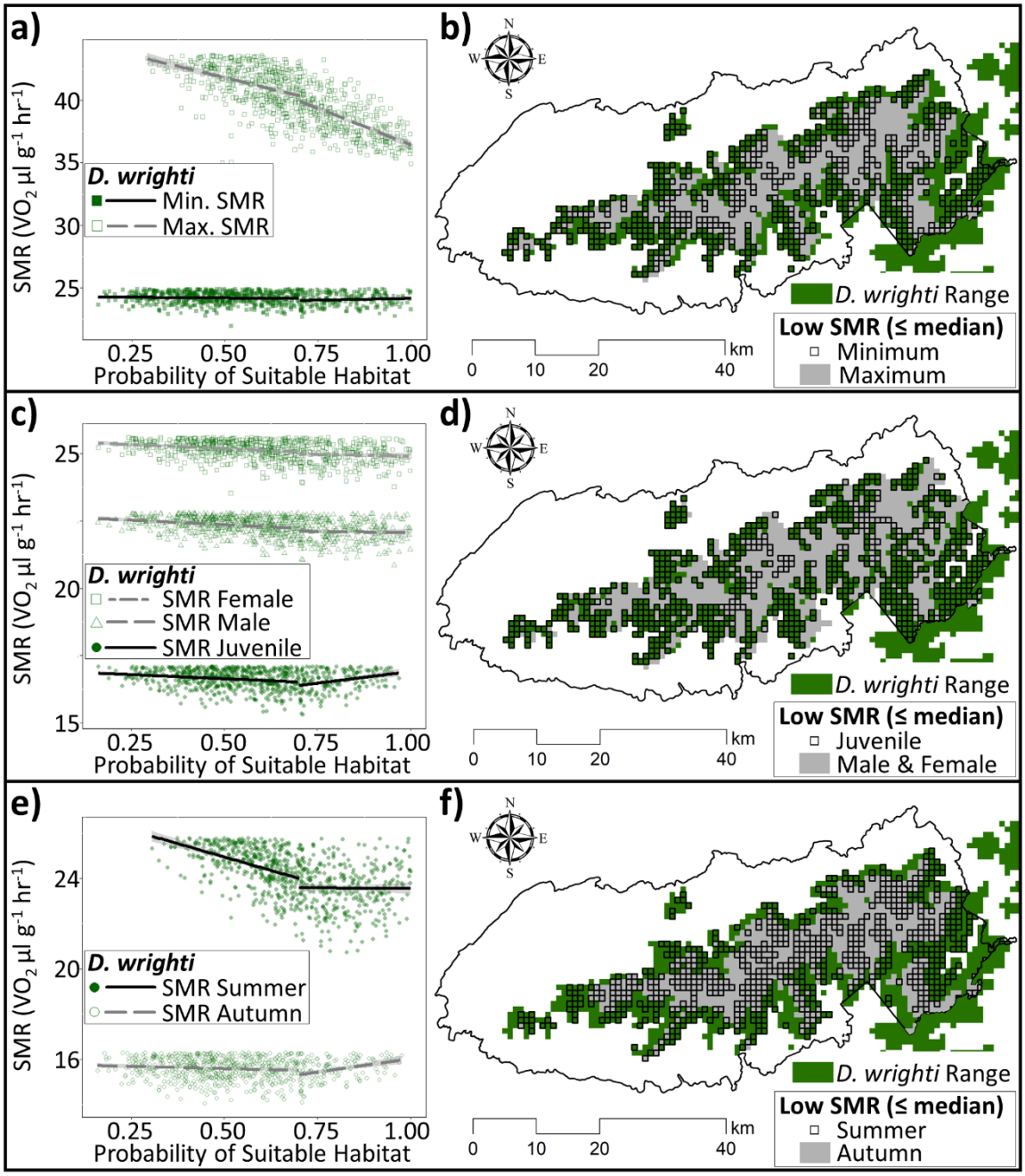

Figure B.7. (a) Minimum and maximum standard metabolic rate plotted against the predicted habitat suitability from species distribution models. (b) Locations of low standard metabolic rate (SMR ≤ median) vary between minimum and maximum SMR. Examples in (a) and (b) are using data for *Desmognathus wrighti* females during autumn. (c) Minimum standard metabolic rate in spring plotted against predicted habitat suitability for *Desmognathus wrighti*. (d) Locations of low standard metabolic rate (SMR ≤ median) vary between adults and juveniles. (e) Minimum standard metabolic rate during summer and autumn plotted against predicted habitat suitability for *Desmognathus wrighti* juveniles. (f) Locations of low standard metabolic rate (SMR ≤ median vary between seasons. (a), (c) , and (e) are plotted with piecewise regression to demonstrate the relationship in low suitable habitat (0.0-0.7) and high suitable habitat (> 0.7)

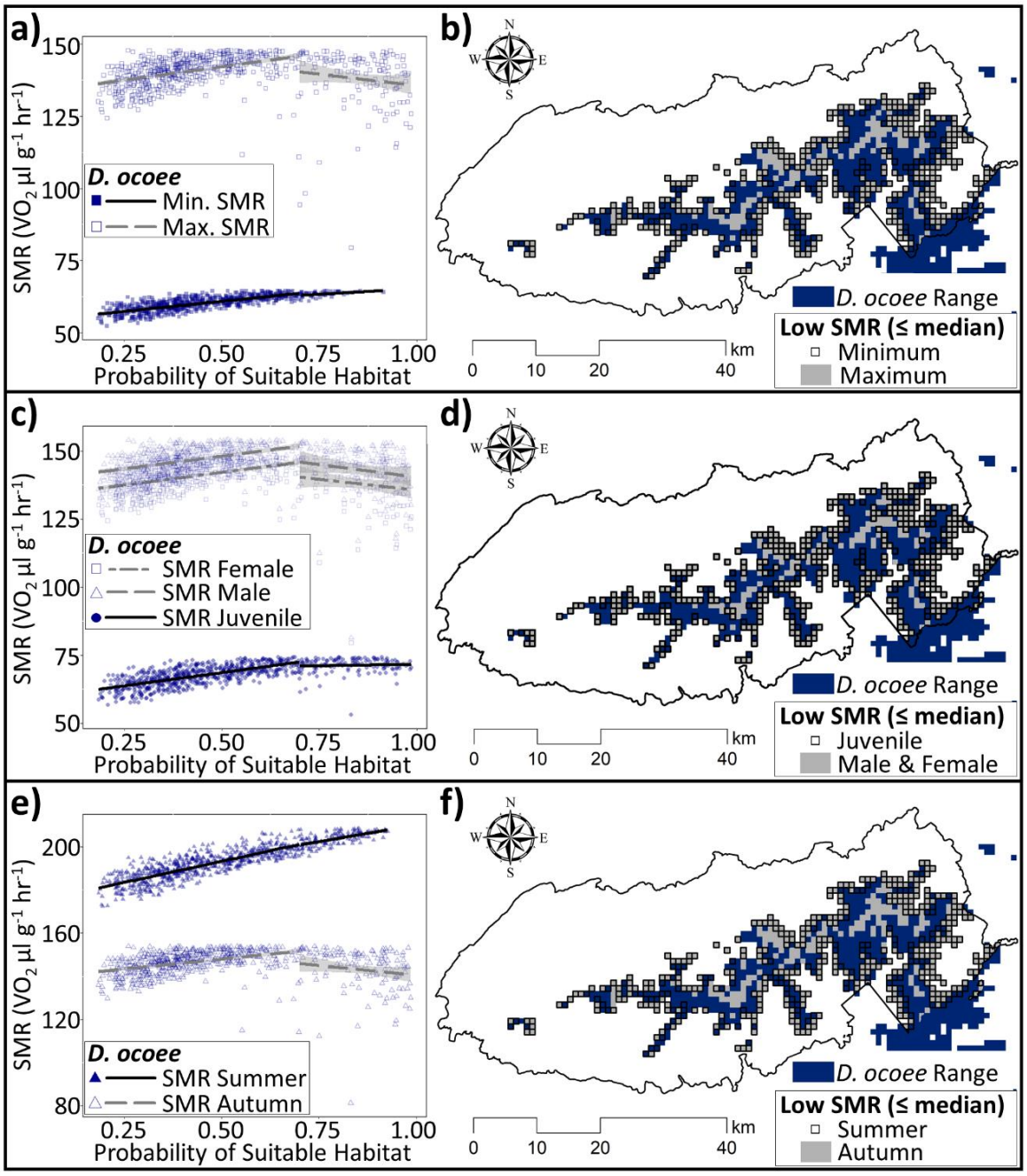

Figure B.8. a) Minimum and maximum standard metabolic rate plotted against the predicted habitat suitability from species distribution models. (b) Locations of low standard metabolic rate (SMR ≤ median) vary between minimum and maximum SMR. Examples in (a) and (b) are using data for *Desmognathus ocoee* females during autumn. (c) Maximum standard metabolic rate during autumn plotted against predicted habitat suitability for *Desmognathus ocoee*. (d) Locations of low standard metabolic rate (SMR ≤ median) vary between adults and juveniles. (e) Maximum standard metabolic rate during summer and autumn plotted against predicted habitat suitability for *Desmognathus ocoee* males. (f) Locations of low standard metabolic rate (SMR ≤ median vary between seasons. (a), (c), and (e) are plotted with piecewise regression to demonstrate the relationship in low suitable habitat (0.0-0.7) and high suitable habitat (> 0.7)

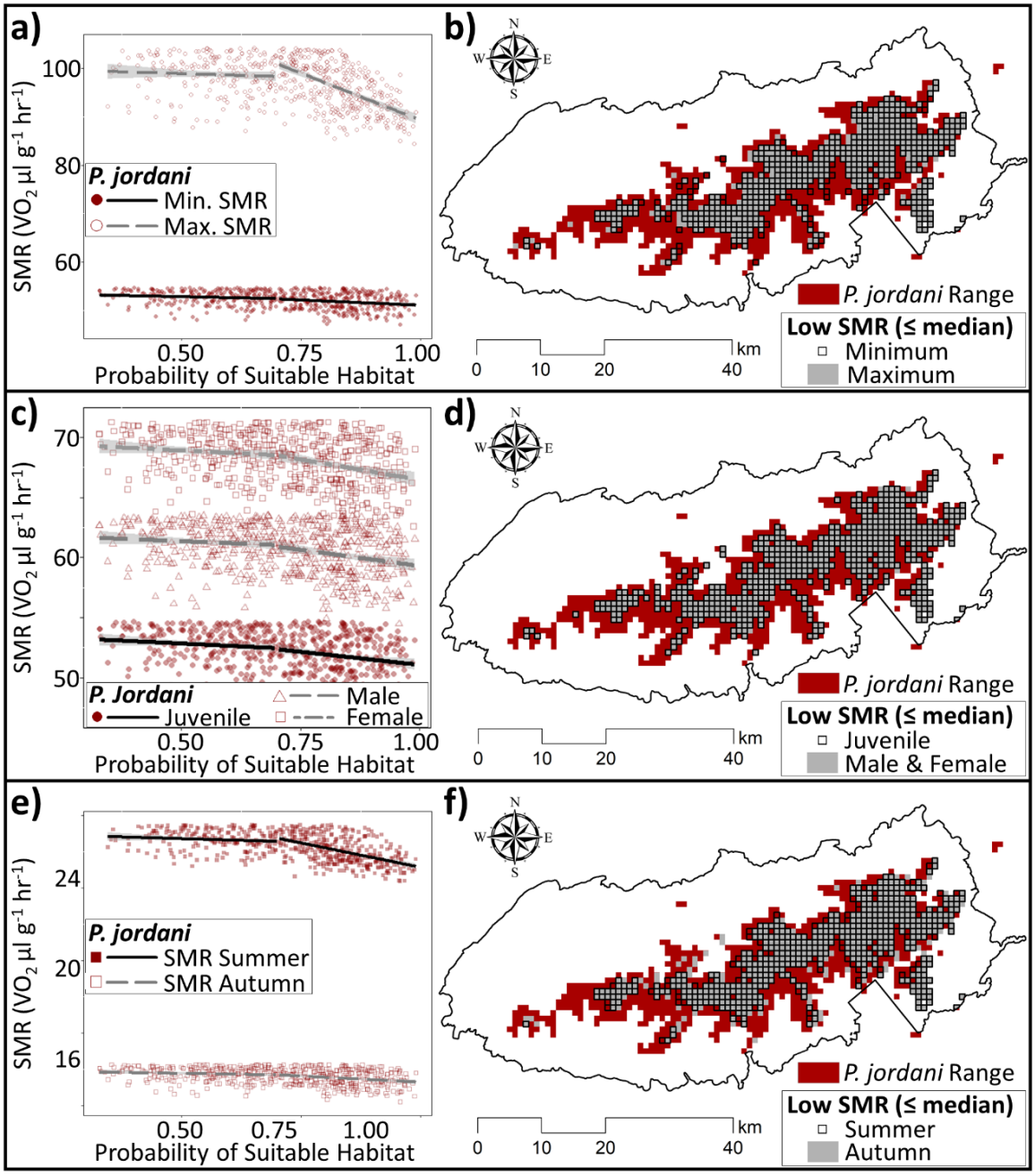

Figure B.9. a) Minimum and maximum standard metabolic rate plotted against the predicted habitat suitability from species distribution models. (b) Locations of low standard metabolic rate (SMR ≤ median) vary between minimum and maximum SMR. Examples in (a) and (b) are using data for *Plethodon jordani* juveniles during autumn. (c) Minimum standard metabolic rate during autumn plotted against predicted habitat suitability for *Desmognathus ocoee*. (d) Locations of low standard metabolic rate (SMR ≤ median) vary between adults and juveniles. (e) Minimum standard metabolic rate during summer and autumn plotted against predicted habitat suitability for *Desmognathus ocoee* males. (f) Locations of low standard metabolic rate (SMR ≤ median vary between seasons. (a), (c) , and (e) are plotted with piecewise regression to demonstrate the relationship in low suitable habitat (0.0-0.7) and high suitable habitat (> 0.7)

Table B.1. The 11 bioclimatic variables used in our species distribution models.

WorldClim Bioclimatic Variables	
Bioclim Code	Description
BIO1	Annual Mean Temperature
BIO2	Mean Diurnal Range (Mean of monthly (max temp - min temp))
BIO3	Isothermality (Mean Diurnal Range/Temperature Annual Range) (×100)
BIO7	Temperature Annual Range (Maximum Temperature of Warmest Month-Minimum Temperature of Coldest Month)
BIO8	Mean Temperature of Wettest Quarter
BIO9	Mean Temperature of Driest Quarter
BIO15	Precipitation Seasonality (Coefficient of Variation)
BIO16	Precipitation of Wettest Quarter
BIO17	Precipitation of Driest Quarter
BIO18	Precipitation of Warmest Quarter
BIO19	Precipitation of Coldest Quarter

Table B.2. Mean mass (g) and standard error of the mean for observed females, males, and juveniles of each study species. Also shown are model estimates for the increase in mass (g) and percent increase in mass per 100 m gain in elevation.

Sex/Stage	Count	Mass (g)	SE	ΔMass (g)/100 m	ΔMass (%)/100 m
Desmognathus wrighti					
Female	59	0.52	0.017	0.017	3.3
Male	150	0.35	0.009	0.017	4.9
Juvenile	82	0.36	0.015	0.021	5.8
Desmognathus ocoee					
Female	41	3.23	0.224	0.31	9.6
Male	76	3.29	0.179	0.32	9.7
Juvenile	44	0.99	0.106	0.19	19.2
Plethodon jordani					
Female	148	5.73	0.113	0.20	3.5
Male	359	4.43	0.059	0.20	4.5
Juvenile	104	3.06	0.114	0.20	6.5

Table B.3. Mean, minimum, and maximum standard metabolic rate (SMR) estimates and the coefficient of variation (CV) for each species. Shown are averages across the entire study period, and during spring, summer, and autumn months.

D. wrighti	Study Period		Spring		Summer		Autumn	
	Mean	CV	Mean	CV	Mean	CV	Mean	CV
Minimum SMR	26.54	0.06	22.27	0.07	35.92	0.03	21.44	0.10
Female	30.11	0.05	25.84	0.05	39.49	0.03	25.01	0.08
Male	27.31	0.05	23.04	0.06	36.69	0.03	22.20	0.10
Juvenile	22.20	0.08	17.93	0.10	31.58	0.05	17.10	0.13
Average SMR	34.04	0.06	30.21	0.06	42.78	0.04	29.15	0.07
Female	37.61	0.05	33.78	0.05	46.35	0.03	32.72	0.06
Male	34.81	0.05	30.97	0.06	43.55	0.04	29.92	0.08
Juvenile	29.70	0.08	25.87	0.09	38.44	0.06	24.81	0.09
Maximum SMR	41.55	0.06	38.14	0.07	49.64	0.05	36.87	0.07
Female	45.12	0.05	41.71	0.06	53.21	0.04	40.44	0.06
Male	42.32	0.06	38.91	0.06	50.40	0.05	37.63	0.07
Juvenile	37.21	0.08	33.80	0.09	45.30	0.07	32.53	0.09
D. ocoee	Study Period		Spring		Summer		Autumn	
	Mean	CV	Mean	CV	Mean	CV	Mean	CV
Minimum SMR	50.14	0.15	45.87	0.16	59.51	0.12	45.03	0.17
Female	57.49	0.14	53.22	0.15	66.87	0.12	52.39	0.16
Male	59.25	0.14	54.98	0.15	68.63	0.11	54.15	0.13
Juvenile	33.66	0.20	29.39	0.22	43.04	0.15	28.56	0.24
Average SMR	57.64	0.12	53.80	0.13	66.37	0.10	52.74	0.13
Female	65.00	0.11	61.16	0.12	73.73	0.10	60.10	0.13
Male	66.75	0.11	62.91	0.12	75.49	0.09	61.86	0.10
Juvenile	41.17	0.14	37.33	0.15	49.90	0.11	36.27	0.17
Maximum SMR	65.14	0.09	61.73	0.10	73.23	0.08	60.46	0.11
Female	72.50	0.09	69.09	0.09	80.59	0.08	67.82	0.10
Male	74.26	0.09	70.85	0.09	82.34	0.08	69.57	0.08
Juvenile	48.67	0.10	45.26	0.11	56.76	0.09	43.99	0.12
P. jordani	Study Period		Spring		Summer		Autumn	
	Mean	CV	Mean	CV	Mean	CV	Mean	CV
Minimum SMR	79.90	0.11	68.91	0.12	102.83	0.10	67.95	0.13
Female	91.52	0.08	79.15	0.08	117.30	0.07	78.10	0.09
Male	80.50	0.11	69.44	0.11	103.59	0.10	68.47	0.15
Juvenile	67.67	0.16	58.14	0.17	87.59	0.15	57.28	0.18
Average SMR	100.47	0.10	87.42	0.10	128.66	0.10	85.34	0.11

Table B.3. continued

Female	114.79	0.08	99.99	0.08	146.73	0.07	97.64	0.08
Male	101.24	0.10	88.09	0.10	129.63	0.09	85.98	0.13
Juvenile	85.40	0.15	74.19	0.15	109.62	0.15	72.38	0.16
Maximum SMR	127.98	0.11	112.43	0.10	163.02	0.11	108.48	0.11
Female	146.12	0.08	128.39	0.08	186.09	0.09	123.88	0.08
Male	128.96	0.10	113.29	0.10	164.29	0.10	109.31	0.13
Juvenile	108.85	0.15	95.61	0.15	138.69	0.15	92.26	0.15

APPENDIX C: CHAPTER 4 SUPPLEMENTARY MATERIAL

Figures

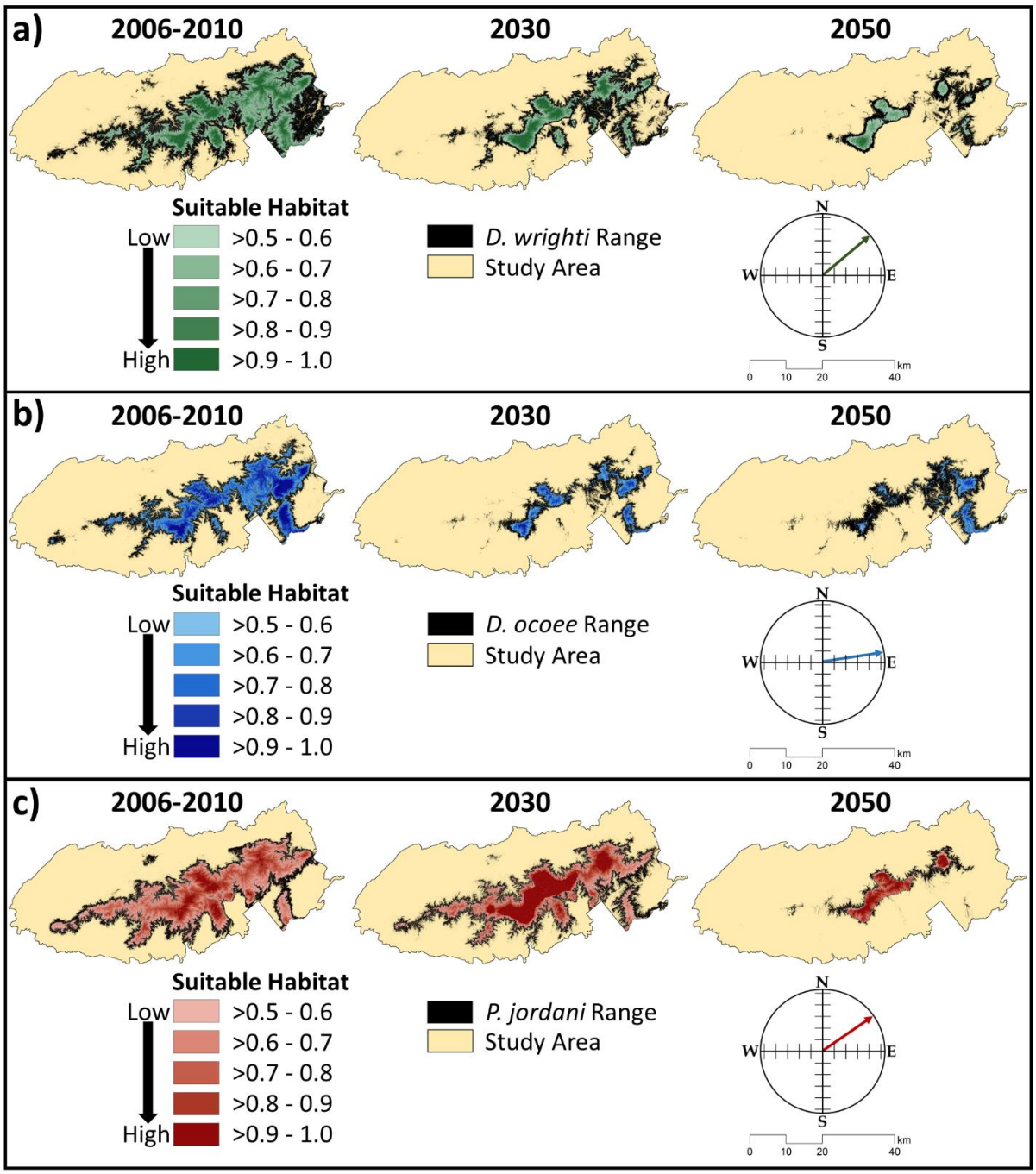

Figure C.1. Microclimatic species distribution models for (a) *Desmognathus wrighti*, (c) *Desmognathus ocoee*, and (e) *Plethodon jordani* displaying the probability of suitable habitat above 0.5 for each species from an average 2006-2010 model, 2030 model, and 2050 model. Probability of suitable habitat > 0.5 is overlaid on the entire estimated species range, denoted in black. Compass shows average directional shift of species' range from 2010 to 2050

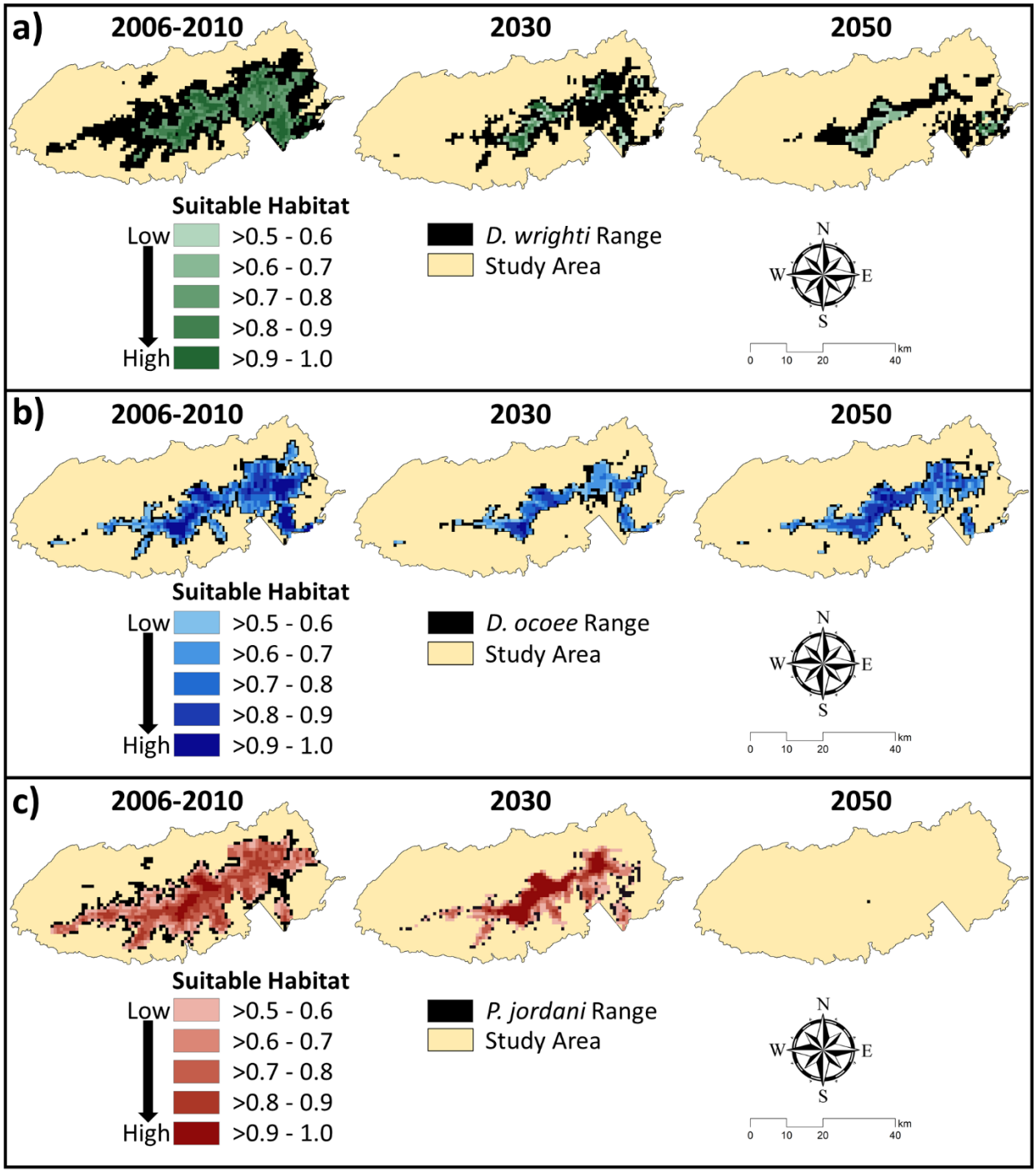

Figure C.2. Coarse resolution species distribution models developed from the NASA NEX-DCP30 dataset for (a) *Desmognathus wrighti*, (c) *Desmognathus ocoee*, and (e) *Plethodon jordani* displaying the probability of suitable habitat above 0.5 for each species from an average 2006-2010 model, 2030 model, and 2050 model. Probability of suitable habitat > 0.5 is overlaid on the entire estimated species range, denoted in black

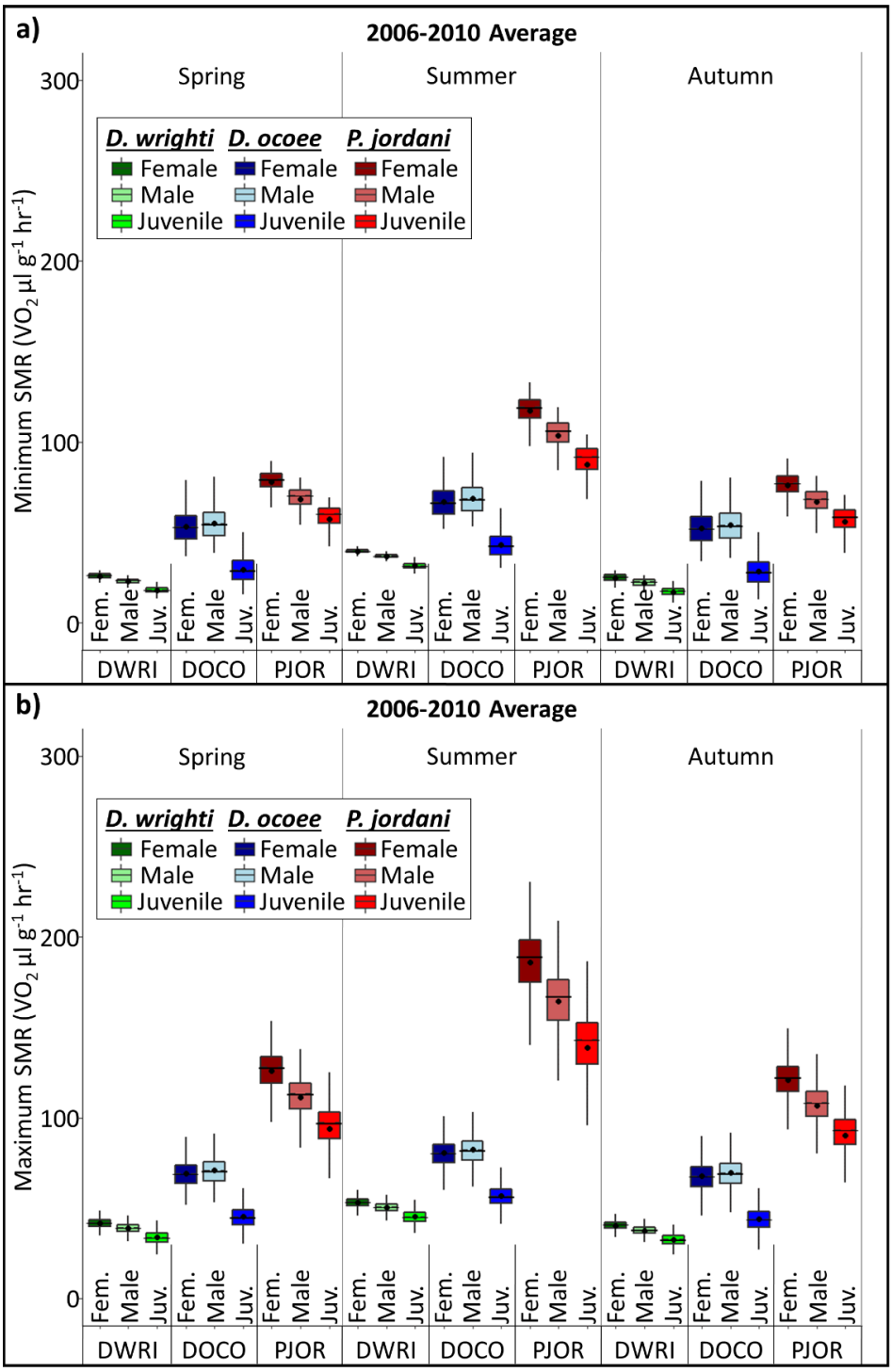

Figure C.3. Seasonal estimates for (a) minimum and (b) maximum standard metabolic rate (SMR) during 2006-2010 for *Desmognathus wrighti* (DWRI), *Desmognathus ocoee* (DOCO), and *Plethodon jordani* (PJOR). Shown are estimates for each sex and stage class (female, male, and juvenile). Points indicate the bootstrapped mean and central error bar lines indicate the confidence interval for the bootstrapped median. Vertical lines indicate the error bar for standard deviation of mean

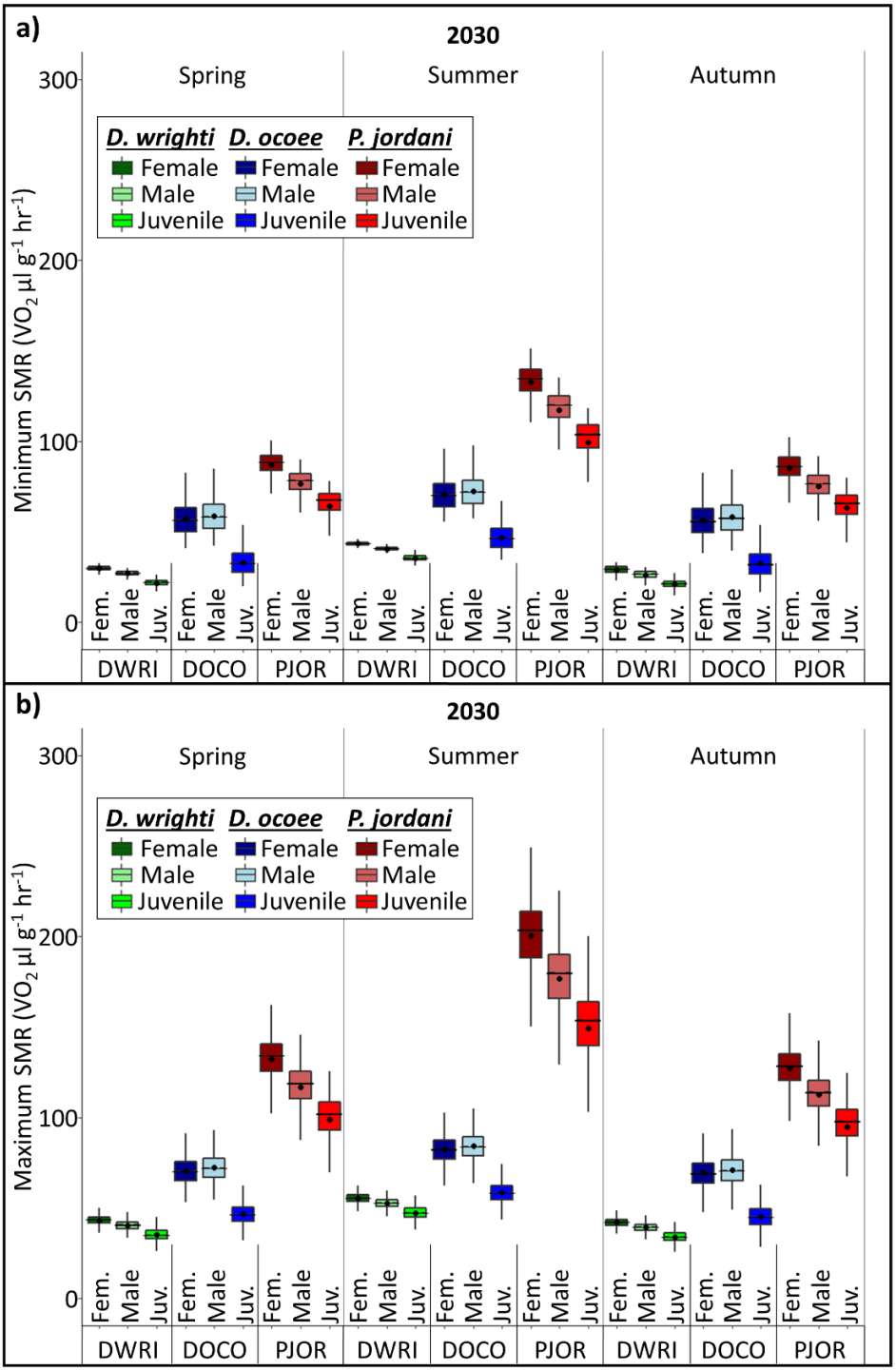

Figure C.4. Future seasonal estimates for (a) minimum and (b) maximum standard metabolic rate (SMR) during 2030 for *Desmognathus wrighti* (DWRI), *Desmognathus ocoee* (DOCO), and *Plethodon jordani* (PJOR). Shown are estimates for each sex and stage class (female, male, and juvenile). Points indicate the bootstrapped mean and central error bar lines indicate the confidence interval for the bootstrapped median. Vertical lines indicate the error bar for standard deviation of mean

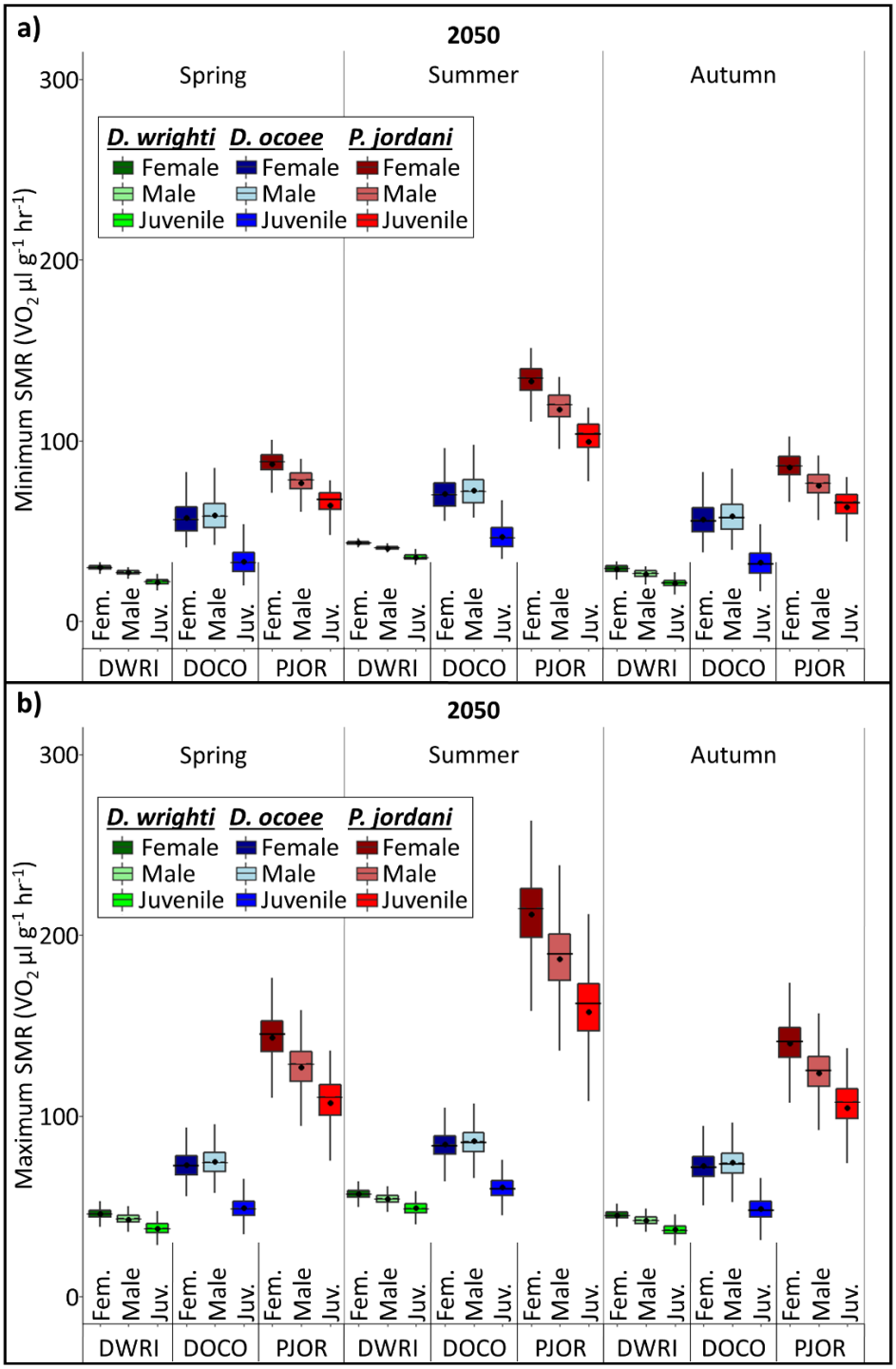

Figure C.5. Future seasonal estimates for (a) minimum and (b) maximum standard metabolic rate (SMR) during 2050 for *Desmognathus wrighti* (DWRI), *Desmognathus ocoee* (DOCO), and *Plethodon jordani* (PJOR). Shown are estimates for each sex and stage class (female, male, and juvenile). Points indicate the bootstrapped mean and central error bar lines indicate the confidence interval for the bootstrapped median. Vertical lines indicate the error bar for standard deviation of mean

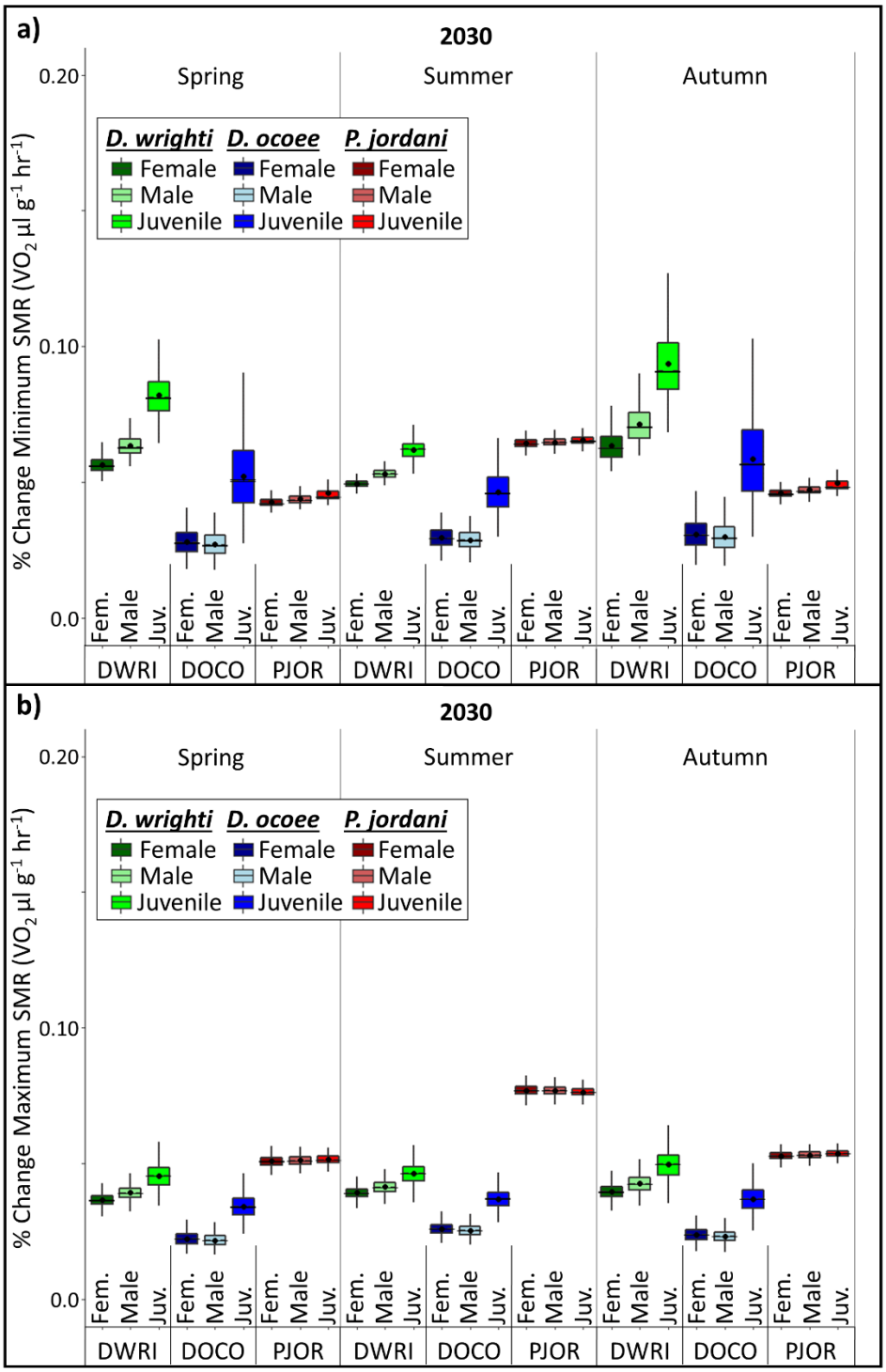

Figure C.6. Percent change in minimum and maximum standard metabolic rate (SMR) between 2010 (2006-2010 average) and 2030 for each season. Shown are estimates for the sex and stage class (male, female, and juvenile) for *Desmognathus wrighti* (DWRI), *Desmognathus ocoee* (DOCO), and *Plethodon jordani* (PJOR). Points indicate the bootstrapped mean and central error bar lines indicate the confidence interval for the bootstrapped median. Vertical lines indicate the error bar for standard deviation of mean

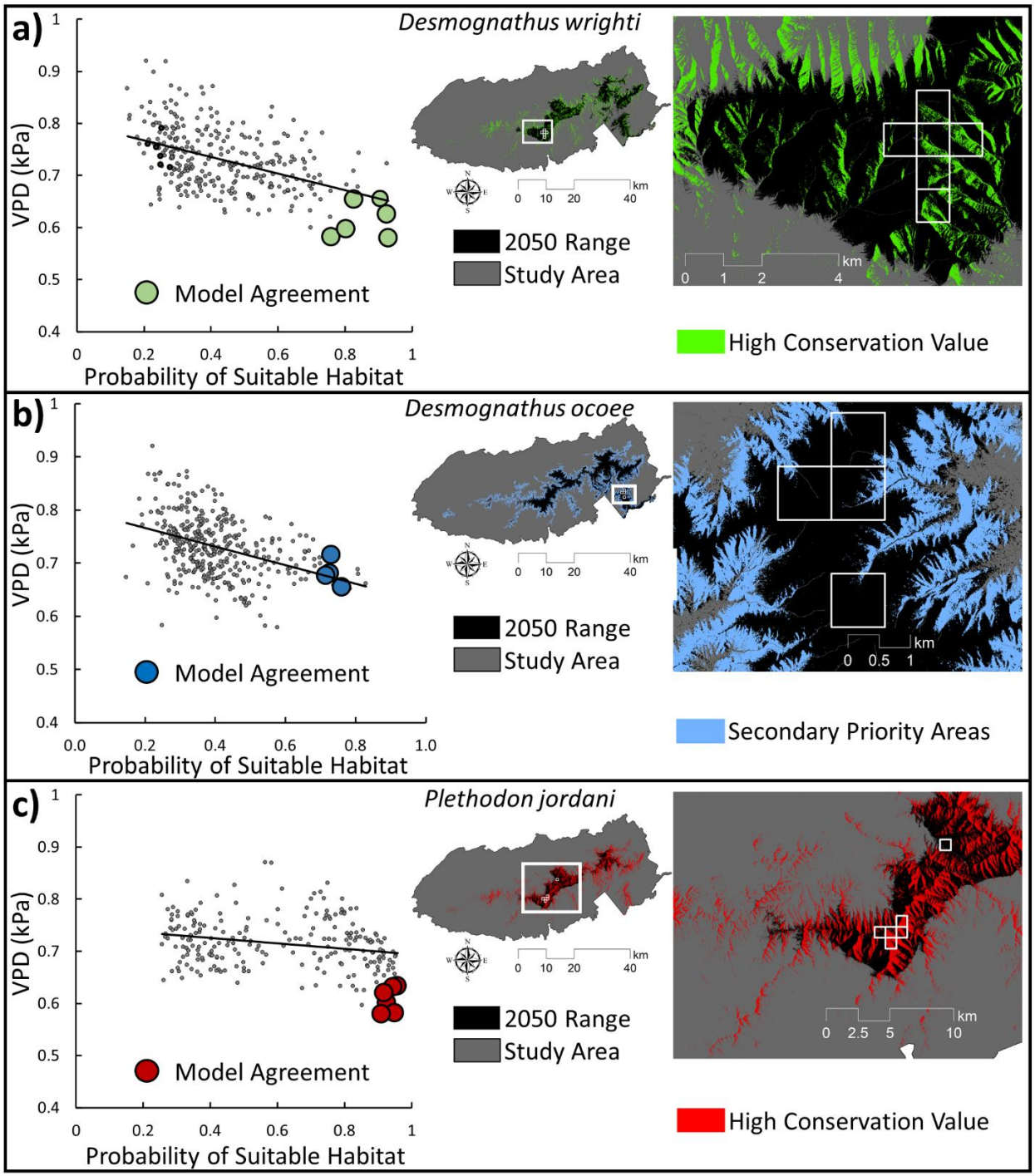

Figure C.7. Multi-scale conservation approach targeting locations with model agreement (large, colored points in graph) between low vapor pressure deficit (VPD) and high probability of suitable habitat to spatially target microscale areas of high conservation value or secondary priority areas within coarse resolution areas (white boxes in map insets). (a) *Desmognathus wrighti*, (b) *Desmognathus ocoee*, and (c) *Plethodon jordani*

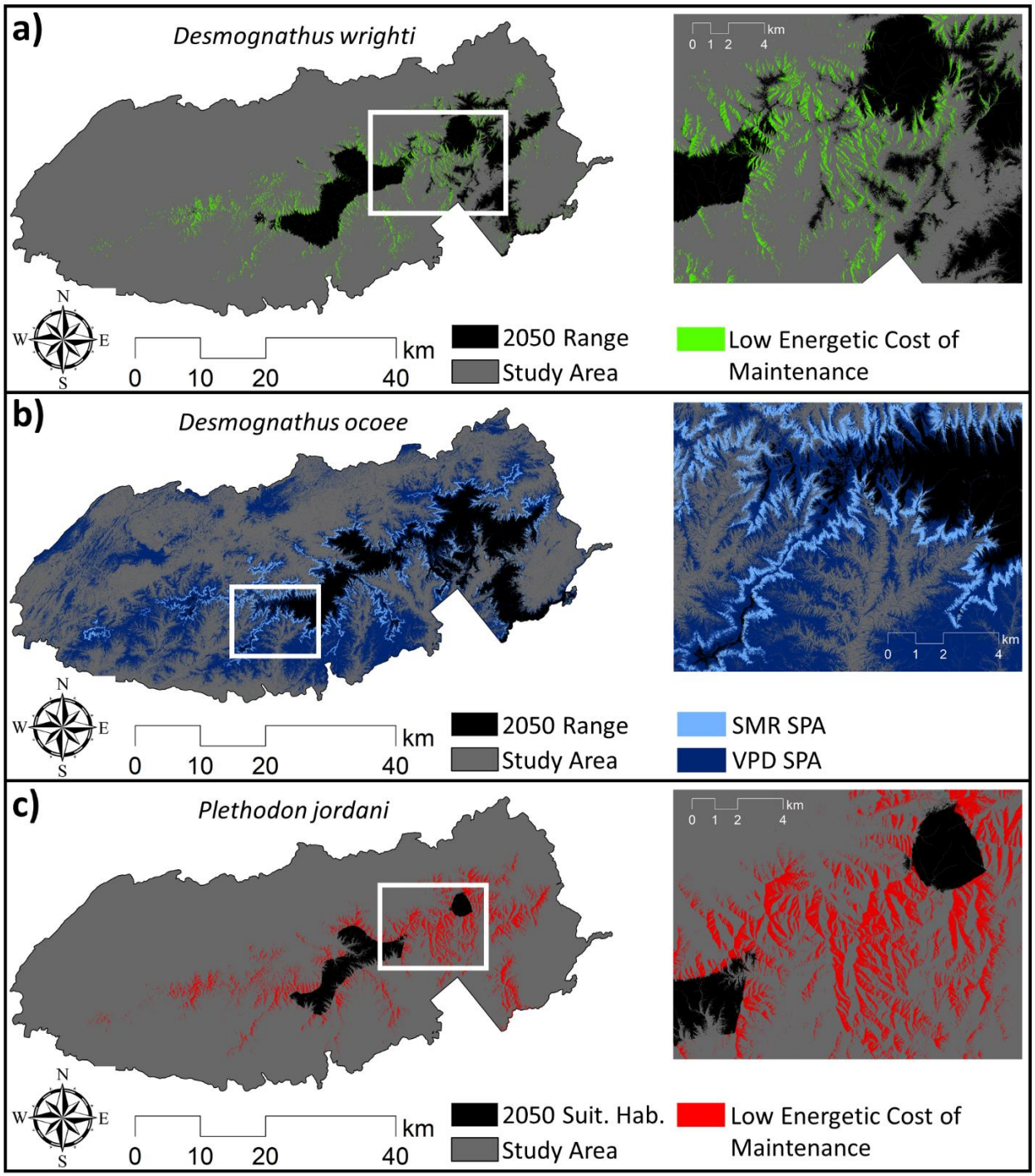

Figure C.8. Low energetic costs of maintenance at the microscale may be useful in targeting functional connectivity between 2050 projections of range extent for *Desmognathus wrighti*. (b) Secondary priority areas (SPA) for microscale standard metabolic rate (SMR) and VPD may be useful for targeting functional connectivity between 2050 range projections for *Desmognathus ocoee*. (c) Low energetic cost of maintenance at the microscale may be useful in targeting functional connectivity between 2050 projections of highly suitable habitat (probability ≥ 0.7) for *Plethodon jordani*

Table C.1. The 11 bioclimatic variables used in our species distribution models.

WorldClim Bioclimatic Variables	
Bioclim Code	Description
BIO1	Annual Mean Temperature
BIO2	Mean Diurnal Range (Mean of monthly (max temp - min temp))
BIO3	Isothermality (Mean Diurnal Range/Temperature Annual Range) (×100)
BIO7	Temperature Annual Range (Maximum Temperature of Warmest Month-Minimum Temperature of Coldest Month)
BIO8	Mean Temperature of Wettest Quarter
BIO9	Mean Temperature of Driest Quarter
BIO15	Precipitation Seasonality (Coefficient of Variation)
BIO16	Precipitation of Wettest Quarter
BIO17	Precipitation of Driest Quarter
BIO18	Precipitation of Warmest Quarter
BIO19	Precipitation of Coldest Quarter

Table C.2. Landscape fragmentation of suitable climatic habitat areas within each species' predicted range from microclimatic species distribution models. Patch density (PD) is equal to the number of patches/km^2 and is shown for only species distribution models (SDM) and the integration of SDMs with functional connectivity, based on high and secondary priority areas, under future climate scenarios (2030 and 2050).

			Species Distribution Model (SDM)		SDM + Connectivity	
Year	**Species**	**Range Area (km^2)**	**Number Patches**	**PD (km)**	**Number Patches**	**PD (km)**
2010	*Desmognathus wrighti*	920.1	250226	272.0	-	-
2010	*Desmognathus ocoee*	604.2	234047	387.4	-	-
2010	*Plethodon jordani*	840.3	157200	187.1	-	-
2030	*Desmognathus wrighti*	482.2	266504	552.7	206560	428.4
2030	*Desmognathus ocoee*	243.0	141896	584.0	80640	331.9
2030	*Plethodon jordani*	722.0	270040	374.0	206560	286.1
2050	*Desmognathus wrighti*	235.4	140458	596.7	89572	380.5
2050	*Desmognathus ocoee*	273.8	138663	506.4	73399	268.1
2050	*Plethodon jordani*	164.4	88532	538.6	65792	400.2

Table C.3. Average difference in probability of suitable habitat between species' distribution models developed from coarse grain, NASA NEX-DCP30 data and microclimatic temperature data. Averages were calculated within the entire species' range, only within areas of highly suitable habitat (probability ≥ 0.7), and only in areas outside of highly suitable habitat. Difference is calculated as NASA NEX-DCP30 prediction – microclimatic predictions.

Species	Time Period	Species' Range	Suitable Habitat ≥ 0.7	Outside Suitable Habitat
Desmognathus wrighti	2006-2010	0.06	-0.08	0.03
Desmognathus wrighti	2030	-0.11	-0.23	-0.14
Desmognathus wrighti	2050	-0.07	-0.15	-0.08
Desmognathus ocoee	2006-2010	0.09	-0.02	0.06
Desmognathus ocoee	2030	0.17	0.00	0.14
Desmognathus ocoee	2050	0.24	-0.13	0.22
Plethodon jordani	2006-2010	0.05	-0.02	0.03
Plethodon jordani	2030	-0.07	-0.09	-0.08
Plethodon jordani	2050	-0.29	-0.59	-0.44

Table C.4. Results from modified t-tests between minimum standard metabolic rate (SMR) or vapor pressure deficit (VPD) with the probability of suitable habitat from species distribution models at a 3 m^2 spatial resolution. Shown are results for the 2006-2010 study period and 2050 study period in () for each sex and stage class of each species and for each season of the study period. Test results include the correlation coefficient, F-statistic, degrees of freedom (df), and *p*-values (**p*-value < 0.05, ** *p*-value < 0.01, and *** *p*-value < 0.001).

Sex/Stage Class	Season	Correlation Coefficient	F-statistic	df	*p*-value
Desmognathus wrighti			2006-2010 (2050)		
Minimum SMR	Spring	-0.18 (-0.02)	36.0 (0.3)	1085 (877)	*** (0.61)
Female	Summer	-0.34 (-0.06)	40.9 (1.1)	310 (338)	*** (0.29)
	Fall	-0.08 (0.01)	21.7 (0.01)	3683 (2041)	*** (0.93)
Minimum SMR	Spring	-0.20 (-0.02)	39.6 (0.4)	994 (858)	*** (0.51)
Male	Summer	-0.36 (-0.07)	44.4 (1.5)	289 (331)	*** (0.22)
	Fall	-0.09 (-0.01)	26.8 (0.01)	3440 (2009)	*** (0.93)
Minimum SMR	Spring	-0.01 (0.12)	0.2 (18.8)	2052 (1371)	0.65 (***)
Juvenile	Summer	-0.07 (0.15)	3.6 (16.2)	667 (742)	0.06 (***)
	Fall	0.04 (0.09)	5.1 (18.5)	4113 (2131)	* (***)
VPD	Spring	-0.57 (-0.22)	125.1 (46.1)	255 (881)	*** (***)
	Summer	-0.47 (-0.23)	72.6 (40.5)	251 (699)	*** (***)
	Fall	-0.38 (-0.14)	101.7 (25.7)	585 (1266)	*** (***)
Desmognathus ocoee			2006-2010 (2050)		
Minimum SMR	Spring	0.68 (0.29)	273.4 (18.8)	326 (205.8)	*** (***)
Female	Summer	0.71 (0.33)	311.4 (25.6)	313 (215)	*** (***)
	Fall	0.63 (0.24)	234.4 (12.7)	356 (203)	*** (***)
Minimum SMR	Spring	0.68 (0.29)	274.3 (18.8)	326 (205)	*** (***)
Male	Summer	0.71 (0.33)	312.0 (25.7)	312 (214)	*** (***)
	Fall	0.63 (0.24)	235.3 (12.8)	355 (202)	*** (***)
Minimum SMR	Spring	0.66 (0.27)	256.8 (17.5)	339 (218)	*** (***)
Juvenile	Summer	0.70 (0.32)	298.5 (25.2)	320 (227)	*** (***)
	Fall	0.60 (0.22)	216.2 (11.1)	379 (217)	*** (***)
VPD	Spring	-0.48 (-0.42)	289.9 (98.4)	959 (471)	*** (***)
	Summer	-0.36 (-0.39)	64.6 (41.8)	446 (232)	*** (***)
	Fall	-0.31 (-0.33)	163.1 (157.2)	1568 (1272)	*** (***)
Plethodon jordani			2006-2010 (2050)		
Minimum SMR	Spring	-0.48 (-0.01)	93.7 (0.01)	309.9 (322)	*** (0.91)
Female	Summer	-0.65 (-0.09)	129.0 (2.9)	180.8 (356)	*** (0.09)

Table C.4. continued

	Fall	-0.31 (0.02)	75.3 (0.3)	708 (232)	*** (0.63)
Minimum SMR	Spring	-0.49 (0.01)	94.5 (0.01)	305 (326)	*** (***)
Male	Summer	-0.65 (-0.07)	129.5 (2.0)	181 (359)	*** (***)
	Fall	-0.32 (0.03)	76.0 (0.4)	684 (326)	*** (***)
Minimum SMR	Spring	-0.49 (0.02)	95.5 (0.1)	298 (334)	0.65 (***)
Juvenile	Summer	-0.65 (-0.05)	129.8 (0.9)	181 (369)	0.06 (***)
	Fall	-0.33 (0.05)	77.0 (0.7)	652 (331)	* (***)
VPD	Spring	-0.46 (-0.11)	114.4 (1.5)	421 (111)	*** (***)
	Summer	-0.36 (-0.11)	45.4 (1.1)	300 (84)	*** (***)
	Fall	-0.26 (-0.04)	45.9 (0.2)	627 (142)	*** (***)

Table C.5. Results from modified t-tests between minimum standard metabolic rate (SMR) or vapor pressure deficit (VPD) with the probability of suitable habitat from species distribution models. Shown are results for the 2050 projections for aggregated data at a 0.85 km^2 spatial resolution. Correlation coefficients are shown for aggregated data along with microclimatic correlations in () for comparison. Test results include the correlation coefficient, F-statistic, degrees of freedom (df), and *p*-values (**p*-value < 0.05, ** *p*-value < 0.01, and *** *p*-value < 0.001).

Sex/Stage Class	Correlation Coefficient	F-statistic	df	*p*-value
Desmognathus wrighti	Aggregated (Microclimate)			
Minimum SMR Average	-0.26 (-0.02)	3.4	48	***
VPD Average	-0.45 (-0.20)	28.4	109	***
Desmognathus ocoee	Aggregated (Microclimate)			
Minimum SMR Average	0.52 (0.28)	33.6	90	***
VPD Average	-0.40 (-0.38)	14.8	81	***
Plethodon jordani	Aggregated (Microclimate)			
Minimum SMR Average	-0.27 (-0.01)	12.8	166	***
VPD Average	-0.24 (-0.09)	3.9	61	***

REFERENCES

Abatzoglou JT, Brown TJ (2012) A comparison of statistical downscaling methods suited for wildfire applications, International Journal of Climatology 32:772-780

Adams DC, Church JO (2008) Amphibians do not follow Bergmann's rule. Evolution 62:413–420. https://doi.org/10.1111/j.1558-5646.2007.00297.x

Addo-Bediako A, Chown SL, Gaston KJ (2001) Revisiting water loss in insects: a large scale view. J Insect Physiol 47:1377–1388. https://doi.org/10.1016/S0022-1910(01)00128-7

Allen RG, Pereira LS, Raes D, Smith M (1998), Crop evapotranspiration—Guidelines for computing crop water requirements-FAO Irrigation and drainage paper 56, FAO, Rome, 300, 6541.

AmphibiaWeb (2020) <https://amphibiaweb.org> University of California, Berkeley, CA, USA. Last accessed 9 Aug 2020.

Araújo MB, Anderson RP, Barbosa AM, et al (2019) Standards for distribution models in biodiversity assessments. Science Advances 5:1–12 http://doi.org/10.1126/sciadv.aat4858

Arif S, Adams DC, and Wicknick JA. (2007) Bioclimatic modeling, morphology, and behavior reveal alternative mechanisms regulating the distributions of two parapatric salamander species. Evolutionary Ecology Research 9:843– 854.

Ashcroft MB (2010) Identifying refugia from climate change. J Biogeogr 37:1407–1413

Ashcroft MB, Gollan JR (2012) Fine-resolution (25 m) topoclimatic grids of near-surface (5 cm) extreme temperatures and humidities across various habitats in a large (200-300 km) and diverse region. - Int. J Climatol 32:2134–2148

Ashcroft MB, Chisholm LA, French KO (2008) The effect of exposure on landscape scale soil surface temperatures and species distribution models. Landsc Ecol 23:211–225

Barton MG, Terblanche JS (2014) Predicting performance and survival across topographically heterogeneous landscapes: The global pest insect *Helicoverpa armigera* (Hübner, 1808) (Lepidoptera: Noctuidae). Austral Entomol 53:249–258. https://doi.org/10.1111/aen.12108

Bellis ED (1962) The influence of humidity on wood frog activity. American Midland Naturalist 68:139.

Bernardo J, Spotila JR (2006) Physiological constraints on organismal response to global warming : mechanistic insights from clinally varying populations and implications for assessing endangerment. 2:135–139. https://doi.org/10.1098/rsbl.2005.0417

Bernardo J, Ossola RJ, Spotila J, Crandall KA (2007) Interspecies physiological variation as a tool for endangerment : validation of an intrinsic determinant of macroecological and phylogeographic structure. 695–698. https://doi.org/10.1098/rsbl.2007.0259

Beven KJ, Kirkby MJ (1979) A physically based, variable contributing area model of basin hydrology. Hydrol Sci Bull 24:43–69

Blaustein AR, Kiesecker JM (2002) Complexity in conservation: Lessons from the global decline of amphibian populations. Ecol Lett 5:597–608. https://doi.org/10.1046/j.1461-0248.2002.00352.x

Blaustein AR, Walls SC, Bancroft BA, et al (2010) Direct and indirect effects of climate change on amphibian populations. Diversity 2:281–313. https://doi.org/10.3390/d2020281

Bramer I, Anderson BJ, Bennie J, et al (2018) Advances in monitoring and modelling climate at ecologically relevant scales. Adv Ecol Res 58:101–161

Brattstrom BH (1979) Amphibian temperature regulation studies in the field and laboratory. Integr Comp Biol 19:345–356. https://doi.org/10.1093/icb/19.1.345

Burnham KP, Anderson DR (2002) Model selection and multimodel inference: a practical information-theoretic approach (2nd ed). Library of Congress Cataloging-in-Publication Data

Carey C, Alexander M (2003) Special Issue: Amphibian Declines. Climate change and amphibian declines: is there a link? Divers Distrib 9:111–121. https://doi.org/10.1046/j.1472-4642.2003.00011.x

Carscadden KA, Emery NC, Arnillas CA, et al (2020) Niche Breadth: Causes and Consequences for Ecology, Evolution, and Conservation. The Quarterly Review of Biology 95:179–214. https://doi.org/10.1086/710388

Caruso NM, Sears MW, Adams DC, Lips KR (2014) Widespread rapid reductions in body size of adult salamanders in response to climate change. Glob Change Biol 20:1751-1759. http://dx.doi.org/10.1111/gcb.12550.

Caruso, N. M. (2015). Surface Retreats Used among Four Genera of Terrestrial Salamanders in the Great Smoky Mountains National Park. BioOne 49(3), 3–10. http://doi.org/10.1670/13-148

Chazdon RL (1988) Sunflecks and their importance to forest understorey plants. Adv Ecol 18:1–63

Chen I, Hill JK, Ohlemüller R, et al (2011) Rapid Range Shifts of Species of Climate Warming. Science. 333:1024–1027. https://dow.org/10.1126/science.1206432

Chen J, Franklin JF (1997) Growing-season microclimate variability within an old-growth Douglas-fir forest. Clim Res 8:21–34

Chen J, Saunders SC, Crow TR, Naiman RJ, Brosofske KD, Mroz GD, Brookshire BL, Franklin JF (1999) Microclimate in forest ecosystem and landscape ecology—variations in local climate can be used to monitor and compare the effects of different management regimes. Bioscience 49:288–297

Clifford P, Richardson S. Hemon D (1989). Assessing the significance of the correlation between two spatial processes. Biometrics 45, 123–134.

Clinton BD (2003) Light, temperature, and soil moisture responses to elevation, evergreen understory, and small canopy gaps in the southern Appalachians. For Ecol Manag 186:243–255

Clusella-Trullas S, Blackburn TM, Chown SL (2011) Climatic predictors of temperature performance curve parameters in ectotherms imply complex responses to climate change. Am Nat 177:738–751. https://doi.org/10.1086/660021

Colson T (2011) National Park Service. 3-m Lidar Digital Elevation Model. https://irma.nps.gov/DataStore/

Connette GM, Crawford JA, Peterman WE (2015) Climate change and shrinking salamanders: Alternative mechanisms for changes in plethodontid salamander body size. Glob Chang Biol 21:2834–2843. https://doi.org/10.1111/gcb.12883

Cushman SA (2006) Effects of habitat loss and fragmentation on amphibians: A review and prospectus. Biol Conserv 128:231–240. https://doi.org/10.1016/j.biocon.2005.09.031

Dai A, Trenberth K (1999) Effects of clouds, soil moisture, precipitation, and water vapor on diurnal temperature range. J Clim 12:2451–2474

Daly C, Neilson RP, Phillips DL (1994) A statistical-topographic model for mapping climatological precipitation over mountainous Terrain. J Appl Meteorol 33(2):140–158

Davis KT, Dobrowski SC, Holden ZA, Higuera PE, Abatzoglou JT (2018) Microclimatic buffering in forests of the future: the role of local water balance. Ecography 42(1):1–11

De Frenne P, Verheyen K (2016) Weather stations lack forest data. Science 351(6270):234

De Frenne P, Zellweger F, Rodríguez-Sánchez F, et al (2019) Global buffering of temperatures under forest canopies. Nat Ecol Evol 3:744–749

Dodd, CK (2003) Monitoring Amphibians in Great Smoky Mountains National Park. U.S. Department of the Interior U.S. Geological Survey. Library of Congress Cataloging-in-Publication Data. Tallahassee, FL USA

Dodd, CK (2004) The Amphibians of the Great Smoky Mountains National Park. The University of Tennessee Press, Knoxville, Tennessee.

DuRant SE, Hopkins WA, Talent LG (2007) Energy acquisition and allocation in an ectothermic predator exposed to a common environmental stressor. Comp Biochem Physiol - Toxicol Pharmacol 145:442–448

Elith J, Ferrier S, Guisan A, et al (2006) Novel methods improve prediction of species' distributions from occurrence data. Ecography 29:129-151

Elith J, Leathwick JR, Hastie T (2008) A working guide to boosted regression trees. J Anim Ecol 77:802–813. https://doi.org/10.1111/j.1365-2656.2008.01390.x

Elith J, Phillips SJ, Hastie T, Dudı M (2011) A statistical explanation of MaxEnt for ecologists. Divers Distrib 43–57. https://doi.org/10.1111/j.1472-4642.2010.00725.x

Elsen PR, Tingley MW (2015) Global mountain topography and the fate of montane species under climate change. Nat Clim Chang 5:772–776

Elsen PR, Monahan WB, Dougherty ER, Merenlender AM (2020) Keeping pace with climate change in global terrestrial protected areas. Sci Adv 6: 25 https://doi.org/10.1126/sciadv.aay0814

Esri Inc. (2020) ArcGIS Desktop (version 10.4.1-10.6.1). Software. Redlands, CA

Evans TG, Diamond SE, Kelly MW (2015) Mechanistic species distribution modelling as a link between physiology and conservation. Conserv Physiol 3:1–16. https://doi.org/10.1093/conphys/cov056.

Fahrig L (2003) Effects of habitat fragmentation on biodiversity. Anu Rev Ecol Evol Syst 34:487–515. https://doi.org/10.1146/132419

Faleiro FV, Machado R (2013) Defining spatial conservation priorities in the face of land-use and climate change. Bio Conservation 158: 248-257 https://doi.org/10.1016/j.biocon.2012.09.020

Farallo VR, Miles DB (2016) The Importance of Microhabitat: A Comparison of Two Microendemic Species of Plethodon to the Widespread P. cinereus. Copeia 104:67–77. https://doi.org/10.1643/CE-14-219

Feder ME, Pough FH (1975) Temperature selection by the red-backed salamander, Plethodon c. cinereus (Green) (Caudata: Plethodontidae). Comp Biochem Physiol 50A:91–98. https://doi.org/10.1016/S0010-406X(75)80207-6

Feder ME (1976) Oxygen consumption and body temperature in neotropical and temperate zone lungless salamanders (Amphibia: Plethodontidae). J Comp Physiol 110:197–208. https://doi.org/10.1007/BF00689308

Feder ME (1983) Integrating the Ecology and Physiology of Plethodontid Salamanders Author (s): Martin E . Feder Published by : Allen Press on behalf of the Herpetologists ' League Stable URL : https://www.jstor.org/stable/3892572 Linked references are availa. 39:291–310

Fielding CA, Whittaker JB, Butterfield JEL, Coulson JC (1999) Predicting responses to climate change: The effect of altitude and latitude on the phenology of the Spittlebug Neophilaenus lineatus. Functional Ecology 13:65–73.

Franklin J, Davis FW, Ikegami M, Syphard AD, Flint LE, Flint AL, Hannah L (2013) Modeling plant species distributions under future climates: how fine scale do climate projections need to be? Glob Chang Biol 19:473–483

Frey SJK, Hadley AS, Johnson SL, Schulze M, Jones JA, Betts MG (2016) Spatial models reveal the microclimatic buffering capacity of old-growth forests. Sci Adv 2(4):e1501392

Fridley JD (2009) Downscaling climate over complex terrain: high finescale (< 1000 m) spatial variation of near-ground temperatures in a montane forested landscape (Great Smoky Mountains). J Appl Meteorol Climatol 48:1033–1049

Geiger R, Aron RH, Todhunter P (2009) The climate near the ground, 7th edn. Rowman and Littlefield, Lanham

Gifford ME, Kozak KH (2012) Islands in the sky or squeezed at the top? Ecological causes of elevational range limits in montane salamanders. Ecography (Cop) 35:193–203. https://doi.org/10.1111/j.1600-0587.2011.06866.x

Gifford ME (2016) Physiology of Plethodontid Salamanders: A Call for Increased Efforts. Copeia 104:42–51. https://doi.org/10.1643/OT-14-223

Gillingham PK, Palmer SCF, Huntley B, Kunin WE, Chipperfield JD, Thomas CD (2012a) The relative importance of climate and habitat in determining the distributions of species at different spatial scales: a case study with ground beetles in Great Britain. Ecography 35:831–838

Gillingham PK, Huntley B, Kunin WE, Thomas CD (2012b) The effect of spatial resolution on projected responses to climate warming. Divers Distrib 18:990–1000

GRASS Development Team (2017) Geographic Resources Analysis Support System (GRASS) Software, Version 7.2. Open Source Geospatial Foundation. Electronic document: http://grass.osgeo.org. LiDAR Analysis of Vegetation Structure: https://grasswiki.osgeo.org/wiki/Lidar_Analysis_of_Vegetation_Structure

Groves CR, Game ET, Anderson MG, et al (2012) Incorporating climate change into systematic conservation planning. Biodivers Conserv 21:1651–1671. https://doi.org/10.1007/s10531-012-0269-3

Hannah L, Flint L, Syphard AD, Moritz MA, Buckley LB, McCullough IM (2014) Fine-grain modeling of species' response to climate change: holdouts, stepping-stones, and microrefugia. Trends Ecol Evol 29:390–397

Helmuth B, Broitman BR, Yamane L, Gilman SE, Mach K, Mislan KAS, Denny MW (2010) Organismal climatology: analyzing environmental variability at scales relevant to physiological stress. J Exp Biol 213:995–1003

Hernandez PA, Graham CH, Master LL, et al (2006) The effect of sample size and species characteristics on performance of different species distribution modeling methods. Ecography 5:773–785

Hicks DJ, Chabot BF (1985) Deciduous forest. In: Chabot BF, Mooney HA (eds) Physiological ecology of North American plant communities. Chapman and Hall, New York, pp 257–277

Hijmans RJ, Graham CH (2006). The ability of climate envelope models to predict the effect of climate change on species distributions. Glob. Chang. Biol., 12, 1–10.

Hijmans RJ, Elith J (2017) Species distribution modeling with R. https://cran.r-project.org/web/packages/dismo/vignettes/sdm.pdf

Hocking DJ, Babbitt KJ (2014) Amphibian contributions to ecosystem services. Herpetol Conserv Biol 9(1):1-17

Hoegh-Guldberg O, Hughes L, McIntyre S, et al (2008) Assisted colonization and rapid climate change. Science (80-) 321:345–346. https://doi.org/10.1126/science.1157897

Hoffmann M, Hilton-taylor C, Angulo A, et al (2010) The Impact of Conservation on the Status of the World's Vertebrates. Science 330 6010: 1503-1509. 10.1126/science.1194442

Homyack JA, Haas CA, Hopkins WA (2010) Influence of temperature and body mass on standard metabolic rate of eastern red-backed salamanders (Plethodon cinereus). J Therm Biol 35:143–146. https://doi.org/10.1016/j.jtherbio.2010.01.006

Homyack JA, Haas CA, Hopkins WA (2011) Energetics of surface-active terrestrial salamanders in experimentally harvested forest. J Wildl Manage 75:1267–1278. https://doi.org/10.1002/jwmg.175

IUCN (2020) The IUCN Red List of Threatened Species. Version 2020-3. https://www.iucnredlist.org.

Jacobsen CD, Brown DJ, Flint WD, et al (2020) Vulnerability of high-elevation endemic salamanders to climate change: A case study with the Cow Knob Salamander (Plethodon punctatus). Glob Ecol Conserv 21:e00883. https://doi.org/10.1016/j.gecco.2019.e00883

Jennings SB, Brown ND, Sheil D (1999) Assessing forest canopies and understorey illumination: canopy closure, canopy cover and other measures. Forestry 72:59–74

Jones HG (2014) Plants and microclimate. A quantitative approach to environmental plant physiology, vol 7, 3rd edn. Cambridge University Press, Cambridge

Jones KR, Watson JEM, Possingham HP, Klein CJ (2016) Incorporating climate change into spatial conservation prioritisation: A review. Biol Conserv 194:121–130. https://doi.org/10.1016/j.biocon.2015.12.008

Jordan T, Madden M, Yang B, Sharma JB, Panda S (2011) Acquisition of LiDAR for the Tennessee portion of Great Smoky Mountains National Park and the Foothills Parkway. Center for Remote Sensing and Mapping Science (CRMS), Department of Geography, The University of Georgia, Athens, Georgia, USA, Tech. Rep. USGS Contract # G10AC0015

Jucker T, Hardwick SR, Both S, Elias DMO, Ewers RM, Milodowski DT, Swinfield T, Coomes DA (2018) Canopy structure and topography jointly constrain the microclimate of human-modified tropical landscapes. Glob Chang Biol 24:5243–5258

Kearney MR, Porter WP (2009) Mechanistic niche modelling: combining physiological and spatial data to predict species' ranges. Ecol Lett 12:. https://doi.org/10.1111/j.1461-0248.2008.01277.x

Kearney MR, Porter WP (2016) NicheMapR – an R package for biophysical modelling : the microclimate model. Ecography 1–11. https://doi.org/10.1111/ecog.02360

Keppel G, Van Niel KP, Wardell-Johnson GW, et al (2012) Refugia: Identifying and understanding safe havens for biodiversity under climate change. Glob Ecol Biogeogr 21:393–404. https://doi.org/10.1111/j.1466-8238.2011.00686.x

Kiefer MT, Zhong S (2013) The effect of sidewall forest canopies on the formation of cold- air pools: a numerical study. J Geophys Res D: Atmos 118:5965–5978

Koizumi H, Oshima Y (1993) Light environment and carbon gain of understory herbs associated with sunflecks in a warm temperate deciduous forest in Japan. Ecol Res 8:135–142

Kozak KH, Wiens JJ (2010) Niche Conservatism Drives Elevational Diversity Patterns in Appalachian Salamanders. Am Nat 176(1): 40-54 https://doi.org/10.1086/653031

Lefsky MA, Cohen WB, Parker GG, Harding DJ (2002) Lidar remote sensing for ecosystem studies. Bioscience 52:19

Leitão PJ, Santos MJ (2019) Improving models of species ecological niches: A remote sensing overview. Front Ecol Evol 7:1–7. https://doi.org/10.3389/fevo.2019.00009

Lembrechts JJ, Nijs I, Lenoir J (2018) Incorporating microclimate into species distribution models. Ecography 42:1267–1279

Lenoir J, Svenning J (2015) Climate-related range shifts – a global multidimensional synthesis and new research directions. Ecography 15–28. https://doi.org/10.1111/ecog.00967

Lenoir J, Hattab T, Pierre G (2017) Climatic microrefugia under anthropogenic climate change: implications for species redistribution. Ecography (Cop) 40:253–266. https://doi.org/10.1111/ecog.02788

Lentini PE, Wintle BA (2015) Spatial conservation priorities are highly sensitive to choice of biodiversity surrogates and species distribution model type. Ecography 1101–1111. https://doi.org/10.1111/ecog.01252

Loarie SR, Duffy PB, Hamilton H, Asner GP, Field CB, Ackerly DD (2009) The velocity of climate change. Nature 462:1052–1055. https://doi.org/10.1038/nature08649

Lookingbill T (2002) Spatial estimation of air temperature differences for landscape-scale studies in montane environments. Agric For Meteorol 114:141–151

Lutterschmidt WI, Hutchison VH (1997) The critical thermal maximum: history and critique. Can J Zool 75:1561–1574. https://doi.org/10.1139/z97-783

Maclean IMD, Wilson RJ (2011) Recent ecological responses to climate change support predictions of high extinction risk. PNAS 108:12337–12342. https://doi.org/10.1073/pnas.1017352108

Marceau DJ (1999) The scale issue in the social and natural sciences. Can J Remote Sens 25:347–356. https://doi.org/10.1080/07038992.1999.10874734

Meineri E, Hylander K (2017) Fine-grain, large-domain climate models based on climate station and comprehensive topographic information improve microrefugia detection. Ecography 40:1003–1013

Merow C, Smith MJ, Silander JA (2013) A practical guide to MaxEnt for modeling species' distributions : what it does , and why inputs and settings matter. Ecography 1058–1069. https://doi.org/10.1111/j.1600-0587.2013.07872.x

Milanovich JR, Peterman WE, Nibbelink NP, Maerz JC (2010) Projected loss of a salamander diversity hotspot as a consequence of projected global climate change. PLoS One 5: https://doi.org/10.1371/journal.pone.0012189

Mokany K, Ferrier S (2011) Predicting impacts of climate change on biodiversity: a role for semi-mechanistic community-level modelling. Divers Distrib 374–380. https://doi.org/10.1111/j.1472-4642.2010.00735.x

Morin X, Thuiller W (2009) Comparing niche- and process-based models to reduce prediction uncertainty in species range shifts under climate change. Ecology 90:1301–1313. https://doi.org/10.1890/08-0134.1

Muñoz DK, Hesed KM, Grant EHC, Miller DAW (2016) Evaluating within-population variability in behavior and fitness for the climate adaptive potential of a dispersal-limited species, Plethodon cinereus. Ecology and Evolution:1–16

NatureServe (2021) NatureServe Explorer [web application]. NatureServe, Arlington, Virginia. Available https://explorer.natureserve.org/. (Accessed: June 22, 2021).

Norman SP, Hargrove WW, Christie WM (2017) Spring and autumn phenological variability across environmental gradients of Great Smoky Mountains National Park, USA. Remote Sens 9(5):407

Novick K, Ficklin DL, Stoy PC, et al (2016) The increasing importance of atmospheric demand for ecosystem water and carbon fluxes. Nat Clim Change 6:1023–1027

Nunez TA, Lawler JJ, McRae BH, Pierce DJ, Krosby MB, Kavanagh DM, Singleton PH, Tewksbury JJ (2013) Connectivity Planning to Address Climate Change. Conserv Biol 27:407–416. https://doi.org/10.1111/cobi.12014

OCM Partners (2019) 2005 NCFMP Lidar: NC Statewide Phase 3 from 2010-06-15 to 2010-08-15. NOAA National Centers for Environmental Information. https://inport.nmfs.noaa.gov/inport/item/49833

O'Donnell KM, Thompson FR, Semlitsch RD (2014) Predicting Variation in Microhabitat Utilization of Terrestrial Salamanders. Herpetologica, 70(3), 259–265. http://doi.org/10.1655/HERPETOLOGICA-D-13-00036

Olalla-Tarraga MA, Rodriguez MA, Hawkins BA (2006) Broad-scale patterns of body size in squamate reptiles of Europe and North America. J Bio 781–793. https://doi.org/10.1111/j.1365-2699.2006.01435.x

Parra-Olea G, Martínez-Meyer E, Pérez-Ponce De León G (2005) Forecasting climate change effects on salamander distribution in the highlands of central Mexico. Biotropica 37: https://doi.org/10.1111/j.1744-7429.2005.00027.x

Perveen S, James LA (2012) Changes in Correlation Coefficients with Spatial Scale and Implications for Water Resources and Vulnerability Data. Prof Geogr 64:389–400. https://doi.org/10.1080/00330124.2011.609783

Peterman WE, Crawford JA, Hocking DJ (2016) Effects of elevation on plethodontid salamander body size. Copeia 104:202–208. https://doi.org/10.1643/OT-14-188

Petranka, JW (1998) Salamanders of the United States and Canada. Smithsonian Institution Press, USA

Petruzzi EE, Niewiarowski PH, Moore FB (2006) The role of thermal niche selection in maintenance of a colour polymorphism in redback salamanders (Plethodon cinereus). Front Zool 8:1–8. https://doi.org/10.1186/1742-9994-3-10

Pinheiro J, Bates D, DebRoy S, Sarkar, D, R Core Team (2020). nlme: linear and nonlinear mixed effects models. R package version 3.1-151. https://CRAN.R-project.org/package=nlme

Possingham HP, Wilson KA, Andelman SJ, Vynne CH (2006) Protected areas: goals, limitations and design. In: Groom MJ, Meffe GK, Carroll CR, editors. Principles of Conservation Biology. Sinauer Associates: Sunderland; 2006. pp. 509–533.

Potter KA, Woods HA, Pincebourde S (2013) Microclimatic challenges in global change biology. Glob Change Biol 19:2932–2939

Pough FH (1980) Advantages of ectothermy for tetrapods. Am Nat 115:92–112. https://doi.org/10.2307/2460833

PRISM Climate Group (2020) Oregon State University, http://prism.oregonstate.edu. Accepted 4 Feb 2004

R Core Team (2020) R: a language and environment for statistical computing. R Foundation for Statistical Computing, Vienna, Austria. http://www.R-project.org/. Computing, Vienna, Austria. http://www.R-project.org/

Randin CF, Engler R, Normand S, et al (2009) Climate change and plant distribution: local models predict high-elevation persistence. Glob Change Biol 15:1557–1569

Riddell EA, Sears MW (2015) Geographic variation of resistance to water loss within two species of lungless salamanders: implications for activity. Ecosphere 6(5):86. http://dx.doi.org/10.1890/ES14-00360.1

Riddell EA, Apanovitch EK, Odom JP, Sears MW (2017) Physical calculations of resistance to water loss improve predictions of species range models. Ecol Monogr 87(1):21-33. https://doi.org/10.1002/ecm.1240

Riddell EA, Odom JP, Damm JD, Sears MW (2018a) Plasticity reveals hidden resistance to extinction under climate change in the global hotspot of salamander diversity. Science Advances 5:1–10

Riddell EA, McPhail J, Damm JD, Sears MW (2018b). Tradeoffs between water loss and gas exchange influence habitat suitability of a woodland salamander. Funct Ecol 32:916–925

Riddell EA, Iknayan KJ, Hargrove L, Tremor S, Patton JL, Ramirez R, Wolf BO, Beissinger SR (2021) Exposure to climate change drives stability or collapse of desert mammal and bird communities. Science 371, 6529. doi: 10.1126/science.abd4605

Ripple WJ, Wolf C, Newsome TM, et al (2017) Extinction risk is most acute for the world's largest and smallest vertebrates. Proc Natl Acad Sci U S A 114:10678–10683. https://doi.org/10.1073/pnas.1702078114

Rissler LJ, Apodaca JJ (2007) Adding More Ecology into Species Delimitation: Ecological Niche Models and Phylogeography Help Define Cryptic Species in the Black Salamander (Aneides flavipunctatus). Syst Biol 56:924–942. https://doi.org/10.1080/10635150701703063

Scherrer D, Körner C (2010) Infra-red thermometry of alpine landscapes challenges climatic warming projections. Glob Chang. Biol 16:2602–2613

Schmitz A, Lawler JJ, Beier P, et al (2015) Conserving Biodiversity : Practical Guidance about Climate Change Adaptation Approaches in Support of Land-use Planning. Natural Areas Journal. 35:1

Schwalm CR, Glendon S, Duffy PB (2020) RCP8.5 tracks cumulative CO 2 emissions. 2020:17–18. https://doi.org/10.1073/pnas.2007117117

Sears MW (2005) Resting metabolic expenditure as a potential source of variation in growth rates of the sagebrush lizard. Comp Biochem Physiol - A Mol Integr Physiol 140:171–177

Shukla PR, J. Skea R, Slade R, et al (2019) Portugal Pereira (eds.) Technical Summary. In: Climate Change and Land: an IPCC special report on climate change, desertification, land degradation, sustainable land management, food security, and greenhouse gas fluxes in terrestrial ecosystems

Singer JD, Willett JB (2003) Applied longitudinal data analysis: modeling change and event occurrence. Oxford University Press, Oxford

Stickley SF, Fraterrigo JM (2021) Understory vegetation contributes to microclimatic buffering of near-surface temperatures in temperate deciduous forests. Land. Ecol 36: 1197-1213. https://doi.org/10.1007/s10980-021-01195-w. Reproduced with permission from Springer Nature.

Suggitt AJ, Gillingham PK, Hill JK, Huntley B, Kunin WE, Roy DB, Thomas CD (2011) Habitat microclimates drive fine-scale variation in extreme temperatures. Oikos 120(1):1–8

Thomas CD, Cameron A, Green RE, et al (2004) Extinction risk from climate change. Nature 427, 145–148

Thornton MM, Thornton PE, Wei Y, Mayer BW, Cook RB, Vose RS (2018) Daymet: annual climate summaries on a 1-km grid for North America, Version 3. ORNL DAAC, Oak Ridge, Tennessee, USA. https://doi.org/10.3334/ORNLDAAC/1343

Thrasher B, Xiong J, Wang W, Melton F, Michaelis A, Nemani R (2013) Downscaled Climate Projections Suitable for Resource Management. Eos Trans 94:321. https://doi.org/10.1023/B

Tingley MW, Koo MS, Moritz C, Rush AC, Beissinger SR. (2012) The push and pull of climate change causes heterogeneous shifts in avian elevational ranges. Global Change Biology 18:3279–3290

Trivedi MR, Berry PM, Morecroft MD, Dawson TP (2008) Spatial scale affects bioclimate model projections of climate change impacts on mountain plants. Glob Change Biol 14:1089–1103

Turner MG, Dale VH, Gardner RH (1989) Predicting across scales: Theory development and testing. Landsc Ecol 3:245–252. https://doi.org/10.1007/BF00131542

Urban MC (2015) Accelerating extinction risk from climate change. Science. 348: 6234, 571-573 doi: 10.1126/science.aaa4984

Urban MC, Bocedi G, Hendry AP, et al (2016) Improving the forecast for biodiversity under climate change. Science 353:6304. https://doi.org/10.1126/science.aad8466

Vanwalleghem T, Meentemeyer RK (2009) Predicting forest microclimate in heterogeneous landscapes. Ecosystems 12:1158–1172

Washitani I, Tang Y (1991) Microsite variation in light availability and seedling growth of Quercus serrata in a temperate pine forest. Ecol Res 6:305–316

Wells, KD (2007) The Ecology & Behavior of Amphibians. The University of Chicago Press. Chicago and London

Welsh HH, Lind AJ (1992) Population Ecology of two Relictual Salamanders from the Klamath Mountains of Northwestern California. In: McCullough D.R., Barrett R.H. (eds) Wildlife 2001: Populations. Springer, Dordrecht. https://doi.org/10.1007/978-94-011-2868-1_33

Whitford, WG, Hutchison VH (1965) Gas exchange in salamanders. Physiological Zoology 38:228–242

Whitford, WG, Hutchison VH (1967) Body size and metabolic rate in salamanders. Physiological Zoology 40: 127–133

Whittaker RH (1956) Vegetation of the Great Smoky Mountains. Ecol Monogr 26(1):1–80

Whittaker RJ, Nogués-bravo D, Araújo MB (2007) Geographical gradients of species richness : a test of the water-energy conjecture of Hawkins et al . (2003) using European data for five taxa. Glob. Ecol. Biog. 16 (1); 76–89. https://doi.org/10.1111/j.1466-822x.2006.00268.x

Wiens JA, Stralberg D, Jongsomjit D, Howell CA, Snyder MA (2009) Niches, models, and climate change: Assessing the assumptions and uncertainties. PNAS 106:19729–19736

Wilson JB (2011) Cover plus: ways of measuring plant canopies and the terms used for them. J Veg Sci 22:197–206

Withers PC (1980) Oxygen consumption of plethodontid salamanders during rest, activity, and recovery. Copeia 1980:781–786

WWF (2020) Living Planet Report 2020 -Bending the curve of biodiversity loss. Almond, R.E.A., Grooten M. and Petersen, T. (Eds).WWF, Gland, Switzerland.

Zeigler SL, Fagan WF (2014) Transient windows for connectivity in a changing world. Mov Ecol 2:1. https://doi.org/10.1186/2051-3933-2-1

Zellweger F, Coomes D, Lenoir J, et al (2019a) Seasonal drivers of understorey temperature buffering in temperate deciduous forests across Europe. Global Ecology and Biogeography 1774–1786. https://doi.org/10.1111/geb.12991

Zellweger F, De Frenne P, Lenoir J, Rocchini D, Coomes D (2019b) Advances in microclimate ecology arising from remote sensing. Trends Ecol Evol 34:327–341

Zuur A, Leno EN, Walker NJ, Saveliev AA, Smith GM (2009) Mixed effects models and extensions in ecology with R. Springer, Berlin